ENGINSOFT

The Simulation Based Engineering & Sciences Magazine

Newsletter

Year 18 n°4

Winter 2021

Loaded tooth contact analysis and dynamic investigation of Spiral Bevel Gears

Large bore engine lubrication system: oil flow and pressure analysis using moving particle simulation

Validation of a model of a methanol fuel supply system for a two-stroke dual-fuel marine diesel engine

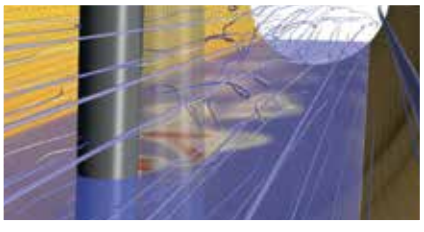

Using high-fidelity FSI simulation and advanced mesh morphing to simulate and mitigate vortex-induced vibrations

ENGINSOFT

Drive Your Career!

Dive into our full training offer!

2022

www.enginsoft.com/training

Flash

Digitalization and sustainability remain two impelling trends in business today and were key themes of the 37th International CAE Conference and Exhibition that was held in November 2021 at the Vicenza Convention Centre, which focused on the role that simulation plays in orchestrating a winning strategy implementation for both of these challenges. This issue of the Newsletter has a report-back on the event and also includes some articles based on a selection of the content that was presented at the hybrid (both in person and broadcast via live streaming on the Internet) event.

Our cover story on the loaded tooth contact analysis and dynamic investigation of a spiral bevel gear undertaken as a joint project between the University of Modena and Reggio Emilia in Italy and the Shahid Bahonar Mechanical Engineering Department of the University of Kerman in Iran, which was presented in the manufacturing breakout session. It looks at an innovative approach to studying spiral bevel gear pairs to reduce vibration and variability in mesh stiffness over time in order to improve the transmission efficiency and durability of a geartrain.

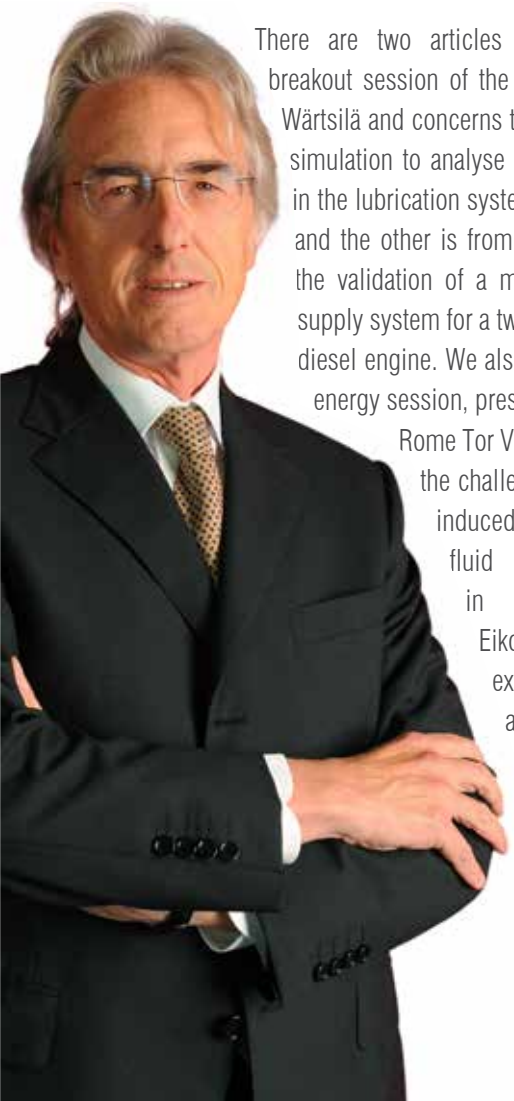

There are two articles from the transportation breakout session of the conference. One is from Wärtsilä and concerns the use of moving particle simulation to analyse the oil flow and pressure in the lubrication system of a large bore engine; and the other is from Alfa Laval and examines the validation of a model of a methanol fuel supply system for a two-stroke dual-fuel marine diesel engine. We also have an article from the energy session, presented by the University of Rome Tor Vergata, which investigated the challenge of controlling vortex-induced vibrations in unsteady fluid structure interactions in industrial applications. Eikosim, one of the exhibitors, presents an article that examines the value of image correlation to validate numerical models for automotive issues, and we have included an article based on one of the five winning posters of the tenth annual Poster award that discusses the hypothesis of transferring a safety device used in cars to powered two-wheelers.

Moving away from the International CAE Conference and Exhibition, we have a series of articles of interest. There is a CFD simulation of an axial piston pump for fluid power sources that require high pressure and variable flow rates; there is a case study that describes the design of a new sensorized foundry die and the implementation of an intelligent monitoring system for it supported by a predictive quality model created through instructional sampling. We have an analysis of stray load loss reduction for a distribution transformer, the simulation of snow drift volume and deposition, and the analysis of the seismic and geological characteristics of a "tunnel-rock massif" to design a tunnel for greater stability and security.

Another article worthy of interest is the one concerning the EU LIFESAVER project, a large-scale pan-European project funded by the European Commission's Horizon2020 Research and Innovation Action Programme, with the goal of addressing this serious threat in order to ensure that every pregnant woman has an adequate living environment with minimal risks to the fetus. The objective is to create and demonstrate a novel digitally cloned in vitro system to emulate prenatal conditions near the placental interface to enable the prediction of the potential risks posed by a drug or chemical to the unborn child. The LIFESAVER concept is based on an original idea to hybridize several innovative technologies and integrate the digital in silico system with the in vitro laboratory system. With a total budget of €6-million and a duration of 48 months, EnginSoft is proud to be the coordinator of this project which brings together a consortium of 14 partners from nine EU countries, comprising leading European research and academic institutions, institutes for health, and industry. Future editions of the Newsletter are sure to cover further details of this project as it develops.

I'd like to take this opportunity to wish you and your families a serene and successful 2022 and express the hope which I am sure we all have, that 2022 will see us finally overcome the Covid-19 pandemic.

Stefano Odorizzi
Editor in chief

Contents

37th International CAE Conference
SPECIAL SUPPLEMENT

Case Studies

Software Update

PAST ISSUES at
www.enginsoft.com/magazine

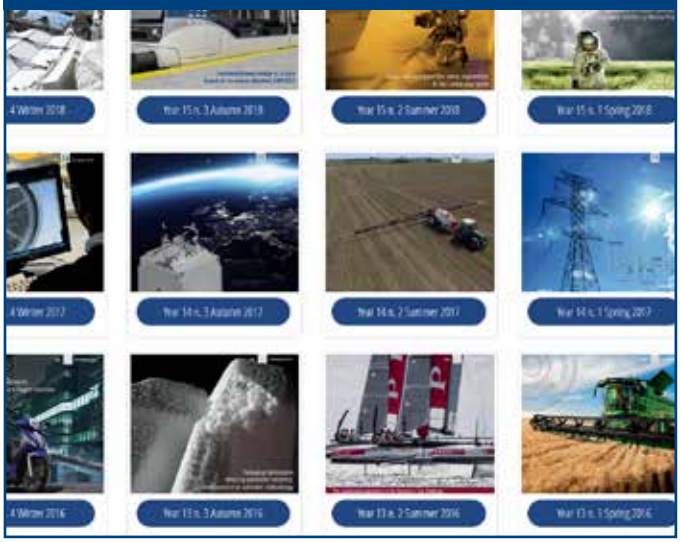

EnginSoft Newsletter
Year 18 n°4 - Winter 2021

To receive a free copy of the next EnginSoft Newsletters, please contact our Marketing office at: info@enginsoft.it

EnginSoft S.p.A.
24126 BERGAMO c/o Parco Scientifico Tecnologico
Kilometro Rosso - Edificio A1, Via Stezzano 87
Tel. +39 035 368711 • Fax +39 0461 979215
50127 FIRENZE Via Panciatichi, 40
Tel. +39 055 4376113 • Fax +39 0461 979216
35129 PADOVA Via Giambellino, 7
Tel. +39 049 7705311 • Fax +39 0461 979217
72023 MESAGNE (BRINDISI) Via A. Murri, 2 - Z.I.
Tel. +39 0831 730194 • Fax +39 0461 979224
38123 TRENTO fraz. Mattarello - Via della Stazione, 27
Tel. +39 0461 915391 • Fax +39 0461 979201
10133 TORINO Corso Marconi, 20
Tel. +39 011 6525211 • Fax +39 0461 979218

www.enginsoft.com
e-mail: info@enginsoft.com

The EnginSoft Newsletter is a quarterly magazine published by EnginSoft SpA

COMPANY INTERESTS
EnginSoft GmbH - Germany
EnginSoft UK - United Kingdom
EnginSoft France - France
EnginSoft Turkey - Turkey
VSA-TTC3 - Germany
www.enginsoft.com

CONSORZIO TCN www.consorziotcn.it • www.improve.it
M3E Mathematical Methods and Models for Engineering www.m3eweb.it
AnteMotion

ASSOCIATION INTERESTS
NAFEMS International www.nafems.it • www.nafems.org
TechNet Alliance www.technet-alliance.com

ADVERTISING
For advertising opportunities, please contact our Marketing office at: info@enginsoft.com

RESPONSIBLE DIRECTOR
Stefano Odorizzi

PRINTING
Grafiche Dalpiaz - Trento

Autorizzazione del Tribunale di Trento
n° 1353 RS di data 2/4/2008

Report back on the 2021 International CAE Conference and Exhibition

The 37th annual edition of the event took place over three days from 17-19 November 2021 in hybrid mode (that is, both physically, in person and virtually, online) and focused on Orchestrating Digital Transformation through Simulation – Channeling Technology Processes and People for competitive advantage. A collaboration with the PHORESTA Onlus organization enabled the CAE Conference and Exhibition's CO_2 emissions to be offset, making this a zero-emissions event.

The conference and exhibition offered participants a perspective on the trends, technologies, issues and how-tos of sustainable and successful digital transformation and on the key role that engineering simulation plays in achieving the desired outcome.

The hybrid aspect added significant value to this year's event, enabling participants and speakers that would otherwise not have been able to attend due to travel or other Covid-19-related restrictions to contribute directly. All the events were broadcast live via real-time streaming in the event's virtual platform, allowing all participants to ask questions of the presenters and receive answers equally, as though they were there in person.

The Conference program was rich and interesting, featuring two inspirational presentations, two special events, four technical sessions, and ten deep-dive exhibitors' events. The first of the two inspirational presentations was entitled "A Stroll on Mars" by NASA's Mars Science Laboratory member, Paolo Bellutta. It allowed attendees to vicariously share the adventures of the man who has travelled the greatest number of kilometers as a remote navigator at the controls of a rover on the Red

The 37th edition in numbers

3	Conference and Exhibition Days
19	Events streamed live
75	Speakers – either on-site or connecting remotely
24	Physical and/or virtual Exhibitors
48	Poster Award Finalists
11	Projects in the Research Agorà

Planet. The second inspirational presentation, "Origami Engineering, nurtured by Japanese folding culture", offered a fascinating look at how the traditional Japanese artform of paper folding is influencing the most avant-garde thinking in engineering for innovative, light weight and highly protective solutions for food packaging, or crash protection in motor vehicles or safety equipment, just to mention a few.

The first of the special events, entitled "Italian Pathways to the Digital Future: an overview of the country's economic recovery and the paths to creating an innovative Italy" was a lively round table discussion between political and business thought leaders and participants about the potential avenues for innovative evolution in Italy from the EU's pandemic economic recovery financing program. The second of these events examined "The hourglass of innovation: challenges and opportunities for European industries" to tackle climate change challenges, with participation from top representatives of European and national networks in strategic who provided a perspective on the opportunities for industry in approaching climate change issues through digitalization.

The four technical breakout sessions covered the automotive, energy, manufacturing, and transportation sectors. Each was opened with a relevant thought leadership keynote addressing the practical application of engineering simulation to real-world challenges in that sector and was followed by detailed technical sessions.

The exhibition, which took place in parallel with the conference, hosted a substantial selection of big-name players in the engineering simulation market both physically at the Vicenza Convention Centre, and online by means of virtual stands in the event platform, and represented a sample of some of engineering simulation's most cutting-edge innovations. The exhibitors were able to interact directly, remotely or on site, with participants and present their application expertise, detailed product demonstrations, explicative videos and more. The event's virtual platform ensured simple and effective B2B networking powered by artificial intelligence (AI) matchmaking, the key innovative feature this year.

As usual, a space was dedicated, both virtually and physically this year, to the dissemination of international research through the Research Agorà. Public and private research bodies and academic institutions participated in the hybrid event and numerous research consortia highlighted the progress of their projects.

This year also celebrated the tenth edition of the annual Poster Award, a now-traditional contest that recognizes and rewards the creative use of CAE technologies by young students and researchers from all over the world, and which was sponsored by SIMAI (the Italian Society for Applied and Industrial Mathematics), the TCN Consortium (Tecnologie per il Calcolo Numerico) and EnginSoft. With around 100 poster submissions from some of the most prestigious universities in Europe, the UK, and the USA across a diverse range of fields, this year's short-list of 48 finalists was hotly contested. The two-tiered voting assessment to select the winning five posters from among them consists of an online vote open to everyone (in which over 3,000 people participated), and the vote of the technical and scientific committee, experts in numeric simulation. The five winners represented interesting applications of CAE technologies to new or ongoing challenges.

Overall, it was a full, informative, and interesting program and the event was well attended both online and in person, in spite of the pandemic. As the longest running international event in this sector, it lived up to its reputation. With the rapid increase in the uptake of digital technologies, spurred on by the pandemic lock downs around the globe, and the relentless pace of innovation in technology, attending next year's event will be necessary in order to keep abreast of it all!

Loaded tooth contact analysis and dynamic investigation of Spiral Bevel Gears

by Moslem Molaie, Giovanni Iarriccio, Francesco Pellicano, Farhad S. Samani, and Antonio Zippo
A joint study by the "Enzo Ferrari" Department of Engineering at the University of Modena and Reggio Emilia in Modena, Italy,
the Centre InterMech MO.RE., in Modena, Italy and
the Shahid Bahonar Mechanical Engineering Department of the University of Kerman, in Kerman, Iran.

Spiral bevel gear pairs (SBGs) play an important role in transferring power between non-parallel shafts in transmission systems. Their high contact ratio, makes SBGs smooth and quiet, allows them to withstand high levels of torque and power, however their complex geometry requires a careful consideration of the parameters that affect transmission efficiency and durability. Vibration is a major issue because it influences the stress distribution, contact pressure, and fatigue life of a geartrain. Several parameters, such as fluctuating mesh stiffness and transmission error in the gear mesh exert an important influence on vibration which is the major source of driveline noise.

Therefore, mesh stiffness (MS) and transmission error (TE) are two key parameters that require intensive research. A variety of methods is used to calculate these two parameters. Loaded tooth contact analysis (LTCA) is used to calculate the static transmission error (STE) and the MS of a gear pair. Different methods can be used to conduct LTCA, including the finite element method (FEM), the experimental method, and the analytical method.

Several software packages to analyze LTCA have been developed and released over the last decade. They use FEM, or standards (for instance, ISO), or both methods to extract MS/TE for different gear sets. In this study, STE and MS were calculated using the MASTA software package, and the results were compared with CALYX software. This paper presents the dynamic results of the case study investigated and illustrates nonlinear phenomena.

Bevel gears are often used to transmit power between non-parallel shafts. They comprise several geometries, the most significant of which are the spiral bevel gears (SBG). The vibration affects the stress distribution, the contact pressure, and the fatigue life of a gearset. Nonlinearity is affected by a number of factors, including backlash and time-varying mesh stiffness. It is to note that gear mesh transmission error is one of the most significant sources of driveline vibration and noise. A variety of approaches is used to study gear pairs. [1-5].

The total displacement of gears during meshing is given by the sum of different deformations, such as deflection due to bending, shear, and surface indentation. Sánchez et al [6] studied the mesh stiffness of pairs of spur gears taking into account the Hertzian effect and presented a formula for approximate mesh stiffness. Sánchez considered bending, shear, compression and contact deflection to obtain the mesh stiffness. For spur gears, the equation proposed in Ref.[6] calculated the load sharing ratio and the load at any point along the contact path. Cheng et al [7], used the finite element method to calculate time-varying mesh stiffness considering the influence of Hertzian deflection and various loads.

Recently, the research on SBGs has focused on tooth contact analysis to obtain static transmission error (STE), which is regarded as the primary cause of vibration. Kickbush et al [8] proposed two finite element models (two-dimensional and three-dimensional) to approximate MS. Tang et al [9] investigated how two distinct STEs affect an SBG's dynamic response. The two STEs evaluated were a pre-designed parabolic function and a sine function. Other research has investigated the influence of faults on the dynamic behavior of gear pairs [10]. Peng et al [11] proposed a new method for estimating load transmission error (LTE) which considers the effect of bearing supports. Wang et al. [12] used a finite element analysis technique to investigate the time-varying mesh stiffness of a gear pair with cracked teeth.

The main objective of the present study is to calculate the mesh stiffness using LTCA. For this purpose, two powerful software, based on FEM, are used to calculate the mesh stiffness with the highest possible accuracy. After obtaining the mesh stiffness, we are able to analyze the behavior of spiral gear pairs in different situations, e.g. in the presence of misalignments.

Loaded tooth contact analysis

Mesh stiffness and dynamic investigation are two of the most prominent and interesting topics that attract great attention from researchers. Investigation of mesh stiffness is significant to understand the behavior of the gear system. Obtaining mesh stiffness is mandatory to simulate the dynamic model of the geartrain.

To calculate the mesh stiffness of a gear pair, a loaded tooth contact analysis (LTCA) must be conducted [11, 13- 15]. Finite element analysis, experimental testing, and simplified analytical models are all suitable methods for performing LTCA. Comparing these methods, one could find that experimental methods [5] require expensive test rigs; and that while the analytical solutions developed for spur/helical gear pairs, they are not well suited to gear pairs with complicated geometries, such as spiral gears. In this context, FEM has been widely used in recent years owing to its reduced costs and its ability to model gear pairs with different geometries [1, 16, 17].

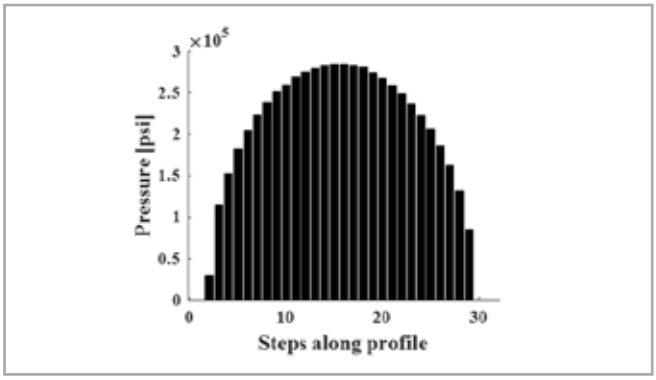

Fig. 1 - Pressure distribution on the tooth surface

Several software have been developed to perform LTCA, two of the most powerful of which are MASTA and Calyx. This study focuses primarily on obtaining the mesh stiffness as accurately as possible. Both Calyx and MASTA are FEM-based, so comparing their results would be likely to ensure their accuracy. With respect to accuracy, the most sensitive output of a LTCA is the contact pressure. Fig. 1 shows the pressure distribution on the tooth surface along the pinion profile. The pressure distribution is parabolic, as predicted by the theory.

The next step, which is undertaken to check the accuracy of the results, is to compare them with the FEM data present in literature, see Bibel et al [18];it should be pointed out that they validated their results with experimental data.

Fig. 2 shows the maximum principal stress on the pinion root at the middle surface. The solid line shows the simulation results, and the solid red circles are the results of Bibel it should be: [18]; we observe a very good match.

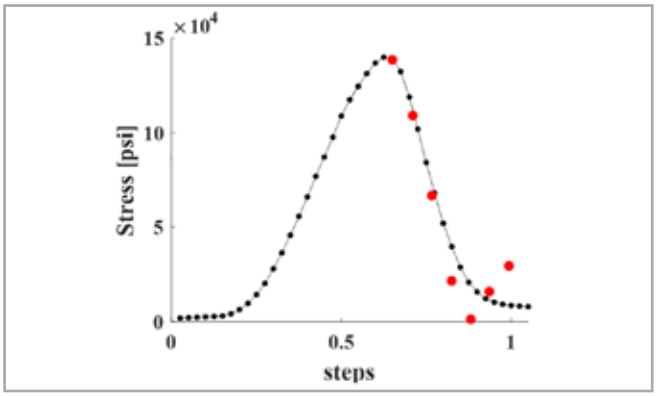

Fig. 2 - Maximum principal stress on the root of the tooth relative to the pinion mid plate (- FEM simulation, • verified FEM results [18]).

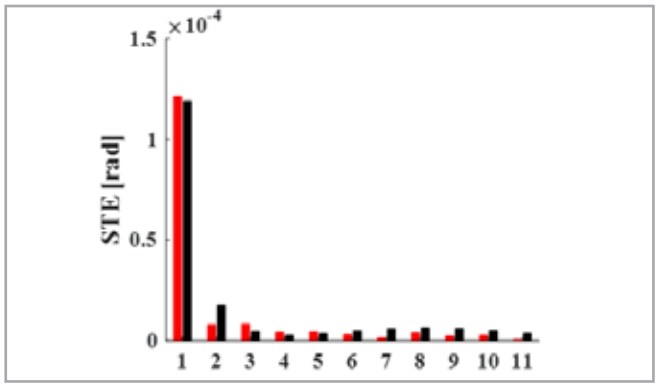

Fig. 3 - Fourier coefficients for rotational deflection (• MASTA, • Calyx)

As mentioned, earlier, two reliable software with powerful solvers were used in this study. The static transmission error is expanded through the Fourier series and the coefficients are shown in Fig.3. The black bars represent the Fourier coefficient from the Calyx simulation results, and the red bars show the MASTA simulation results.

Dynamic investigation

In this section, a model is provided to study the dynamics of an SBG gear pair. Consider the bevel gear pair in Fig. 4: the translational degrees of freedom for both the driver and driven gears are constrained in all directions; the gears can rotate about their axes, but no further rotation is allowed. In addition, the following assumptions are made: a pure involute profile with dry contact and no friction; and thermal effects are ignored.

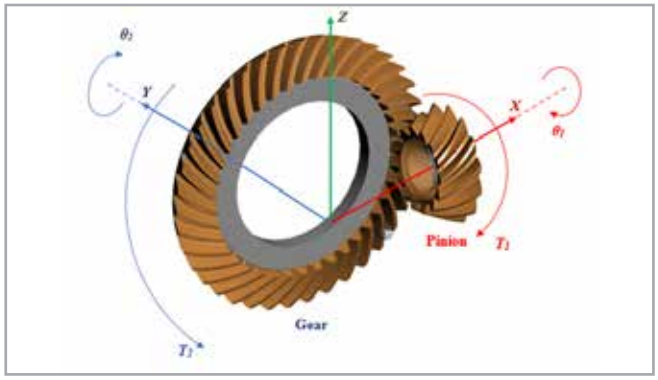

Fig. 4 - Dynamic model of a gear system with rotational degrees of freedom

The dynamic equations of motion of this system (Fig. 4) are given by [16, 19-23]:

$$\begin{aligned} &I_1\ddot{\theta}_1 + C_m r_{b1}\left(r_{b1}\dot{\theta}_1 - r_{b2}\dot{\theta}_2 - \dot{e}\right) \\ &\qquad + K_m r_{b1} f\left(r_{b1}\theta_1 - r_{b2}\theta_2 - e\right) = T_1 \\ &I_2\ddot{\theta}_2 - C_m r_{b2}\left(r_{b1}\dot{\theta}_1 - r_{b2}\dot{\theta}_2 - \dot{e}\right) \\ &\qquad - K_m r_{b2} f\left(r_{b1}\theta_1 - r_{b2}\theta_2 - e\right) = -T_2 \end{aligned} \qquad (1)$$

Due to assembly and manufacturing errors, or changes in tooth profile, the backlash between mating teeth varies; this is called geometric transmission error, or e(t). The linear dynamic transmission error (DTE) along the line of action is defined as $\lambda = r_{b1}\theta_1 - r_{b2}\theta_2$. The two equations (1) are merged, and the following equation is obtained

$$m_{eq}\ddot{\lambda} + C_m(\dot{\lambda} - \dot{e}) + K_m(t) f(\lambda - e) = {}^{T_1}/_{r_{b1}} \qquad (2)$$

where $m_{eq} = \left(\frac{r_{b1}^2}{I_1} + \frac{r_{b2}^2}{I_2}\right)^{-1}$.

Equation (2) presents the equivalent displacement of the gear mesh.

$$f(\lambda - e) = \begin{cases} \lambda - e - b, & \lambda - e > b \\ 0, & -b \le \lambda - e \le b \\ \lambda - e + b, & \lambda - e < -b \end{cases} \qquad (3)$$

f(λ-e) is the backlash function of the displacement (Equation (3)). The backlash function multiplied by the stiffness returns the restoring force [2]. Whenever λ-e is between -b and +b, the contact loss occurs [24]. For λ-e>b, the contact occurs in forward flank, while if λ-e<-b, unwanted contact occurs at the back. In addition, the torsional mesh stiffness of the gear set is a time-varying function, which is periodic with the fundamental mesh frequency $\omega_m = 2\pi/60\, N_1\gamma_s$.

The equivalent mesh stiffness can be expanded by using the

$$\begin{cases} \omega_m = \dfrac{2\pi}{60} N_1 \gamma_s \\ S = (N_p - 1)/2 \end{cases} \Rightarrow K(t) = k_0 + \sum_{j=1}^{S} a_j \cos(j\omega_m t) + \sum_{j=1}^{S} b_j \sin(j\omega_m t) \qquad (4)$$

Where k_0, a_j, and b_j are the coefficients of the Fourier series. Fig. 5 shows the rotational deflection of the Gear.

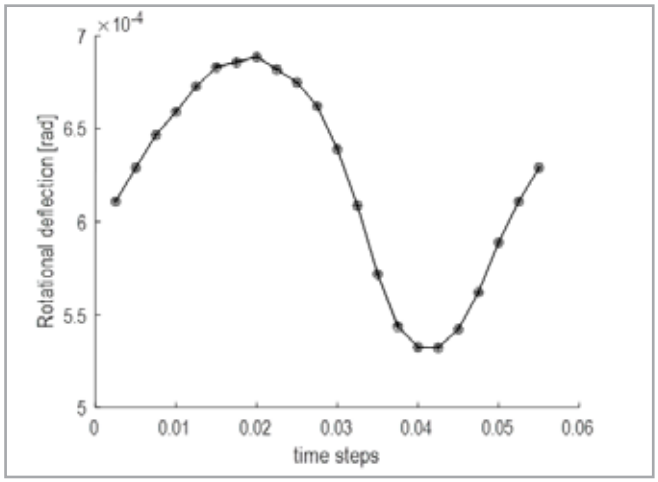

Fig. 5. Rotational deflection of the Gear

In order to normalize the governing equation, new parameters are introduced as follows:

$$\tau = \omega_n t \qquad \bar{e} = \frac{e}{b} \qquad \bar{T}_{eq} = \frac{T_1}{b \cdot r_{b1} \cdot m_{eq}} \qquad (5)$$
$$\omega_n = \sqrt{\frac{k_0}{m_{eq}}} \qquad \bar{\lambda}' = \frac{d\bar{\lambda}}{d\tau}, \bar{\lambda} = \frac{\lambda}{b} \qquad \zeta = \frac{C_m}{2m_{eq}\omega_n}$$

Consequently, Equations (2), (3), and (4) can be rewritten as follows:

$$\overline{\lambda}'' + 2\zeta(\overline{\lambda}' - \overline{e}') + \overline{K}_m(\tau) f(\overline{\lambda} - \overline{e}) = \overline{T}_{eq} \quad (6)$$

$$f(\overline{\lambda} - \overline{e}) = \begin{cases} \overline{\lambda} - \overline{e} - 1 & \overline{\lambda} - \overline{e} > 1 \\ 0 & -1 \le \overline{\lambda} - \overline{e} \le 1 \\ \overline{\lambda} - \overline{e} + 1 & \overline{\lambda} - \overline{e} < -1 \end{cases} \quad (7)$$

$$\overline{K}_m(t) = 1 + \sum_{j=1}^{S} \frac{a_j}{I_{eq}\omega_n{}^2} \cos(j\omega_m t) + \sum_{j=1}^{S} \frac{b_j}{I_{eq}\omega_n{}^2} \sin(j\omega_m t) \quad (8)$$

Equation (6) is a second-order nonlinear differential equation with time-varying parameters.

This governing equation is solved numerically via the "RADAU scheme", which is an implicit scheme of the Runge–Kutta algorithm with step control, capable of handling problems that require a high numerical stability; see, e.g. [1, 2, 16, 17, 23]*.

Numerical results

The design data of the SBG pair considered is listed in Table 1. Note that the gear pair considered was previously used by Bibel et al. [18]. The bifurcation diagrams and root mean square (RMS) are obtained by varying the excitation frequency, i.e., the rotational speed of the pinion.

Parameters	Pinion	Gear
Pitch angle	18.43	71.57
Number of teeth	12	36
Module (mm)	4.941	
Backlash (mm)	0.1	
Nominal torque (N·m)	358.1	
Module of elasticity, E (GPa)	209	
Poisson ratio, v	0.3	
Face width, w (mm)	25.4	
Pressure angle, α	20°	
Mean spiral angle	35°	
Damping ratio, ζ	0.01	

Table 1. Geometric parameters of the SBG pair

Simulations are performed in the range of ω⁄ω_n ϵ (0.1,2.5), forward and backward.

For each frequency, the final condition of previous set is considered as the initial condition for the new step. For the backward simulation, the vibration is periodic (see Fig. 6), except in the interval $\omega/\omega_n \in (2,1.3)$ when subharmonic bifurcation occurs.

Fig. 7 shows the amplitude–frequency diagram. The primary resonance as well as, super-harmonic resonance, and a parametric

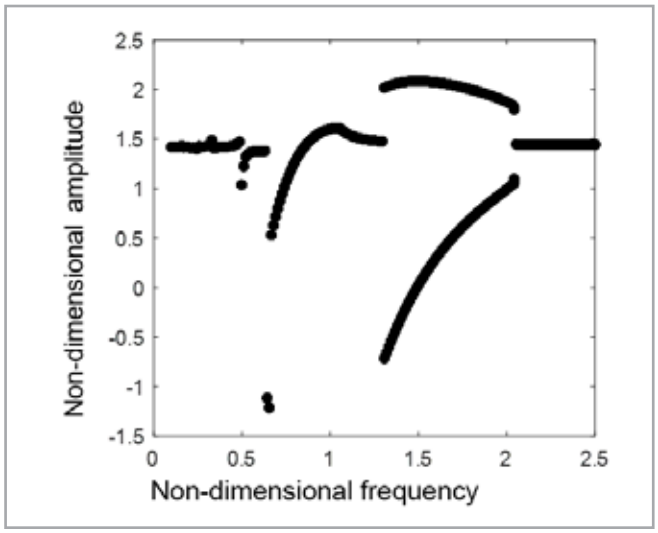

Fig. 6 - Bifurcation diagram based on backward simulation

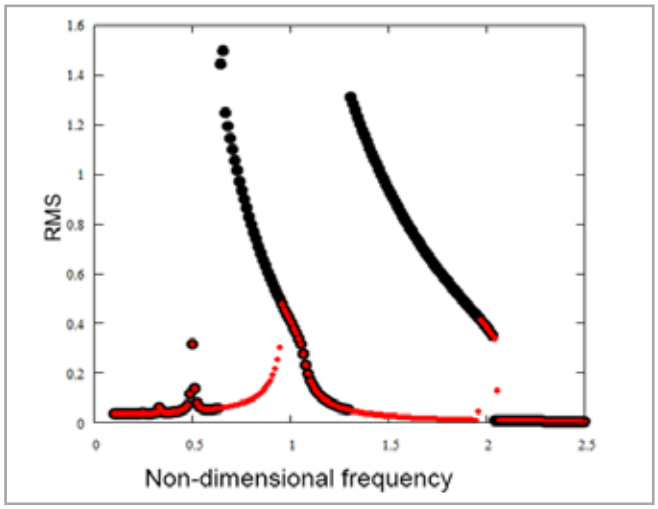

Fig. 7 – RMS diagram of forward and backward simulations

resonance (ω/ω_n =0.5 and 2, respectively) are identified. These results show that the system experiences steady behavior until it approaches super-harmonic, primary and parametric resonances.

Conclusion

This study was conducted to calculate mesh stiffness and transmission error. The results were compared using two important FEM software programs (MASTA and Calyx), and finally the accuracy of the results was evaluated considering the data from a recent study by Bibel et al. As the results showed, the accuracy of the output results was acceptable.

Furthermore, the dynamic response of the system was also evaluated in this study. Subharmonic and super harmonic phenomena are illustrated for some special harmonics. Backside contact and contact loss was observed during the dynamic investigation of the SBG.

The dynamic equation presented is derived after some simplifications, namely: one degree of freedom and neglecting the effect of friction between two coupled teeth. It would be insightful for future studies to increase the number of DOFs or to consider

the effect of friction on the dynamic response in order to analyze the dynamic behavior of the system in greater detail.

The output of this study may be a significant step towards further investigation of the dynamic behavior of an SBG system.

In other words, the comparison made in this study allows the effect of different parameters (for instance, misalignment, tip/root modification, andcrowning) on mesh stiffness, as well as the dynamic behavior of SBG sets a result of these effects to be investigated.

Funding: The authors thank the Emilia Romagna region of Italy for supporting this research through the project "DiaPro4.0 – Sistema 'cost effective' multisensore di Diagnostica- Prognostica integrato in azionamenti meccanici dell'Industria 4.0" – (PG/2018/632156).

Acknowledgments: The authors would like to thank EnginSoft's team for their support in this research.

For more information:
Daniele Sacchi - EnginSoft
d.sacchi@enginsoft.com

List of Symbols	
a_j, b_j	Fourier coefficients
C_m	Damping coefficient between the mesh gear teeth of the pairs
E	Module of elasticity
e(t)	Time-varying no-load transmission error
I_1, I_2	Rotary inertia of pinion and gear
m_{eq}	Equivalent mass
N_1	Teeth number of the pinion
N_p	Number of samples for mesh stiffness computation
k_0	Average value of torsional mesh stiffness of the gear pair
k	Time-varying mesh stiffness of the gear pair
K_m	Equivalents of the torsional mesh stiffness of the gear pair
r_{b1}, r_{b2}	Base radii of pinion and gear
S	Number of harmonics
T_1	Constant driver torque
T_2	Constant breaking torque
w	Face width
α	Pressure angle
γ_s	Input shaft speed
ζ	Damping ratio
θ_1	Driver angular displacement
θ_2	Driven angular displacement
b	Backlash
λ	Linear dynamic transmission error along the line of action
v	Poisson ratio
ω_m	Fundamental mesh frequency

References

[1] Molaie, M., F.S. Samani, and H. Motahar, Nonlinear vibration of crowned gear pairs considering the effect of Hertzian contact stiffness. SN Applied Sciences, 2019. 1(5): p. 414.

[2] Samani, F.S., M. Molaie, and F. Pellicano, Nonlinear vibration of the spiral bevel gear with a novel tooth surface modification method. Meccanica, 2019. 54(7): p. 1071-1081.

[3] Özgüven, H.N. and D.R. Houser, Mathematical models used in gear dynamics—a review. Journal of sound and vibration, 1988. 121(3): p. 383-411.

[4] Guo, H., J. Zhang, and H. Yu, Dynamic modelling and parametric optimization of a full hybrid transmission. Proceedings of the Institution of Mechanical Engineers, Part K: Journal of Multi-body Dynamics, 2019. 233(1): p. 17-29.

[5] Paouris, L., et al., Inefficiency predictions in a hypoid gear pair through tribodynamics analysis. Tribology International, 2018. 119: p. 631-644.

[6] Sánchez, M.B., M. Pleguezuelos, and J.I. Pedrero, Approximate equations for the meshing stiffness and the load sharing ratio of spur gears including hertzian effects. Mechanism and Machine Theory, 2017. 109: p. 231-249.

[7] Ma, H., et al., An improved analytical method for mesh stiffness calculation of spur gears with tip relief. Mechanism and Machine Theory, 2016. 98: p. 64-80.

[8] Kiekbusch, T., et al., Calculation of the combined torsional mesh stiffness of spur gears with two-and three-dimensional parametrical FE models. Strojniški vestnik-Journal of Mechanical Engineering, 2011. 57(11): p. 810-818.

[9] Tang, J.-y., et al., Effect of static transmission error on dynamic responses of spiral bevel gears. Journal of Central South University, 2013. 20(3): p. 640-647.

[10] Su, X., M.M. Tomovic, and D. Zhu, Diagnosis of gradual faults in high-speed gear pairs using machine learning. Journal of the Brazilian Society of Mechanical Sciences and Engineering, 2019. 41(4): p. 1-11.

[11] Peng, S., et al., New determination to loaded transmission error of the spiral bevel gear considering multiple elastic deformation evaluations under different bearing supports. Mechanism and Machine Theory, 2019. 137: p. 37-52.

[12] Wang, Q., et al., An analytical-finite-element method for calculating mesh stiffness of spur gear pairs with complicated foundation and crack. Engineering Failure Analysis, 2018. 94: p. 339-353.

[13] Simon, V.V. Loaded tooth contact analysis and stresses in spiral bevel gears. in International Design Engineering Technical Conferences and Computers and Information in Engineering Conference. 2009.

[14] Qu, W., H. Ding, and J. Tang, An innovative semi-analytical determination approach to numerical loaded tooth contact analysis (NLTCA) for spiral bevel and hypoid gears. Advances in Engineering Software, 2020. 149: p. 102892.

[15] Simon, V., Load distribution in hypoid gears. J. Mech. Des., 2000. 122(4): p. 529-535.

[16] Motahar, H., F.S. Samani, and M. Molaie, Nonlinear vibration of the bevel gear with teeth profile modification. Nonlinear Dynamics, 2016. 83(4): p. 1875-1884.

[17] Faggioni, M., et al., Dynamic optimization of spur gears. Mechanism and machine theory, 2011. 46(4): p. 544-557.

[18] Bibel, G.D., K. Tiku, and A. Kumar, Prediction of Contact Path and Load Sharing in Spiral Bevel Gears. 1994, NORTH DAKOTA UNIV GRAND FORKS.

[19] Yinong, L., L. Guiyan, and Z. Ling, Influence of asymmetric mesh stiffness on dynamics of spiral bevel gear transmission system. Mathematical Problems in Engineering, 2010. 2010.

[20] Chang-Jian, C.-W., Nonlinear dynamic analysis for bevel-gear system under nonlinear suspension-bifurcation and chaos. Applied Mathematical Modelling, 2011. 35(7): p. 3225-3237.

[21] Kahraman, A., J. Lim, and H. Ding. A dynamic model of a spur gear pair with friction. in 12th IFToMM World Congress. 2007.

[22] Liu, G. and R.G. Parker, Nonlinear dynamics of idler gear systems. Nonlinear Dynamics, 2008. 53(4): p. 345-367.

[23] Bonori, G., Static and dynamic modeling of gear transmission error. 2006, Ph. D. Thesis, University of Modena and Reggio Emilia.

[24] Liu, G., Parker, R. G, Nonlinear dynamics of idler gear systems. Nonlinear Dyn. 53.4, 345-367 (2008)

by Luciano Perinel[1], Alessio Cherini[1], Irene Gallici[1], Gianluca Parma[2]
1. Wärtsilä Italy - 2. EnginSoft

Large bore engine lubrication system: oil flow and pressure analysis using moving particle simulation

Lubrication is critical to the efficiency and longevity of the moving parts of an engine, particularly large internal combustion engines. By definition, a lubrication system is designed to deliver a stable, clean film of oil at the correct temperature and with the correct flow. It must prevent direct contact between the moving parts; reduce friction; reduce wear; cool, seal and clean; absorb shocks, and reduce noise. All of these functions combined contribute to the durability of components and systems, and to the overall operation of the engine.

Predicting and simulating the effectiveness of engine lubrication is particularly challenging, both with respect to oil splash in the sump and forced flow in the oil circulation system. With regard to the latter, a computational fluid dynamics (CFD) model of the oil channels must allow for the inertial effect resulting from the complex motion of the engine parts, and must simultaneously be able to simulate the transient nature of the flow at very different spatial scales. In a large combustion engine with a meter-long crankshaft, the flow within the bearings and leakage through small gaps, strongly affect the oil flow and pressure behavior.

In this study, the focus was on the oil supply system for the big-end-bearings of an 18-cylinder engine, which is one of the largest four-stroke gas engines in existence, ideal for base load applications.

Wärtsilä and EnginSoft created a moving-particle simulation model, a meshless method of solving Navier-Stokes equations, which allows complex geometries with moving parts to be simulated. The model of the Wärtsilä engine included all relevant moving parts, such as crankshaft, bearings, connecting rod, pistons, and their motion. Modelling and simulating the engine using finite-volume CFD techniques would be impractical due to the geometric complexity of the oil system, and especially due to the motion of the engine parts, which would make it impractical to manage the mesh movement. By simulating the flow through the channels, the moving particle simulation model allowed the transient pressure behavior to be calculated in crucial areas. Comparison of two bearing configurations revealed differences in pressure stability, spikes and low-pressure values that could potentially lead to cavitation problems. The results of the comparative analysis are presented and explained, along with accompanying illustrations.

In this article, the forced lubrication system of an 18-cylinder engine is studied by means of a fluid dynamic model of the lubrication channels. Particular attention is paid to the pressure trend and behavior in the oil channels and in the vicinity of the big-end bearing (BEB). The purpose of the study is to evaluate the effect of a change in the bearing design on the surrounding pressure field.

Due to the nature of the system, a traditional finite volume CFD approach would be unfeasible due to the many moving parts and the complexity of their motion. Therefore, a meshless CFD approach based on the moving particle simulation (MPS) method is used.

Moving particle simulation (MPS) method

The moving particle simulation (MPS) method, originally called moving particle semi-implicit method, was conceived by Prof. Koshizuka of Tokyo University in 1996 [1]. It is a meshless method for resolving fluid motion by solving Navier-Stokes equations in incompressible conditions. It discretizes the fluid domain using particle elements, and each particle becomes a computational node carrying information about position, velocity, temperature, and all variables of interest. Since the core of the computation is the particles, the Navier-Stokes equations are written in a Lagrangian framework, in contrast to traditional mesh-based methods, which use the Eulerian approach. In the Lagrangian approach, particles are tracked and followed during their motion, whereas in the Eulerian approach the viewpoint is fixed to the computational grid (see Fig. 1).

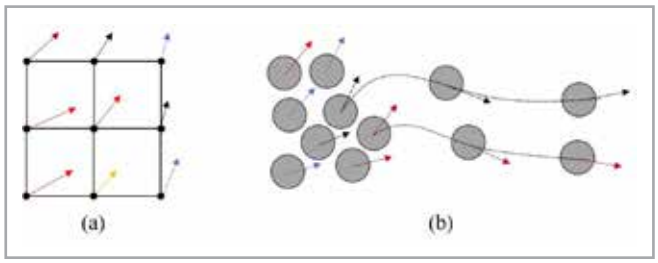

Fig. 1 - Difference between the Eulerian approach (a) and the Lagrangian approach (b).

Its meshless nature makes the MPS approach highly flexible and well-suited to applications involving moving parts where mesh generation and deformation using a mesh-based method can be exceedingly difficult.

In this work, the Particleworks MPS solver developed by Prometech Software Inc. is used to analyze the oil flow in the engine lubrication system.

Model description and boundary conditions

The complete engine consists of 18 pistons with connecting rods, mounted on a crankshaft. The crankshaft is supported by ten main bearings (MB) with their respective main bearing caps; internal channels running through the engine components distribute the lubricating oil to all the bearings (see Fig. 2). The bearings are of the hydrodynamic type. The crankshaft rotates at a constant

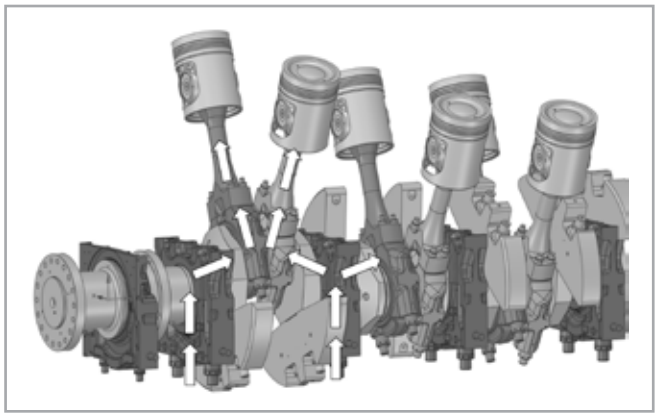

Fig. 2 - Diagram of the engine and oil flow path.

speed, converting the reciprocating motion of the pistons into rotary movement.

Oil enters the system through the main bearing caps, lifting the main bearings; then it is delivered to the big-end bearings (BEB) via the crankshaft oil channels. Finally, it reaches the small-end bearings (SEB) through the connecting rod oil channels. Figs. 2 and 3 show the oil path and diagram of the internal lubrication system.

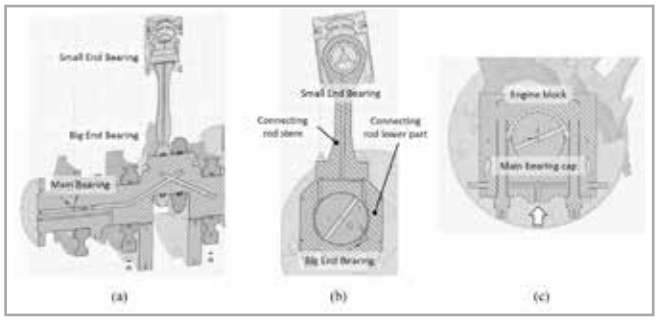

Fig. 3 - Internal lubrication channels. Crankshaft (a), connecting rod (b) main bearing cap, main bearing channel and engine block (c).

Fig. 4 shows a cross-section of the crankpin and its oil channel, the lower part and stem of the connecting rod, and the BEB that is interposed between.

The lubricating oil from the crankpin oil channel reaches the SEB by flowing through the clearance between the pin and BEB, its groove, and then the oil channels inside the connecting rod. The rotation of the crankshaft, together with the alternating movement

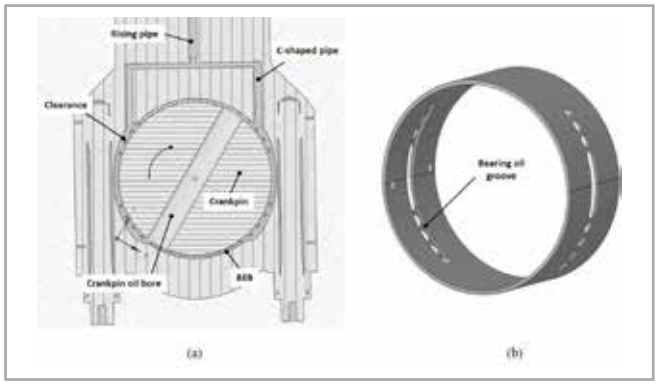

Fig. 4 - (a) Section of crankpin, BEB, connecting rod and C-shaped pipe. (b) BEB geometry.

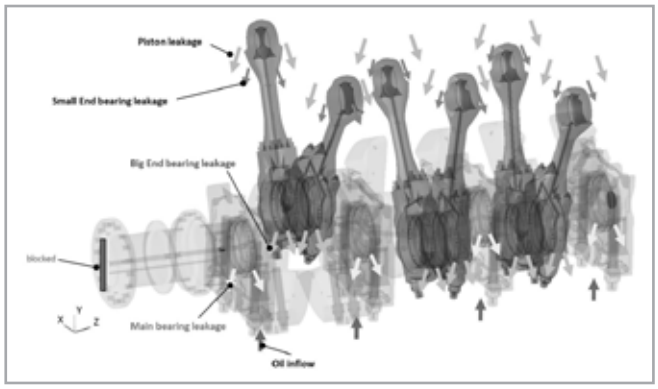

Fig. 5 - Distribution of inflow and outflow boundary conditions.

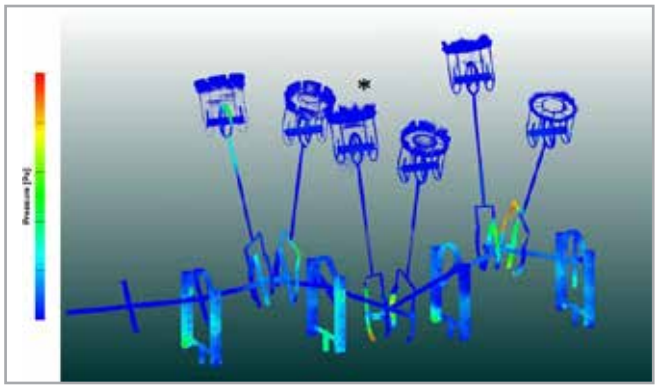

Fig. 6 - Pressure distribution in the simulated domain.

of the connecting rod and the engine oil pump, ensure sufficient oil flow through the channels that feed all the bearings. The moving particle simulation only takes into account the first three turns of the crank, six pistons, and four main bearing caps. An inflow with the prescribed volumetric flow rate is applied to the base of each main bearing caps, and outflow rate conditions are applied in the bearing regions to simulate oil leakages that will then be collected in the oil sump. Fig. 5 summarizes the oil sources and leaks.

Analysis conditions

The same simulation method is applied to two different BEB geometries. The crankshaft rotation speed, inlet and outflow rates are kept constant throughout the simulation.

The particle size and the integration time step are the two main parameters that play a key role in the simulation. The particle size must be small enough to address the smallest gap of interest in the geometry. A 2mm particle size is chosen in the MPS model to capture the smallest passages in the channels and grooves. The film of lubricating oil between the bearings and crankshaft pins is not the scope of the current work. Particle size affects solution accuracy and simulation time (smaller particles increase solution accuracy and computation time).

The second key parameter is the integration time step, which must be set to ensure the numerical stability of the simulation. Its value depends on the maximum velocity in the system, and simulation of the two geometries was in the range of 8E-6s. An adaptive time-step is used to allow the solver to adjust according to the solution.

An implicit pressure solver is used to improve the accuracy of the pressure field calculation. The simulation was performed on two CPU cores (Intel Xeon Silver 4114) along with an NVIDIA V100 GPU. The benefit of using a graphic processing unit (GPU) is the remarkably high performance-to-cost ratio due to the large number of computing cores in the GPU card. For example, an NVIDIA V100 has 5120 CUDA cores and is capable of 15.7 TFLOPS in single precision, with performance comparable to 48-64 CPU cores.

MPS Results

The goal of the activity is to compare two BEB designs, with attention to the pressure distribution in the oil channels and the pressure behavior in the vicinity of the bearings in question. During the transient simulation, the pressure values in different areas of the channels are monitored, focusing on the two central connecting rods to avoid boundary effects.

An overview view of the oil flow in the full domain shows that the highest pressure values are found in the lower part of the connecting rod (see Fig. 6). Due to the motion of the power system parts, pressure waves generated in the system are periodic and are continuously reflected from the thrust side and the anti-thrust side of the BEB.

Fig. 7 shows the evolution of the pressure field around the BEB of the central pair of pistons (marked with an asterisk in Fig. 6). The pressure field is smooth and the pressure waves are well captured by the solver. The left corner of the C-shaped channel is reached periodically by a pressure peak (red values in frames 4 and 6), which is followed by low pressure values.

Low-pressure values are predicted near the corners of the C-shaped tube and other areas of the BEB. This may result in

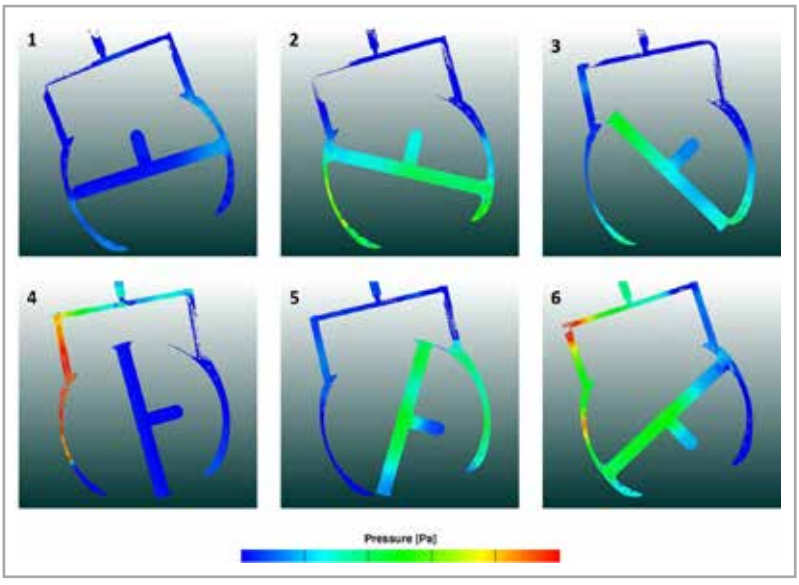

Fig. 7 - Pressure evolution in the connecting rod oil channels.

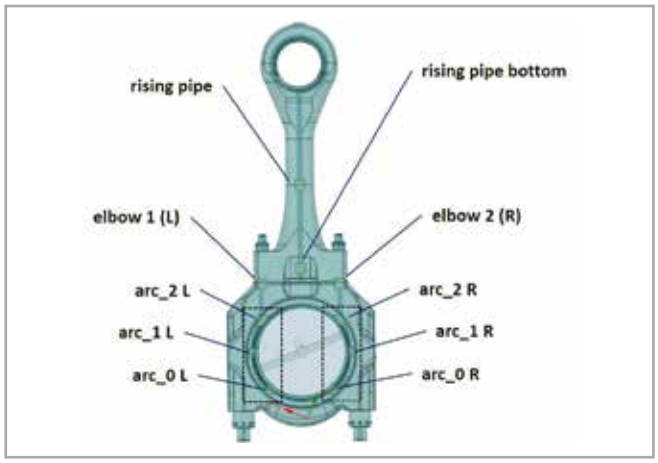

Fig. 8 - Locations of control regions used to monitor pressure within the lubrication channel.

an improper lubrication. The predicted pressure trends were confirmed by experimental investigations.

To measure the magnitude of the pressure shocks, ten control regions are defined in the connecting rod channels: three on the thrust side of the connecting rod; three on the anti-thrust side of the connecting rod; one in each corner of the C-shaped tube; and two in the rising pipe of the connecting rod. Fig. 8 highlights the locations of these control regions.

Along with the pressure measurement, quantitative indices are defined to compare the different BEB design configurations. Specifically, the following quantities are monitored: average pressure and standard deviation, peak pressure, time at low pressure, and pressure derivative at peak occurrence.

A high average pressure with a low standard deviation is desirable; it means that the flow is uniform and the risk of inadequate lubrication is low. Pressure peaks, time at low pressure, and pressure derivative should be as low as possible to ensure longevity of the engine components.

Fig. 9 shows an example of the pressure signal measured in the control regions described above. These signals reveal spikes, and some control regions have long intervals at extremely low pressure followed by sudden spikes. This behavior can be observed in particular in control regions arc0_L, arc1_L, and elbow_1(L).

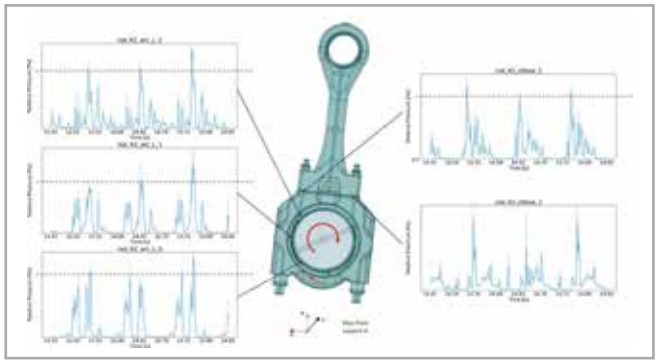

Fig. 9 - Example of pressure signals measured in the control regions. The horizontal dashed line corresponds to the average peak values.

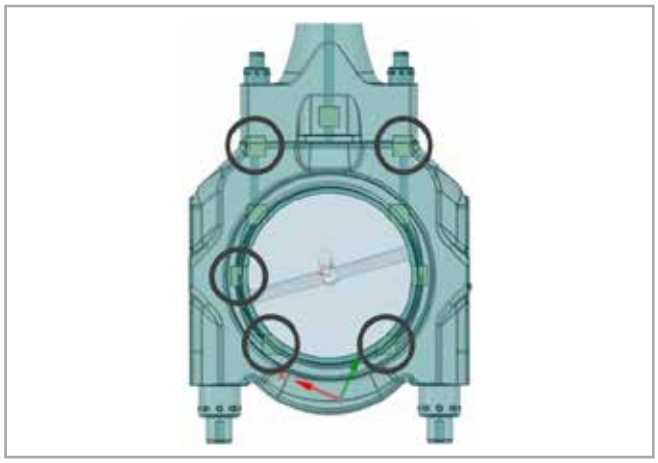

Fig. 10 - The most critical regions in the big-end bearing.

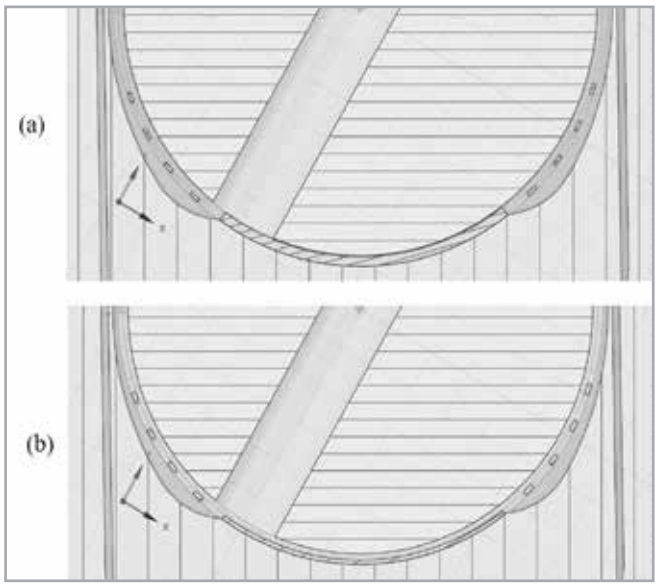

Fig. 11 - Detail of the lower passage joining the two sides of the bearing. Original bearing (a) compared to the improved design (b).

A thorough analysis of the previous indices over the entire domain shows that the most critical regions are the lower regions of the bearing (arc0_L, arc0_R), the left middle section (arc1_L), and both corners of the C-shaped channel (Fig. 10).

These regions all feature long periods at low pressure followed by steep spikes with high pressure derivatives.

The locations of the most critical regions suggest a potential improvement in the bearing design. From the simulation data, it is clear that the new bearing design (see Fig. 11b) has two substantial advantages: it reduces pressure spikes and provides pressure continuity on both sides of the bearing.

Comparing the simulation results for the two configurations shows an overall improvement in all quality indices. The oil has a higher average pressure overall and a lower standard deviation; pressure peaks and pressure derivatives are reduced by 20-30%. As a result, the internal channels are more filled and the oil flow is smoother.

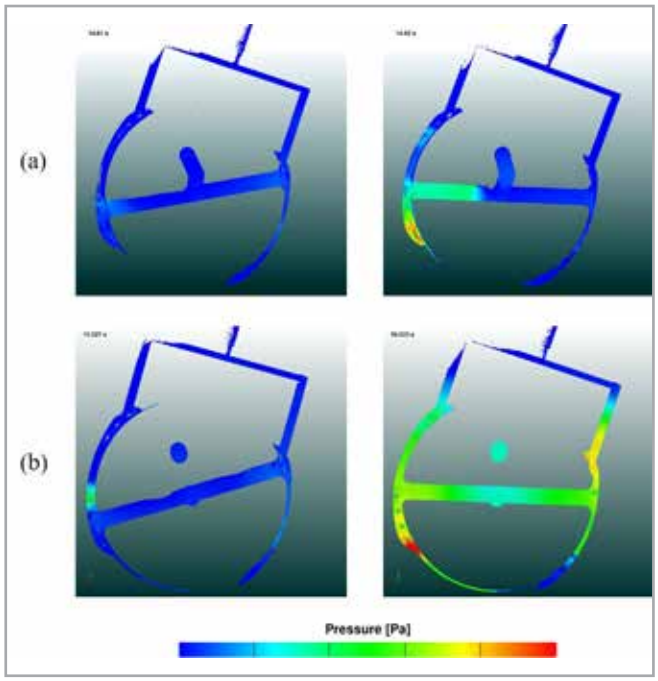

Fig. 12 - Pressure comparison in big-end bearing. Row (a) refers to the original bearing, row (b) to the new design.

Fig. 12 shows the comparison of pressure distribution between the original (a) and improved (b) designs. The new bearing design helps balance the pressure in the system, which is more uniform overall than the original design.

Figs. 13 and 14 show the comparison of the pressure spikes and derivative signals measured for the two configurations. The grey lines represent the peak values of the original design, while the black lines refer to the improved design.

The blue and orange signal lines refer to the new geometry. Most regions depicted in the images show good improvement (lower pressure peaks and lower pressure derivatives).

Conclusions

The lubrication system of a large bore engine was analyzed using Particleworks moving particle simulation (MPS) software. MPS is a meshless method of solving the Navier-Stokes equations which easily accommodates complex moving geometries, such as crankshafts, connecting rods, and pistons.

The simulation method was applied to two different big-end bearing geometries. The pressure behavior for both designs was compared in terms of pressure peaks, average values, and minimum values. The first big-end bearing design showed higher pressure peaks, higher pressure derivatives, and longer periods at low pressure. This combination is associated with higher pressure shocks and potentially inadequate lubrication.

The modified big-end bearing design allows pressure waves to propagate between the thrust and anti-thrust sides of the connecting rod, helps reduce spikes and stabilizes overall oil pressure behavior.
The predicted pressure trends and behavior of both designs were confirmed by experimental investigations.

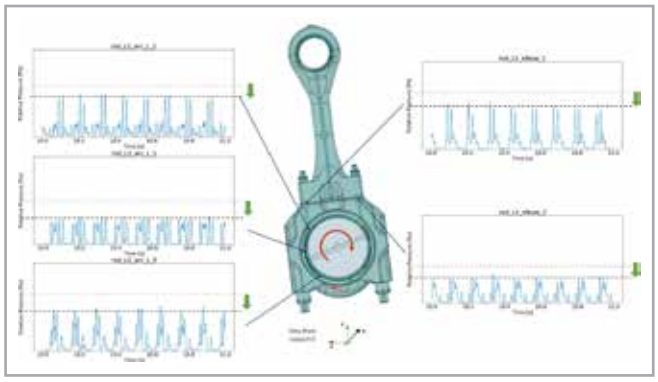

Fig. 13 - Pressure measurement comparison between the original and improved designs. The black dashed line represents the peak values of the improved design; the grey line indicates the peak values of the original design. The blue signal line is for the improved BEB configuration.

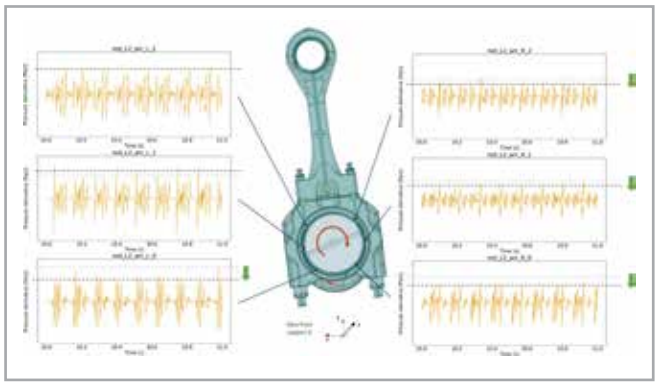

Fig. 14 - Pressure derivative comparison between the original and improved designs. The black dashed line represents the derivative values of the improved design; the pink line indicates the derivative values of the original design. The orange signal line refers to the improved BEB configuration.

References

[1] Koshizuka, S., Oka, Y. (1996). Moving-particle semi-implicit method for fragmentation of incompressible fluid. Nuclear science and engineering, 123. Pag. 421-434

For more information:
Gianluca Parma - EnginSoft
g.parma@enginsoft.com

Validation of a model of a methanol fuel supply system for a two-stroke dual-fuel marine diesel engine

Courtesy of Alfa Laval

by Nicoletta Spazzadeschi[1], Danish Taufiq[1], Davide Rossin[1], Erik Mazzoleni[2], Marco Gatti[2]
1. Alfa Laval - 2. EnginSoft

Methanol is one of the strategic fuels to achieve the International Maritime Organization's ambitious decarbonization goals over the next decades. As an expert in the marine sector, Alfa Laval is a leader in designing and supplying methanol fuel supply systems for marine diesel engines. In this study, Alfa Laval and EnginSoft present the results of a simulation of the methanol fuel supply system currently used on a methanol carrier. The scope of the study was to develop and validate a 1D computation fluid dynamics (CFD) model to reproduce the existing dataset collected from an actual system, in both steady-state and transient conditions, and its interaction with the upstream and downstream parts of the overall fuel line, from tank to engine. The validated model will enable Alfa Laval to simulate the system's behavior under different conditions and to remotely support customers, forming the basis of a new digital approach to product development.

The International Maritime Organization's targets for decarbonization

The shipping sector plays a key role in the global economy, transporting people and goods worldwide. Carrying around 80% of the world's trade volume and 70% of its value, marine vessels are estimated to account for 2.9% of worldwide carbon dioxide emissions [1].

The International Maritime Organization (IMO) has adopted a strategy to progressively reduce the marine industry's greenhouse gas (GHG) emissions, in line with the Paris Agreement on climate change in which in 2015 adhering countries agreed to a commitment to limit the greenhouse effect.

The IMO strategy to progressively reduce the GHGs from shipping, adopted by the Marine Environment Protection Committee (MEPC) in 2018 [2], to progressively reduce the GHG from shipping includes the objectives of:

- reducing CO_2 emissions per transport work, as an average across international shipping by at least 40% by 2030, compared to the levels of 2008
- reducing total annual GHG emissions by at least 50% by 2050, compared to 2008.

Methanol's role as a decarbonization fuel

Methanol (CH_3OH) is a chemical used in thousands of products. While it can be produced from different sources, it is traditionally made from fossil feedstocks via syngas. Renewable methanol, instead, is produced either from biomass (bio-methanol) or from captured CO_2 and H_2 produced from water by electrolysis via renewable electricity (e-methanol). Compared to other fuels, methanol can reduce CO_2 emissions by 65% to 95%, depending on the feedstock [3]. The use of renewable methanol as a fuel is therefore strategic for those sectors, including shipping, which are transitioning to decarbonization. In addition, its combustion is sulfur oxide-free and generates low nitrogen oxides emissions compared to other conventional fossil fuels [3].

Methanol in marine diesel engines

The main marine engine manufacturers have developed technologies to burn methanol in diesel engines [4].

With its expertise in marine fuel handling and conditioning, Alfa Laval has contributed to methanol technology development from the very beginning, working on the first methanol fuel

supply system prototype. Today, Alfa Laval has a strong experience in designing and supplying methanol fuel supply systems, with 12 systems currently installed and operating onboard methanol carriers, with a total of 100,000 hours of operation, plus several other systems in the final stages of development.

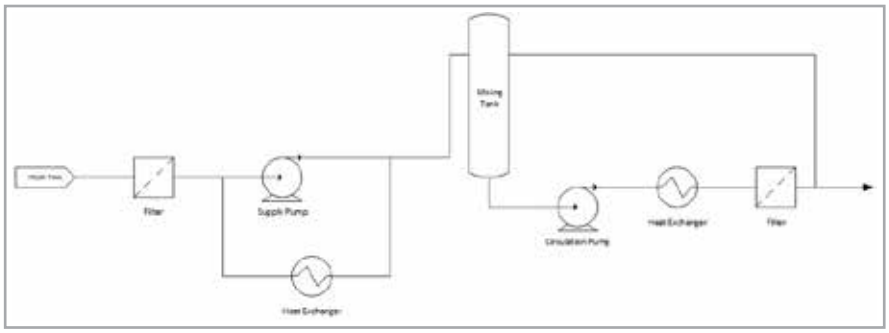

Fig. 1 – Simplified flowchart of the methanol line in the methanol fuel supply system.

The use of methanol as a fuel for the first container vessel is expected by 2023. This is a step towards sustainable zero-emission vessels, in line with the IMO's decarbonization strategy. With its commitment to sustainability, Alfa Laval is fully involved in the development of technology to support methanol and other alternative fuels [5].

Simulation's role in product development at Alfa Laval

In addition to traditional and consolidated engineering practices, Alfa Laval is adopting advanced engineering tools to support the product development process, with the aims of ensuring cost-effective design and increasing the efficiency of methanol fuel supply systems.

One of the first modeling and simulation activities was dedicated to the methanol fuel supply system because of its strategic role in Alfa Laval's portfolio, which is expected to increase in the near future. The objective is to develop virtual models of methanol fuel supply systems and validate them through field data retrieved from operating systems. Once validated, the models can be used as the basis for analyzing the behavior of the process under non-standard conditions, and for providing remote customer support.

Methodology

In this study, Alfa Laval worked with EnginSoft to develop a fluid dynamic model of an existing methanol fuel supply system. This model will generate numerous benefits, such as simplifying the understanding of real system behavior and providing a tool for making better engineering decisions.

Software

The Flownex simulation environment was used to model the system. Flownex is a one-dimensional computational fluid dynamic (CFD) modeling software. The 1D CFD modeling approach is suitable for system simulations and enables the physical behavior of the entire module to be modeled, studied and analyzed, taking into account different operating conditions.

Process description

The methanol fuel supply system modeled in this study is a system designed to feed a two-stroke, dual-fuel marine diesel engine with methanol. It consists of a two-stage pressure module with an intermediate mixing tank (see Fig. 1), designed to pump fuel from the storage tank to the engine at the operating conditions required by the engine, under varying loads. The system also includes heat exchangers, filters, and valves to meet engine requirements for temperature and degree of filtration in a fully automatic mode. The methanol fuel supply system is also equipped with an ethylene-glycol/water solution circuit to provide heating/cooling media for the heat exchangers in methanol operation, preventing contamination of any of the ship's utilities in the event of an internal leakage in the heat exchangers.

Model basis

The main parameters studied were pressures, temperatures, flow rates, and valve opening in both the low-pressure and high-pressure recirculation loops.

Methanol pumps

Both the supply pump (LP) and the circulation pump (HP) were modeled using the "Fan or Pump" component available in the Flownex library. The flow-prevalence curves, the net positive suction head required (NPSHr) curves, and the efficiencies were taken from the datasheets of the pumps installed in the system. This permitted the pumps to be simulated in terms of performance, power consumption, heat transferred to the fluid, and cavitation risk.

Filters

The filters were modeled as pressure drop-generating components, since this is the main effect related to the fluid dynamics of the model. In fact, fuel purity, which is an important parameter in the actual supply system, was not considered as a parameter in the present study.

Therefore, the filters were modeled using the "User specified pressure drop" component. The flow-to-pressure drop curves were obtained from the datasheets of the filters actually installed in the methanol fuel supply system.

Heat exchangers

The modeled system includes two heat exchangers in methanol operation, one in the low-pressure section (LP HE), and one in the high-pressure section (HP HE). The model was implemented and validated against the system's data.

Initially, the "heat exchanger primary"component was used. Four thermal balances at different liquid-phase methanol (MeOH) mass flows and inlet temperatures were used as reference cases to calculate the required heat transfer rate as input to the component.

The pressure drop values were used to interpolate the factors Ck, α, and β used in the following equation:

$$\Delta p = C_k \rho^{\beta} Q^{\alpha}$$

Subsequently, to obtain more accurate results, the "Shell Tube Heat Exchanger" component available in the Flownex library was used to model a more accurate geometry[1]. All data needed as input to the model (geometry, fouling factor, materials, etc.) was obtained either from the available datasheet or from Alfa Laval's in-house experience.

Mixing tank

he mixing tank was initially modeled by splitting the model of the liquid portion and the model of the gas portion, and using the "Open Container" and "Air Volume" components available in Flownex Library, respectively, and associating them via a script (see Fig. 2). By doing so, any changes in level during dynamic load variations, or at start-up and shutdown, were automatically reflected in a corresponding change in the available vapor space above the liquid level, and thus in pressure. Later, the "Accumulator" component was used, which simplified the system while obtaining the same results[1].

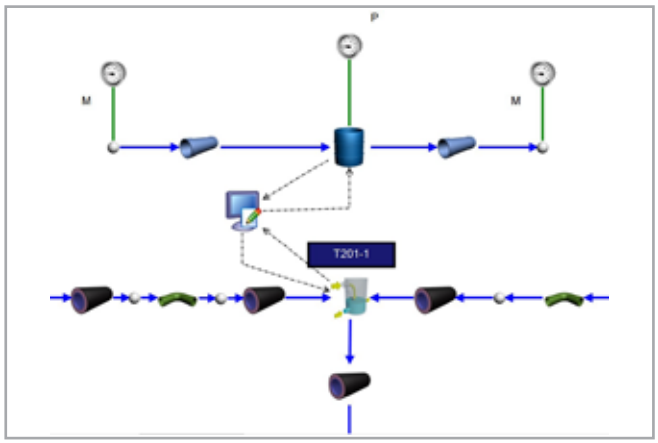

Fig. 2 – Model of the mixing tank.

Other components

All pipes and bends were modeled using the "Insulated pipe" and "Bend" components according to the actual 3D geometry of the methanol fuel supply system. The on/off valves were modeled using the "Basic Valve" component, with the actual valve flow coefficient (Cv) of the valves used in the system. The same approach was taken for the control valves, modeled using the "Ansi control valve" with the actual valve Cv and characteristics. The flow meter, similarly to the filters, was modeled with a "user specified pressure drop".

Glycol-water circuit

The glycol-water circuit consists of a pump that circulates an ethylene glycol-water (GW) solution to a plate heat exchanger to achieve the desired GW temperature set point. The GW is circulated to the two heat exchangers in methanol operation and then back to an expansion tank. The plate heat exchanger maintains the GW temperature by exchanging heat with low temperature water (LT water). To obtain accurate results and make use of the available data, the GW system was also modeled.

Process control parameters

In order to deliver methanol at the operating conditions required by the engine at varying engine loads, the methanol fuel supply system is operated under pressure control at two points in the process (low-pressure and high-pressure sections), and under temperature control at the outlet battery limit. The control logic that acts on the methanol fuel supply system is based on software developed in-house by Alfa Laval, which enables fully automated system operation.

At this stage of the model development, the pressure and temperature controls were modeled using the proportional, integral, derivative (PID) control available in Flownex. The PID parameters were tuned to reproduce the trends in some actual pressure and temperature datasets.

Validation of the model

To validate the developed model, several datasets from methanol fuel supply systems in operation on vessels were analyzed in depth and used as references. The parameters used as inputs to the model, as well as the resulting outputs, are listed in Table 1.

The boundary conditions applied to the model are the methanol temperatures and pressures at the module inlet and the corresponding flow rate at the module outlet. For LT water, the flow rate, pressure, and temperature conditions provided during

Parameters
LP loop
Methanol pressure at module inlet
Pressure at mixing tank
Methanol temperature at module inlet
Methanol flowrate (before the mixing tank)
LP recirculation valve opening
HP loop
Methanol pressure at module outlet
Methanol temperature at module outlet
HP recirculation valve opening
GW circuit
LT water inlet temperature
GW temperature to MeOH/GW HE
GW circuit pressure at pump discharge
LT water flowrate
GW HE flow control valve

Table 1: Parameters used to validate the model divided into three blocks: the LP loop (from the module inlet to the mixing tank), the HP loop (from the mixing tank to the module outlet) and the GW circuit.

[1]The validation results presented in the "Results" section refer to the model without this improvement.

the module design were used as boundary conditions. The GW flow rate is directly dependent on the flow-head curve of the GW pump, and on the GW pressure. Since the latter had already been considered in Table 1, and the characteristic curve was taken from the pump's datasheet, the GW flowrate was not further validated.

The data available for the methanol flow rate refers to a flowmeter placed at the inlet of the mixing tank, i.e. between sections LP and HP. Therefore, this dataset can be used as-is as a boundary condition for the model only in steady-state conditions, assuming the same flowrate at the system outlet. By contrast, during transient phenomena characterized by flow variations over time, this set of measured flowrates cannot be used directly as a boundary condition.

Transient state simulation/test

Outlet battery limit's on/off valve

The validated model was initially used to simulate the transient phenomena that occur:

- at a sudden opening of the on/off valve at the outlet battery limit when the fuel supply system is in full recycle mode (startup condition and filling line to the engine);
- at a sudden closing of the on/off valve at the outlet battery limit when the fuel supply system is in operation (in case of engine switch to diesel oil).

The PID parameters of the model were tuned to reproduce the experimental pressure peaks generated during the opening and closing of the outlet battery limit valve.

Cyclic flow variations

The model was used to simulate a cyclic mass flow trend observed in a set of experimental data measured during a sea trial to evaluate the system's functionality assuming extreme sea conditions. Based on the key engine requirements, the methanol fuel supply system must be designed and controlled to withstand load variations without exceeding ±0.5 bar at the module outlet.

Fig. 3 represents a dataset taken over a 1,000-second time period. This dataset accurately represents very severe conditions under which the system should maintain its pressure variations within the required limits. These values were rounded off to the following sinusoidal function[2] for input into the simulation software:

$$mi = 1250 \sin\left(\frac{2\pi}{25} t\right) + 1250$$

where ±1,250 kg/h is the amplitude of change in flow with an average period of 25 seconds and a mean value of 1,250 kg/h, as inferred from the trend shown in Fig. 3.

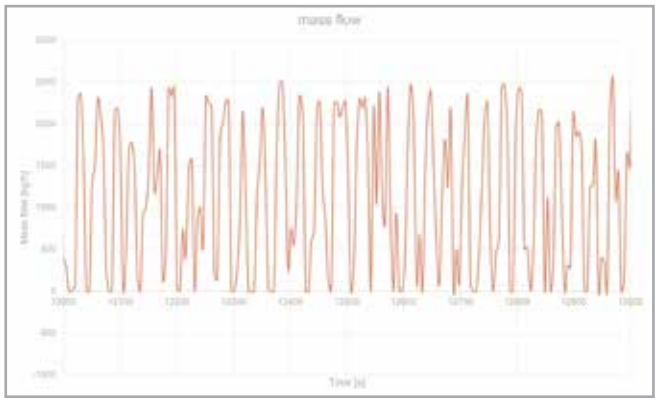

Fig. 3 – Experimental mass flow.

For the transient simulations, the coefficients of the PID controllers controlling the pressure were specified according to the control logic being used in the actual system. The pressure variation at the LP/HP interstage (before the mixing tank) and at the module outlet were considered as parameters for validation.

Results and discussion

Validation results

Table 2 shows the values of the input parameters to the model as well as the results obtained from the simulation, and the corresponding plant values. The validation refers to a steady-state dataset. A maximum deviation of 5% of the results was considered acceptable for the methanol lines, while a larger tolerance was allowed for the auxiliary lines.

Parameters	Simulation	Plant	Deviation [%]
LP loop			
Module inlet pressure [barg]	-0.02	N/A[3]	
Pressure set point before mixing tank [barg]	3.99	3.94	1.3
Module inlet temperature [°C]	23.0	23.0	0.0
Methanol consumption [kg/h]	1820	1823[4]	0.2
LP recirculation valve opening [%]	94.7	92.8	2.0
HP loop			
Pressure set point at module outlet pressure [barg]	8.99	8.91	0.9
Methanol Temperature after HP HE [°C]	34.9	34.7	0.6
HP recirculation valve opening [%]	77.7	78.0	0.4
GW circuit			
GW circuit pressure (after the pump) [barg]	1.91	2.10	9.0
GW temperature before HP HE [°C]	34.9	34.9	0.0
GW HE flow control valve [%]	100.0	100.0	0.0

Table 2: Simulation and plant results.

The deviations in the LP and HP loop parameters are well below the considered threshold. Therefore, the model can be considered to be in line with the required accuracy.

In the GW loop, there is a larger discrepancy between the simulated and experimental pressure values. This is due to the presence of a manual throttling valve in the loop, an element for which no data was available at the exact opening point from the operational plant.

[2] The recent software update allows raw data to be entered directly into the simulation.
[3] Corresponds to tank atmospheric pressure, liquid static head, and loss of the interconnecting piping.
[4] Measured before the mixing tank.

Transient simulation results

Simulation of the module outlet valve opening

Fig. 4 shows the trend in methanol flow rate and the supply pressure upon the sudden opening of the on/off valve located at the outlet battery limit of the methanol fuel supply system. The two charts on the right in Fig. 4 reveal how consumption increases due to the empty pipe attached to the module outlet and the consequent pressure drop. Due to the sampling rate of the flow meter and the maximum detectable flow, the top right graph has a stepped shape. The charts on the left represent this behavior quite well, although the simulated pressure drop is less significant.

The magnitude of the simulated peak flow cannot be compared, but the trend is reliable. Overall, it can be said that the peak consumption and pressure drop following the opening of the outlet battery limit valve is well represented by the model. However, adjustments to the flowmeter sampling rate and maximum detectable flow will be further evaluated to provide a more reliable dataset.

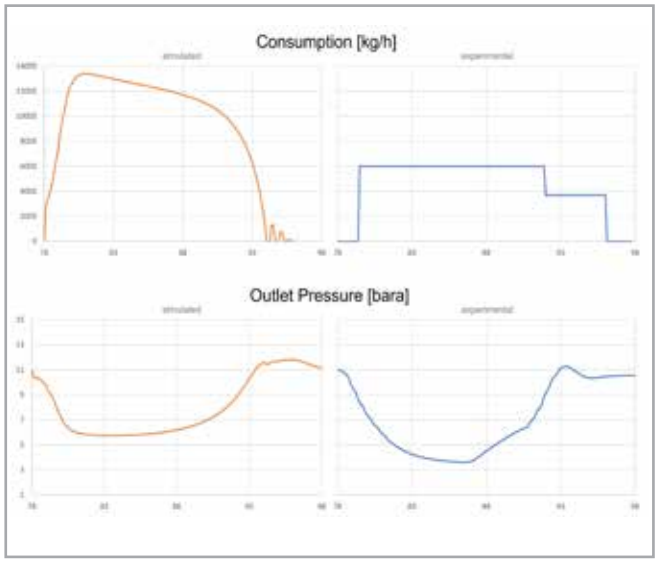

Fig. 4 – The graphs show the methanol flowrate (top) and the module outlet pressure (bottom) trends from the data acquired from the plant (right) and from the simulation (left).

The good correlation between the resulting trends and the actual behavior of the module also reveals that the model represents the real system well, while the control logic can be improved. This will be possible due to the recently added functionality that allows the actual control logic to be implemented in the software, instead of converting it into pre-built PID controllers.

Cyclic consumption simulation

As mentioned in the section on cyclic flow variations, the approximation of the input mass flow data only allows for the study of the resulting pressure variation and its magnitude. Fig. 5 shows the experimental pressure trend at the two control points. At the module outlet, the pressure variation is ±0.1, while before the mixing tank the pressure variation is ±0.05 bar. Fig. 5a shows some pressure spikes that cannot be reproduced as input using the function approximated in the section on cyclic flow variations.

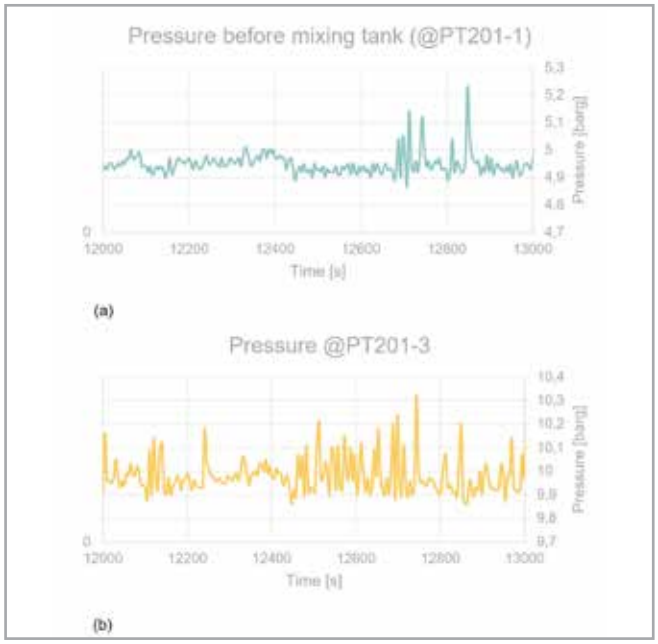

Fig. 5 – Experimental pressure variations at checkpoints.

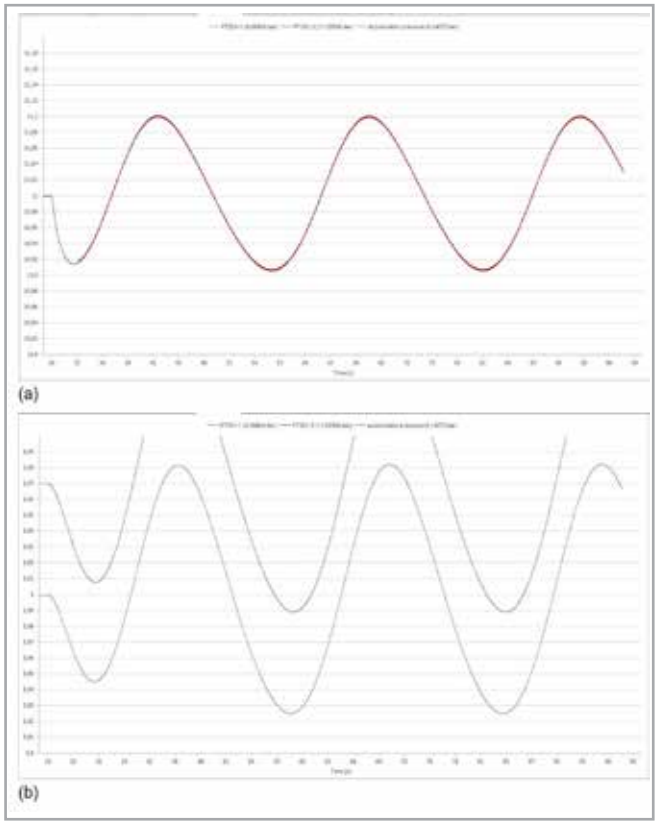

Fig. 6 – Simulated pressure trends.

Fig. 6 represents the simulated trends over a shorter time frame. The outlet pressure (Fig. 6a) has a variation of ±0.1 barg, while the interstage pressure (Fig. 6b) has a pressure variation of ±0.08 barg, slightly higher than actual pressure.

The simulation of the severe cyclic flow variation reflects the experimental pressure variation and complies with the engine requirements. The acceptable accuracy obtained allows this model to be used to simulate other conditions and understand if the resulting pressure variations are within acceptable ranges.

About Alfa Laval

Alfa Laval is active in the areas of Energy, Marine, and Food & Water, offering its expertise, products, and service to a wide range of industries in some 100 countries. The company is committed to optimizing processes, creating responsible growth, and driving progress – always going the extra mile to support customers in achieving their business goals and sustainability targets.

Alfa Laval's innovative technologies are dedicated to purifying, refining, and reusing materials, promoting more responsible use of natural resources. They contribute to improved energy efficiency and heat recovery, better water treatment, and reduced emissions. Thereby, Alfa Laval is not only accelerating success for its customers, but also for people and the planet. Making the world better, every day. It's all about Advancing better™.

Alfa Laval has 16,700 employees. Annual sales in 2020 were SEK 41.5 billion (approx. EUR 4 billion). The company is listed on Nasdaq OMX.

Conclusions

Alfa Laval is adopting new methods of approaching fuel supply system design and development based on data analysis and system modeling.
In this paper, the model-based approach was applied to a fuel supply system processing methanol, which is a key step towards sustainable shipping.

The results of the modeling activities presented show a reliable degree of prediction of the actual system's behavior, fit for purpose, at a degree of approximation that was judged to be acceptable. Further optimization to the same system that can be performed starting from this study includes:

- Implementing Alfa Laval's automation software in the model, instead of using standard simple PID logic;
- Simulating other transient states by directly inputting experimental data without having to define a function to describe the data trend;
- Simulation based on the experimental data related to the configuration of the methanol fuel supply system with the flowmeter located at outlet battery limit;
- Simulation of the system behavior under different boundary conditions.

The availability of additional data from the deployed systems would be useful to further validate the 1D CFD model in various scenarios and to support future modeling activities.

For more information:
Erik Mazzoleni - EnginSoft - e.mazzoleni@enginsoft.com
and Davide Rossin - Alfa Laval - davide.rossin@alfalaval.com

References

[1] American Bureau of Shipping (2021). Setting the Course to low carbon shipping. View of the value chain. Low Carbon Shipping Outlooks, 3.
[2] International Maritime Organization (2018). RESOLUTION MEPC.304(72) (adopted on 13 April 2018) - INITIAL IMO STRATEGY ON REDUCTION OF GHG EMISSIONS FROM SHIPS.
[3] Hobson, C., Màrquez, C. (2018). Renewable methanol report - Methanol Institute.
[4] American Bureau of Shipping (2021). Sustainability whitepaper – Methanol as marine fuel.
[5] Alfa Laval, Altamarine (2019). Innovative LPG Fuel Supply System for MAN B&W LGI-P Engines: Design Challenges and Performance Results. CIMAC 2019.


Courtesy of Alfa Laval

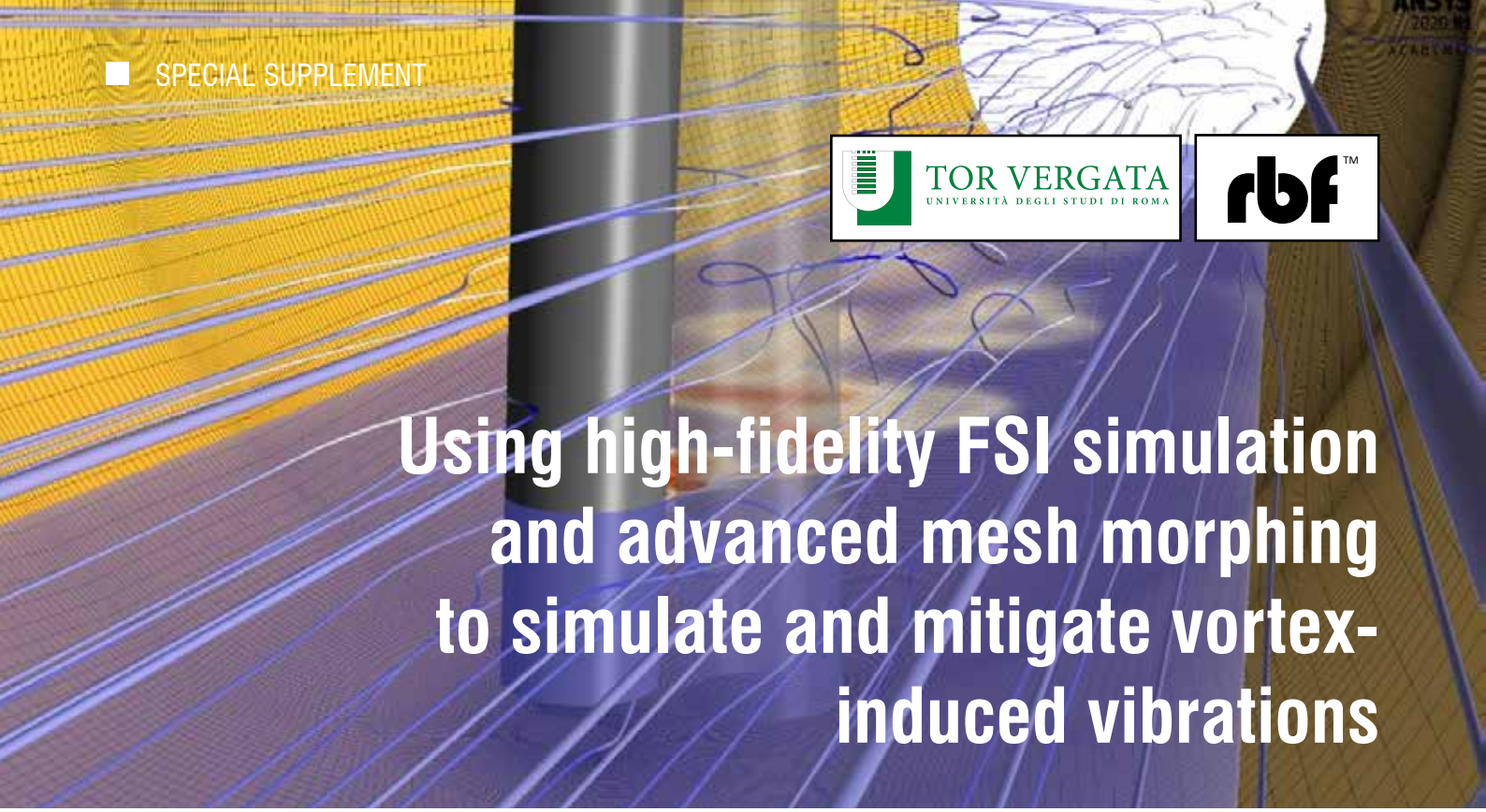

Using high-fidelity FSI simulation and advanced mesh morphing to simulate and mitigate vortex-induced vibrations

by Alessandro Felici[1], Stefano Porziani[2] and Marco Evangelos Biancolini[1]
1. University of Rome Tor Vergata - 2. RBF Morph srl

This study discusses the complex and challenging problem of controlling vortex-induced vibrations (VIV). The fluid-structure interactions (FSI) involved pose two types of problems: firstly, structural and fluid analysis skills are required and the various experts need to interact correctly for a successful outcome; secondly, accurate modelling requires state-of-the-art tools to combine the computational fluid dynamics (CFD) and the computational structural mechanics (CSM).

Advanced mesh morphing enabled by the radial basis function (RBF) is key here: it enables you to create an efficient and fast workflow for strong coupled fluid structure interaction analysis while making that workflow parametric with respect to the design, so that you ultimately have the ability to steer the design toward the desired VIV behavior.

We used structural modes embedding technique to render the fluid solution "flexible". The dynamic characteristics of the system were calculated with Ansys Mechanical for the Finite Element Analysis (FEA); these were then incorporated into Ansys Fluent to solve the fluid aspect using RBF Morph mesh morphing software. The method is demonstrated for a specific application: the design of a thermowell immersed in a water flow. The numerical results obtained were compared with experimental data and showed a satisfactory agreement, thus demonstrating that the superposition of structural modes approach, with a suitable mesh morphing configuration, is able to address unsteady FSI problems with the necessary accuracy for industrial applications.

Today there is an increasing need to develop multi-physics approaches to address complex design challenges. The numerical methods adopted must include coupled field analyses that allow the combined effects of the multiple physical phenomena acting on a given system to be evaluated. One of the most interesting multi-physics phenomena with a wide range of applications is the interaction between a fluid and a structure. This interaction can occur for several reasons: it may be the working principle of the system; it may focus on creating a lightweight design for the structure; or it may be used to refine the design.

Fluid structure interaction (FSI) plays a key role in a wide range of engineering fields, such as automotive, aerospace, marine, civil and biomedical. To numerically solve the interaction, the deformation of the computational fluid dynamics (CFD) mesh is needed to accommodate the changes in the shape of the structure. In the present work, a radial basis functions (RBF) based mesh morphing algorithm is used to change the CFD mesh according to the deformed shape of the structure. The FSI approach we propose allows the mesh to be adapted to the shape of the deformable structure by superposition of its natural modes during the course of the CFD calculation.

The underlying notion for the proposed workflow is to compute the fluid forces on the surface of the structure, along with the inertial loads at each step, as modal forces to determine the amplitude of each modal shape. By superimposing the modal shapes, the overall deformation of the structure can be obtained at each instant and can be imposed in the CFD model by morphing the CFD mesh. The method is implemented to study an industrial problem: the vortex-induced vibration of a thermowell immersed in a stream of fluid.

Thermowells are cylindrical fittings used to protect temperature sensors (such as thermometers or thermocouples) installed in industrial processes. In such a configuration, the fluid transfers heat to the wall of the thermowell which, in turn, transfers heat to the sensor. The use of a thermowell, in addition to protecting the sensor from the effects of the pressure and chemicals of the process fluid, allows the sensor to be easily replaced without emptying the tank or pipes. However, thermowells are subject to potential flow-induced vibrations generated by vortex shedding that may cause failure due to bending fatigue. Consequently, particularly in modern applications involving high-strength piping and high fluid velocity, the dynamics of the system must be carefully evaluated to prepare ad-hoc countermeasures, such as twisted square thermowells, to limit this phenomenon. A numerical method capable of reliably reproducing the fluid-structural coupling is therefore needed to rapidly evaluate different designs and reduce the time to market of new products.

Modal FSI implementation

Beginning with the undeformed configuration, the flexible components of the system are modelled and studied using a structural modal analysis in order to extract a suitable set of eigenvalues and eigenvectors.

The obtained modes are used to generate an RBF solution for each shape. At this stage, the far-field conditions and rigid surfaces must be constrained, while the FEM results must be mapped to the deformable surfaces of the CFD domain. The RBF solutions obtained constitute the modal basis that, suitably amplified, permits the structural deformation under load to be represented, generating an intrinsically aeroelastic domain. This process is known as “RBF structural modes embedding”. To accelerate the mesh morphing phase, the deformations associated with each modal shape are stored thereby containing the numerical cost of the morphing process to a small fraction (around 10%) of the cost of a single CFD iteration.

The proposed FSI modelling technique belongs to the class of weak approaches because, for the purposes of an unsteady analysis, the loads are considered to be fixed during each time-step. The modal forces are calculated on the prescribed surfaces (i.e. the deformable ones) by projecting the nodal forces (pressures and shear stresses) onto the modal shapes. The mesh is updated at each time step during the course of the CFD transient calculation according to the calculated modal coordinates. The mesh morphing tool used was RBF Morph, with Ansys Fluent for the CFD, and Ansys Mechanical 2021 R1 for the FEM solver.

Experimental study

The industrial problem studied concerns a vortex-induced vibration on a thermowell immersed in a fluid flow. The case study experiment was measured and recorded by Emerson Electric Co., the multinational corporation that owns Rosemount which manufactures the thermowell studied (www.emerson.com/en-us/asset-detail/rosemount-twisted-square-a-new-twist-on-thermowell-design-1800740).

The purpose of the experiment was to evaluate the flow-induced vibrations on a traditional cylindrical thermowell design, shown in Fig. 1. The 470.219 mm-long sensor was equipped with an accelerometer in the tip and immersed in a flow of water inside a 152.4 mm-diameter pipe.

The water velocity ranged from 0 m/s to 8.5 m/s. The accelerometer enabled the evolution of the tip displacement to be reconstructed. The results gathered are summarized in Fig. 2 in terms of the mean square root of the tip displacement as a function of the fluid velocity.

Two lock-in regions are observed: an in-line vibration lock-in region, and a transverse vibration lock-in region. In the in-line vibration lock-in region, the maximum Root Mean Squar (RMS) tip displacement in the direction of the flow is 2.33 mm, recorded at a fluid velocity of 2.44 m/s. In the transverse vibration lock-in region, the maximum RMS tip displacement in the cross-flow direction is 8.3 mm, recorded at a fluid velocity of 6.4 m/s. The vibrations are induced by organized vortices that shed in sheets along the axial length of the stem and that generate alternating forces. If the shedding frequency approaches a natural frequency of the thermowell or its half, transverse or in-

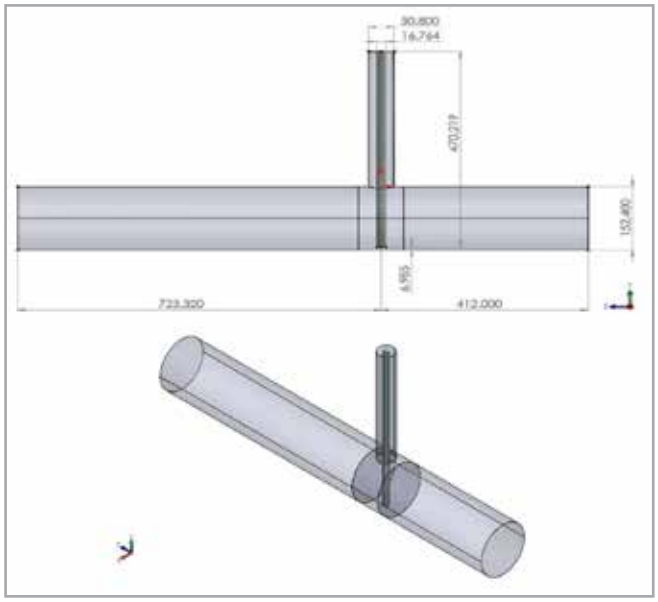

Fig. 1 - CAD model of the analyzed system

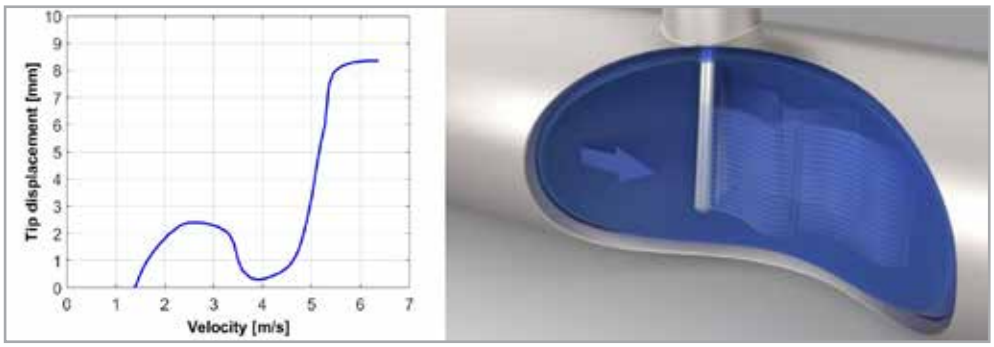

Fig. 2 - Experimental results, RMS tip displacement vs fluid velocity

line vibrations are excited and a failure of the sensor may occur. Failure conditions have been reached for the cylindrical thermowell at velocities greater than 6.4 m/s. The purpose of this work was to numerically capture the transverse vibration lock-in region of the cylindrical thermowell.

Numerical analysis

The study presented in this paper was conducted by using the FSI module included in the RBF Morph package. The FSI module allowed to tackle the VIV analysis using the structural modes embedding method. The workflow is sketched in Fig.3. The structural and fluid domains each have to be modelled in appropriate locations and with consistent units. During initialization, the structural modes calculated by Ansys Mechanical are transferred into the Ansys Fluent CFD model by RBF Morph. Once the modes are incorporated, the "flexible" CFD model is able to: adapt the shape according to the modal coordinates, evaluate the modal forces acting on the wetted surfaces, and evolve the time solution of the structural modal coordinates.

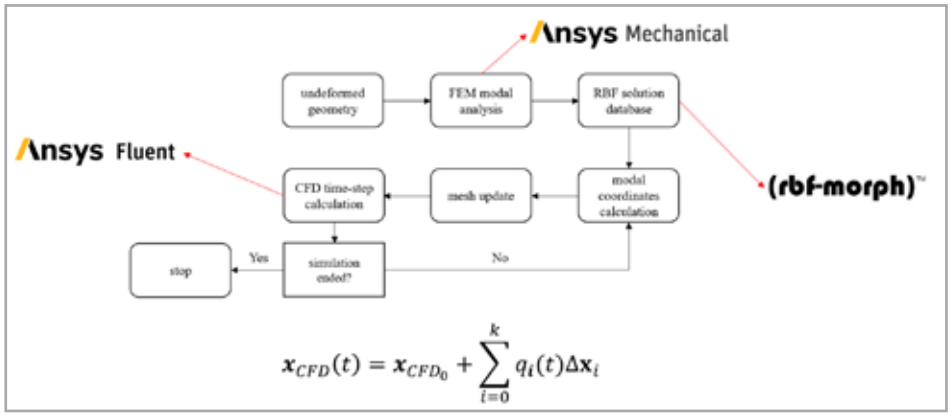

Fig. 3 - FSI workflow based on structural mode embedding by RBF Morph

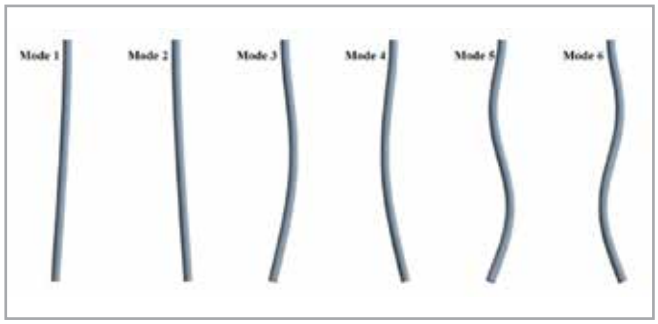

Fig. 4 - First six modal shapes calculated with the FEA model

The first six modes were extracted from the FEM modal analysis and adopted to populate the modal base adopted for the FSI analysis. The shapes of the six modes are shown in Fig. 4 where the first, second and third shapes can be seen bending in the two directions.

The shapes of the modes were extracted in terms of the displacements of the FEA mesh nodes belonging to the sensor surface and normalized with respect to mass; then they were used for the RBF Morph configuration depicted in Fig. 5. It is worth noting that once the configuration for one of the modes is completed it can be easily and automatically replicated for the entire modal base required.

The top left of Fig.5 shows the morphing domain, which is restricted to the region where shape deformations are expected to occur; RBF source points are created to control the morphing of fixed parts (top right of Fig.5) and the deforming parts (bottom left of Fig.5). For this particular case, the proximity of the tip of the thermowell to the boundary wall of the pipe created a challenging problem. In fact the large displacements that the thermowell is expected to undergo due to the vortex induced vibrations, combined with the need to maintain a cylindrical shape for the pipe wall, would result in a significant distortion of the mesh if the nodes in the pipe wall were imposed as fixed.

To avoid this high mesh distortion, an advanced corrective strategy was implemented to allow nodes belonging to the pipe wall that are close to the tip in the clearance region to slide on the cylindrical surface. First, a "shadow" area was defined so that the portion of the pipe surface defined by the projection of the thermowell tip would follow the sensor tip during the morphing action.

Then, a projection of the deformed pipe surface mesh onto the original cylindrical surface, after mesh morphing, was made. This complex task was accomplished by combining three pre-calculated RBF solutions.

The first two solutions allowed the shadow area to be assigned an appropriate rotation around the axis of the pipe, and a translation in the direction of the axis itself, in order to keep it constantly under the tip; the third solution, based on RBF Morph's STL-target technology,

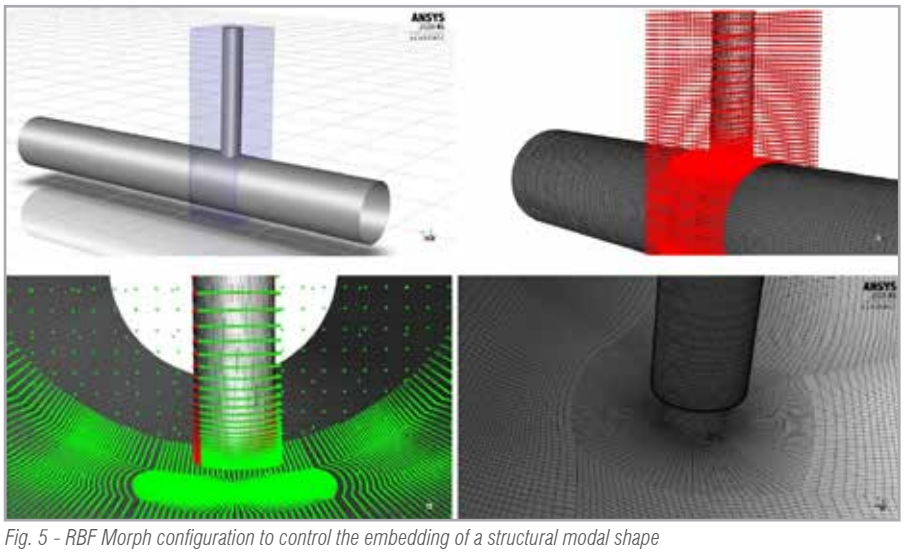

Fig. 5 - RBF Morph configuration to control the embedding of a structural modal shape

allowed the selected nodes to be projected onto a target surface (and thus to recover the cylindrical shape of the pipe).

The bottom right image of Fig. 5 represents the surface mesh around the thermowell tip obtained after morphing by applying the described correction procedure. Note the high quality of morphing, the correct placement of the shadow area, and the preservation of the cylindrical shape of the pipe.

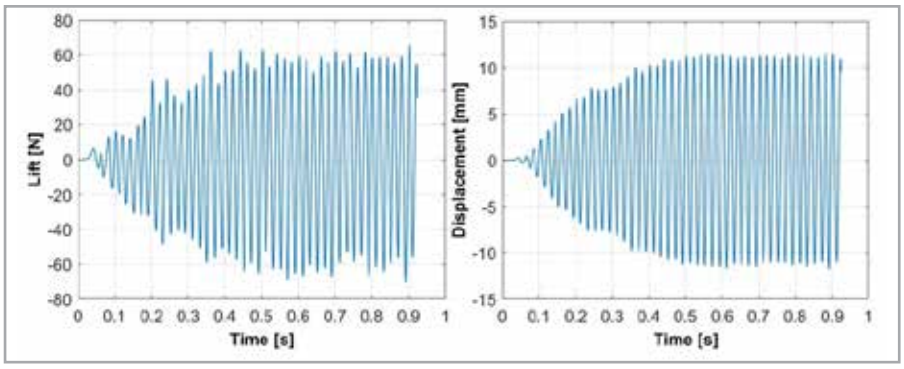

Fig. 7 - Temporal evolution of the lift on the thermowell (left) and the transverse displacement of the tip (right)

The fluid dynamics domain was discretized with a structured, multiblock mesh consisting of 3.16M hexahedra. To accurately solve the boundary layer up to the wall, the thickness of the first cell layer was set to obtain a dimensionless wall distance (y+) of less than one. The SST k-ω turbulence model was adopted. At the inlet, the velocity-inlet boundary condition was set by imposing a flow velocity of 6.4 m/s. At the outlet, a pressure condition was set. The unsteady incompressible RANS calculation was performed with a time-step of 10^{-4} s. The structural damping ratio was set to 0.041, following guidance found in the literature and a parametric study (www.springerprofessional.de/en/analysis-of-vortex-induced-vibration-of-a-thermowell-by-high-fid/19244678). The mesh was updated at each time step by calculating the modal coordinates and amplification factors of the corrective solutions.

Results

Fig. 6 shows the contours of the magnitude of velocity on a plane perpendicular to the thermowell axis for two different flow times corresponding to the maximum transverse displacements, in both the positive and negative directions.

Fig. 7 illustrates the temporal evolution of side force on the thermowell; it also shows the temporal evolution of the transverse tip displacement. The maximum RMS transverse tip displacement of 8.304 mm shown is in good agreement with the experimental data

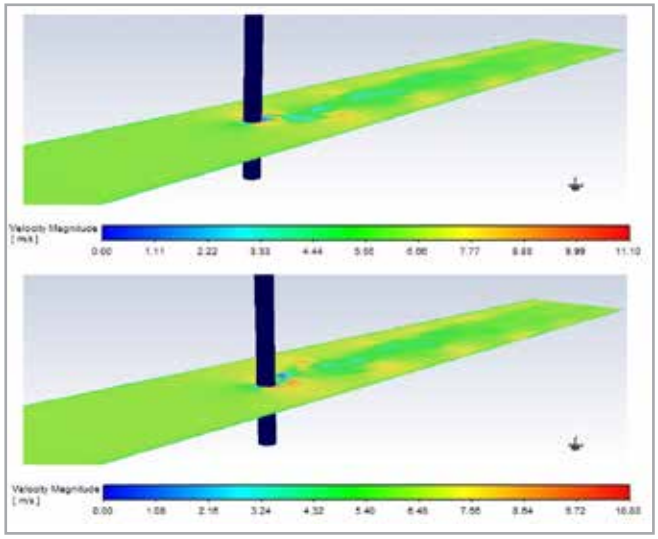

Fig. 6 - Velocity magnitude oscillation contours at t=0.8425 s (top) and t=0.8525 s (bottom)

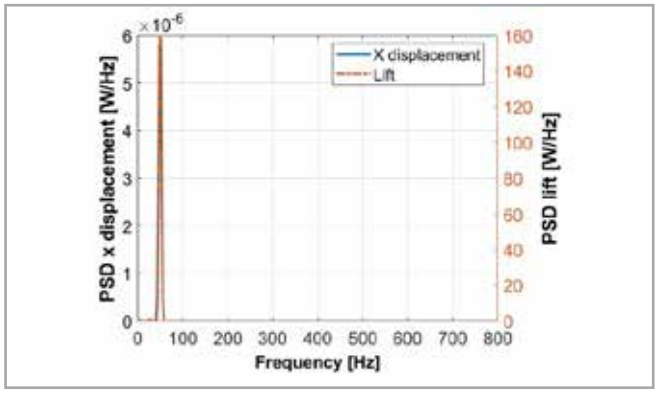

Fig. 8 - Power spectral density distributions of the lift and of the transverse displacement of the tip

available. The power spectral density distributions of the two signals (the temporal evolution of side force and transverse tip displacement) as a function of frequency are shown in Fig. 8. A dominant frequency of 48.8 Hz was observed for both signals, confirming the correct acquisition of the lock-in condition.

Conclusions

The work presented focused on an FSI analysis methodology based on the modal superposition approach. It was applied to the study of vortex-induced vibration of a thermowell. The problem of mesh adaptation was addressed with an RBF-based mesh morphing technique that provided a particularly fast and robust configuration.
The configuration studied represents a particularly challenging problem for the mesh morphing tool. The proximity of fixed and moving boundaries, in fact, results in strong mesh distortions that significantly limit the tolerable displacement. The morphing software used allowed a particularly efficient set of corrective solutions to be configured that enabled the very large displacements relative to the dimensions to be managed. The results of the unsteady FSI analysis conducted were compared with the experimental data and provided a good agreement with the measurements.

This work won the AIAS 2021 Software Simulation Award.

For more information:
Marco Evangelos Biancolini
Università di Roma Tor Vergata
biancolini@ing.uniroma2.it

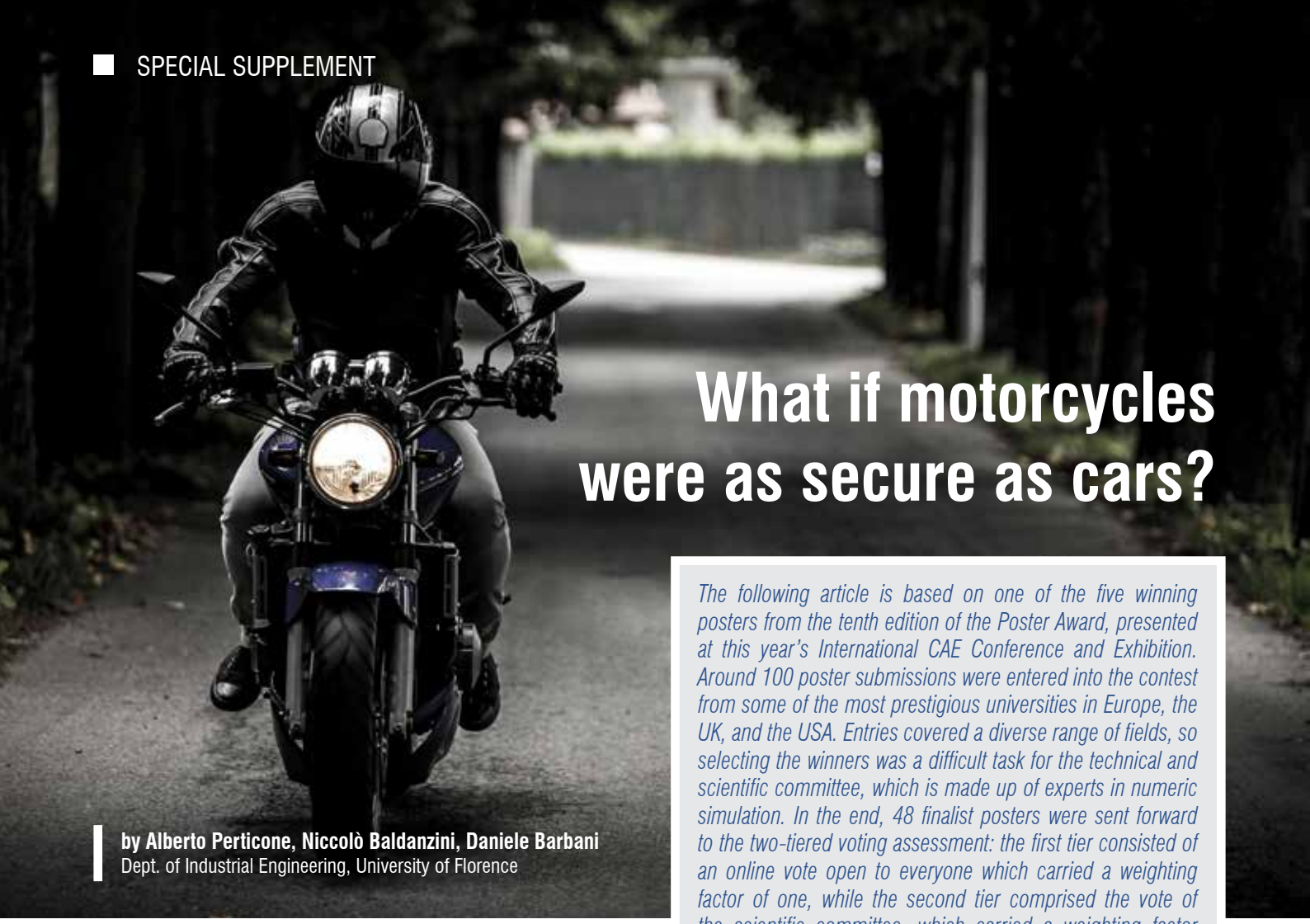

What if motorcycles were as secure as cars?

by Alberto Perticone, Niccolò Baldanzini, Daniele Barbani
Dept. of Industrial Engineering, University of Florence

The following article is based on one of the five winning posters from the tenth edition of the Poster Award, presented at this year's International CAE Conference and Exhibition. Around 100 poster submissions were entered into the contest from some of the most prestigious universities in Europe, the UK, and the USA. Entries covered a diverse range of fields, so selecting the winners was a difficult task for the technical and scientific committee, which is made up of experts in numeric simulation. In the end, 48 finalist posters were sent forward to the two-tiered voting assessment: the first tier consisted of an online vote open to everyone which carried a weighting factor of one, while the second tier comprised the vote of the scientific committee, which carried a weighting factor of three. Over 3,000 people participated in the online vote, which together with the assessment of the scientific committee produced the five winning posters. This poster was submitted by the Department of Industrial Engineering at the University of Florence in Italy.

Worldwide, powered two-wheeleres (PTWs) are typically over-represented in crash statistics. In 2019, motorcyclist fatalities per vehicle mile traveled occurred nearly 29 times more frequently than passenger car occupant fatalities in traffic accidents.

To date, the European Union has made enormous progress in road safety, halving the number of fatalities on European roads since 2000. In 2019, there was an unprecedented annual drop of 17% which was a clear, though unmeasurable, result of the COVID-19 pandemic.

This aside, progress has stalled in recent years. Tragically, almost 19,000 people still die on European roads every year; this is unacceptable. Moreover, the desire for new vehicles resulted in 1.4 million motorcycles and mopeds being registered in Europe in 2019. These vehicles also attract buyers because they offer their riders a value-for-money, time-saving, enjoyable, and low-polluting travel option.

Since road safety research over the past 20 years has successfully focused on protecting car occupants, we began our research project nudged by a simple question: what if motorcycles were as secure as cars? We wondered about the possibility of achieving a transference of safety devices from cars.

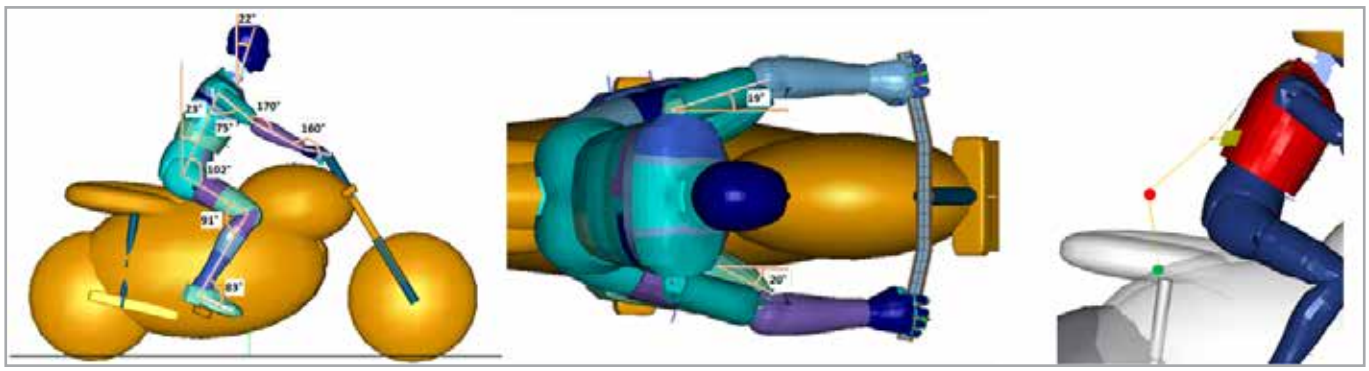

Fig. 1 – MATD dummy positioned on motorcycle ad fitted with the protective device

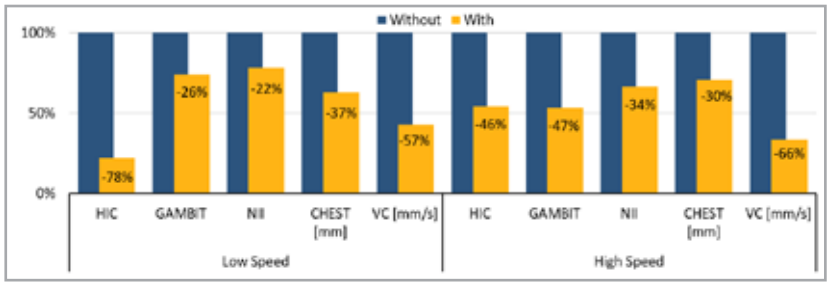

Fig. 2 – Comparison of injury indices at low (≤40km/h) and high (up to 80km/h) speed with and without the protective device

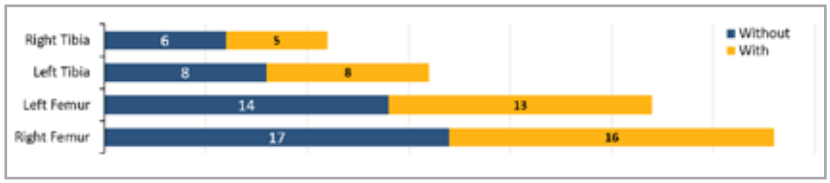

Fig. 3 – Frequency of occurrence of bony fractures. Comparison for N=25 simulations repeated w/o protective device

To understand the customer needs, we interviewed them and the survey led us to devise a belted safety jacket. The concept behind this device is intended to strongly copy the strength and purpose of seat belts in cars. Imagine a high-visibility vest, like those we keep in our cars and put on after accidents to be more visible to other motorists, with some belts segment sewn into the back. You put it on, climb onto your motorcycle, fasten the seatbelt, and start your trip — lightweight, easy to use, and very effective.

A test campaign was mandatory to be 100% sure of the solution's effectiveness. We used some databases that report accidents in the US and EU.

Databases are useful for keeping to real-world phenomenology and avoiding the use of accident configurations with no tangible feedback. The next step was to create a full virtual environment to test the device. We opted for multibody formulations and selected the multibody (facet MB) MATD dummy, derived from Hybrid III and suitable for motorcyclists, for the rider. We crashed a multibody (MB) touring motorcycle onto a deformable (FE) Geo Metro car model. The MADYMO environment reproduced 25 real-world accident configurations to test the protective device.

The entire model was parameterized in HyperStudy to automatically match each simulation with the corresponding crash event in the dataset. Six variables were made parametric: the impact velocity for each vehicle (x2), the contact points (x2), the Relative Heading Angle (RHA), and the Boolean presence of the safety device. The results were processed by evaluating several biomechanical indices.

At a glance, an overall reduction is visible for each index. Leg fractures also registered a slight reduction. Considering only serious injuries (AIS3+), the device reduced them by 79%, introducing only one worse injury to the head at the highest speed of the set (61 km/h) for the motorcycle.

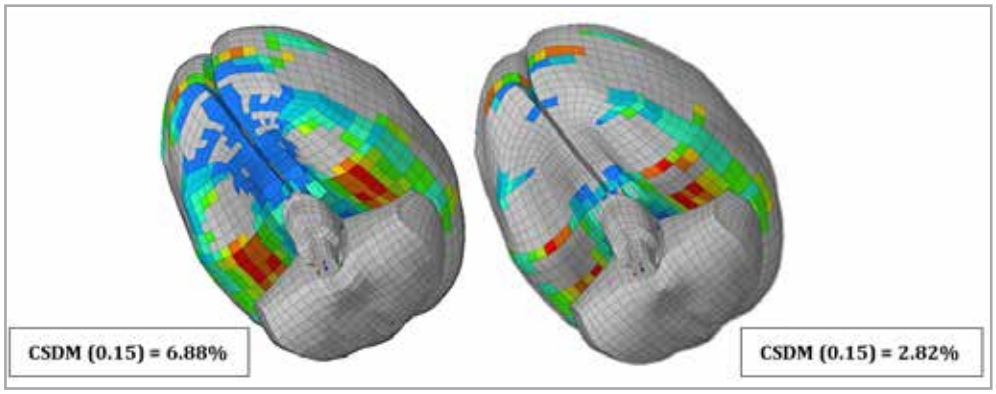

Fig. 4 – Cumulated Strain Damage Measure (CSDM), as a correlate for diffuse axonal injury, compared between the case without the protective device (on the left side) and that one with it (right side).

Some targeted tests aimed at confirming these positive results were then performed in a different environment. Using LS-Dyna, we replaced the previous dummy with a Human Body Model. In this manner, we derived important information about the biomechanical injuries sustained during accidents, such as brain damage.

Preliminary evaluation revealed encouraging results as different regions of the body benefited. However, not all speed ranges and impact positions seemed to experience the same benefit.

Further investigation of a larger dataset is recommended before drawing conclusions. In addition, the use of different motorcycles would improve the overall assessment by providing insights into other dynamics, both with, and without the device. These additional steps will hopefully help provide riders of powered two-wheelers with this highly valuable device to protect them during accidents.

For more information:
Alberto Perticone - University of Florence
alberto.perticone@unifi.it

Innovative European research project combines new technologies from diverse disciplines to protect fetuses from harmful substances

The EU LIFESAVER Project: Living Impact on Fetal Evolution: Shelter - Analyze - Validate - Empower Regulations

LIFESAVER
Living Impact on Fetal Evolution

Pregnant women can suffer from many conditions that require ongoing or acute treatment and care, not only because of health risks, but also because of environmental pollutants such as chemicals, contaminants, antibacterial substances, and others, which may also affect the unborn child, resulting in premature birth.

Premature birth kills one baby every thirty seconds, and poses a serious and growing threat to the health and well-being of the future European population. The risks of preterm birth are not limited to premature death of a baby, but also may lead to serious complications in future life: the children can suffer from extra infection, poor vision, breathing problems, diabetes, hypertension, and increasing risks of cerebral palsy, bowel damage, stroke and even lower IQ. This will affect their lives and presents a significant burden to society over several generations.

At present, the only conclusive process to ensure the safety and efficacy of biomedical products is to test them on humans through clinical evaluation. However, due to the unknown and potentially harmful effects on the developing fetus of such tests, less than 1% of all clinical trials in the US include pregnant women while more than 98% of trials actively exclude them.

Because of the crucial role of the placenta in supporting fetal development, the presence of potentially harmful drugs and exogenous chemicals and particles, such as phenols, antibiotics, phthalates, hormones, or plastics, is of great concern. Moreover, the development of health care treatments for the prenatal state is hampered by a lack of fundamental knowledge about the actual structure, properties, and function of placental tissues. Susceptibility to interference from chemicals and medicine exposure resulting in adverse pregnancy outcomes varies at the different stages of embryonic/fetal development.

ENGINSOFT · SEQVERA · 1921 2021 Università Cattolica del Sacro Cuore · ELVESYS · EVERCYTE · INL · CELLINK A BICO COMPANY · PROACTIVE · NUI Galway OÉ Gaillimh · INRiM · THE PLANET CALLS · IDEA CONSULT thinking ahead · Malta Life Sciences Park · 3s Instituto de Investigação e Inovação em Saúde Universidade do Porto · Fondazione Poliambulanza Istituto Ospedaliero

Fig.1 - LIFESAVER Project partners

The EU LIFESAVER project is a large-scale pan-European project funded by the European Commission's Horizon2020 Research and Innovation Action Programme, with the goal of addressing this serious threat in order to ensure that every pregnant woman has an adequate living environment with minimal risks to the fetus.

It aims to generate and validate the data that forecasts potential effects of environmental pollutants and drug treatments for pregnant women and eventual premature births, which are usually very difficult to assess.

The overall objective of LIFESAVER is to create and demonstrate a novel digitally cloned in vitro system to emulate prenatal conditions near the placental interface. This in vitro system is capable of high biological fidelity and enables the corresponding prediction of the potential risks posed by a drug or chemical to the unborn child. The LIFESAVER concept is based on an original idea to hybridize several innovative technologies and integrate the digital in silico system with the in vitro laboratory system.

The pioneering LIFESAVER project enables the design, production and implementation of a platform with all the correct key components of placental tissue to enable sufficient emulation of typical/atypical prenatal conditions. The combination of "immortal" perinatal telomerase cells with an in vitro bioprinted, mechanically and fluidically stimulated placental structure **has never before been tried** to the same extent.

LIFESAVER platform can in future enable proper emulation of uteri functionalities for testing all drugs and chemicals reducing national healthcare costs.

The added value of LIFESAVER in the spirit of the Green Deal call is in scientifically-based tools for experimental screening, digital pre-screening and analysis of chemicals and pharmaceuticals on their potential to cross placental tissues barriers. This will provide rationale for a risk classification on existing and new compounds, as well as justifications of regulations and risk assessment/mitigation measures towards the potential effects of these compounds on pregnant women and fetal health.

With a total budget of €6-million and a duration of 48 months, the project, coordinated by EnginSoft, brings together a consortium of 14 partners from nine EU countries, comprising leading European research and academic institutions, institutes for health, and industry.

The strength of the project lies in its high multi-disciplinarity and the final platform will be the result of the integration of the researchers' know-how. In fact, the project brings together specialists in digital models; experts in biomaterials, tissues, placental cells and fetal membranes; and professionals in additive manufacturing processes, microfluidics, and nano-biosensors as well as many others.

Looking forwards, the LIFESAVER platform will enable the correct emulation of uterine function to test all drugs, not only those specially targeted to female health, and chemicals that affect maternal/fetal health, as well as those for non-gender-related collateral diseases. This would result in reduced national healthcare costs (due to reduced hospitalization of women with non-communicable diseases) and the improved well-being of pregnant women and their unborn children.

Finally, LIFESAVER addresses new market opportunities in digitalized solutions for improving healthcare and wellness for pregnant women, and new in vitro biological digital twin devices in general. It will also strengthen the competitiveness and growth of companies working in environmental, medical and laboratory data analysis, bioprinting, tissue and cell engineering, and pharmacology.

The project started in November 2021 and runs until November 2025.

The project leading to this application has received funding from the European Union's Horizon 2020 research and innovation programme under grant agreement No 101036702.

For more information:
Carla Baldasso - EnginSoft
c.baldasso@enginsoft.com
or visit www.lifesaverproject.eu

Digital image correlation for automotive structures

by Florent Mathieu
EikoSim

As part of the monitoring of mass-produced automotive parts, many parts are repeatedly tested to ensure their integrity once they are put into service. For example, the test we discuss in this article concerns the "gust of wind" tests to an opening structure (see Fig. 1).

Loading tests on a door were conducted with stereo-digital image correlation (DIC) tracking at the Renault Technocentre. The aim of these tests is to perform real-time tracking to quantify the displacements inflicted on the door and to explore image correlation for automotive purposes. We thus seek to quantify the displacement field globally over the entire structure to ensure the validity of the corresponding numerical model.

For this purpose, the door is brought to its stop and a progressive force is applied in steps to its end, replicating opening by a strong gust of wind. This rigid body motion is extended beyond the point of the door's opening stop. In addition, between each loading step, the door is reset and reverts to its initial position.

Displacement sensors (LVDT type) are placed at several points on the door. The first wire sensor is placed at the end of the door, near the cylinder that allows the displacement. A second wire sensor is placed at the bottom of the door near the hinge axis. It is this second sensor that will be compared with the image correlation results.

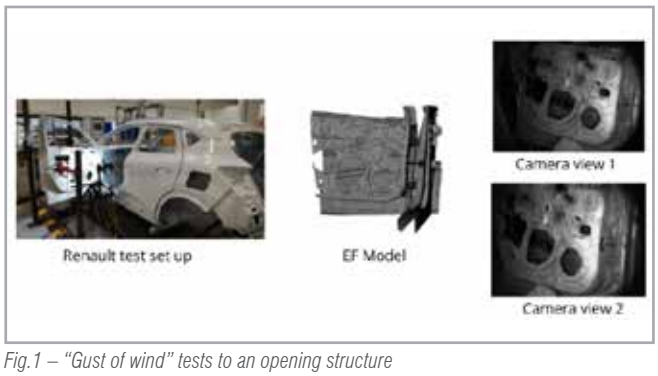

Fig.1 – "Gust of wind" tests to an opening structure

Fig.2 – Positioning of the cameras

Displacement tracking by image correlation field measurement

As shown in Fig. 2, a pair of cameras is positioned in front of the door to be tested. The size of the structure makes it impossible to visualize the whole door and perform the analysis over the entire surface with sufficient accuracy. A reduced study area (shown in Fig. 3) was therefore determined on which to conduct the analysis and comparison during the study.

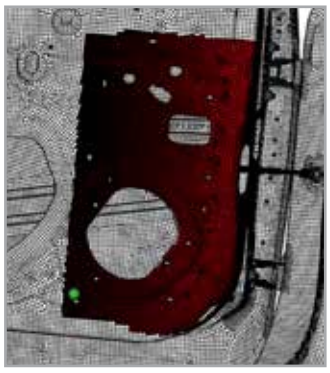

Fig.3 – Reduced study area identified for the study

Despite the large rigid body movements of the part, the cameras are able to capture all the door opening kinematics over the area studied, which includes the position of the

wire sensor (green dot in Fig. 3). The results presented in the following section will be scaled. However, it should be noted that the measurement is expressed directly on the finite element mesh of the part, which allows an immediate comparison with the displacement fields that were predicted by the design calculation for the stress under consideration.

Results and perspectives

The measured displacements are projected directly onto the finite element model provided by Renault, as shown in Fig. 4. As expected, a greater opening movement of the door is measured towards the exterior and the end than on the inside. These results can also be seen by looking specifically at the comparison with the wire sensor. To do so, a virtual displacement sensor (green dot in Fig. 3) is placed on the mesh, using EikoTwin's displacement sensor creation function, at the actual location of the physical sensor. Fig. 5 shows the comparison between the two sensors for the first few load steps.

Here we see consistent displacement values between the real wire sensor and the DIC measurement. However, a discrepancy is present and becomes larger as the door opens. This discrepancy is due to the difference in normals between the wire sensor (sliding normal, which changes with the opening angle of the door) and the camera normal, which is fixed. The optical measurement on the mesh has an additional advantage here for large displacements, as it does not need to be repositioned in the model frame.

It is also appropriate that this test focuses on the behavior of the door during the relaxation phases. Indeed, between each loading step, a return to the initial state is performed. The door is expected

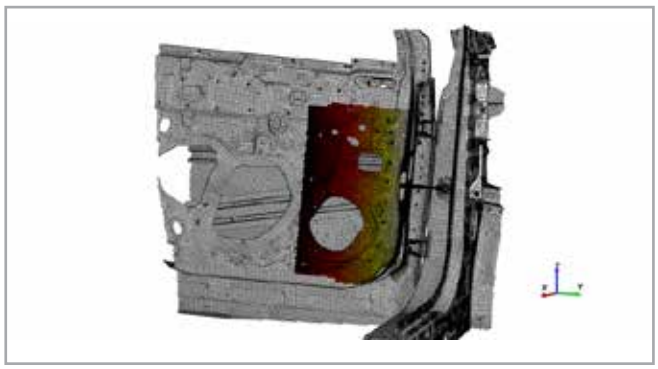

Fig.4 – The measured displacements are projected directly onto the finite element model

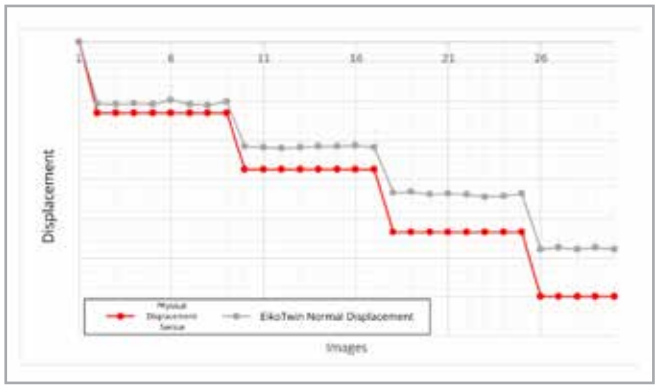

Fig.5 – Comparison between the two sensors for the first few load steps

About EikoSim

EikoSim is a software company that enables users to leverage validated simulation models to support design decisions. The company supports managers of engineers in charge of structural simulations. It assists its customers in explaining discrepancies between tests and models so that they can respond more quickly to program requests and reduce delivery times to the end customer. The EikoTwin software solution applies image analysis and simulation model management to improve both simulations and development cycles.

to revert to its initial position between each step, as predicted by the numerical model, which corresponds to a return to zero displacement in the measurement.

As shown in Fig. 6, given the above-mentioned deviation between the real and virtual sensors, the door does not return to zero between two loading phases, contrary to the numerical model's prediction.

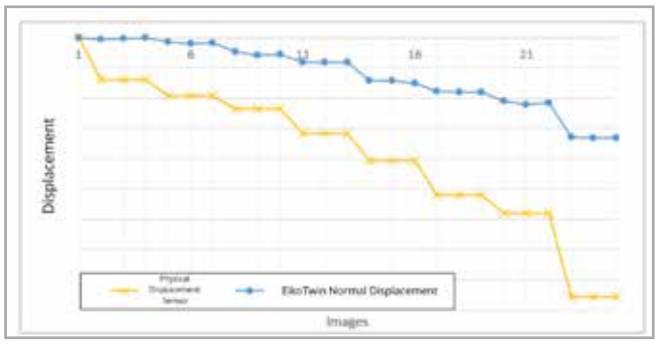

Fig.6 – The door does not return to zero between two loading phases

Furthermore, this deviation from the initial position increases as the imposed displacement increases, which is essential information for the future calibration of the numerical model.

In conclusion, the measurement conducted showed displacement fields obtained during the loading phases to be homogeneous and consistent with the tensile force applied and the wire sensor used for this test. However, a deviation was noted, due to the presence of a variable angle between the normal of the wire sensor and the door's movement at an angle that varies over time.
The measurement also revealed unexpected behavior during the relaxation stages, as well as the presence of residual displacement. Contrary to what was predicted by the numerical model, the door does not return to its original position between each step, as shown by the image correlation and also by the wire sensor.

Test data was collected in this area for the first time and highlights the image correlation's value for automotive issues. These tests are encouraging and provide qualitative and quantitative results in previously unmeasured areas of study, allowing the associated numerical model to be updated.

For more information:
Florent Mathieu - EikoSim
florent.mathieu@eikosim.com

CFD simulation of an axial piston pump with Ansys CFX

by Sara Bonati
CASAPPA

Thanks to their compactness and efficiency, swashplate axial piston pumps are widely used as fluid power sources in fixed and mobile applications that require high pressure and variable flow rates. In order to guarantee high performances, reliability and reduced time-to-market, their development process requires more and more the use of advanced simulation tools.

With specific reference to fluid dynamic simulation, different approaches are available; nowadays, the most common one is still represented by the lumped parameter method (0D-1D models). The advantages of this approach are the fast computation time and the ease of attaining convergence, but some physical phenomena are inevitably simplified or even neglected at all. In this sense a three-dimensional approach is the most advanced and accurate method; however, there are still considerable challenges to be overcome before reach a comparable level of usability: CPU time and convergence issues, in order to solve complex transient analyses characterized by small clearances and high pressure drops.

This work presents the CFD model of an axial piston pump and compares it to a validated 0D model. The main objective of this study was to analyze the flow field inside the pump, focusing on the aspects that involved the main inner volumes, such as the filling and emptying dynamics in the piston chambers and the flow field inside the ducts. Finally, particular attention was paid to the pressure transition phases, investigating their potential role in triggering erosion.

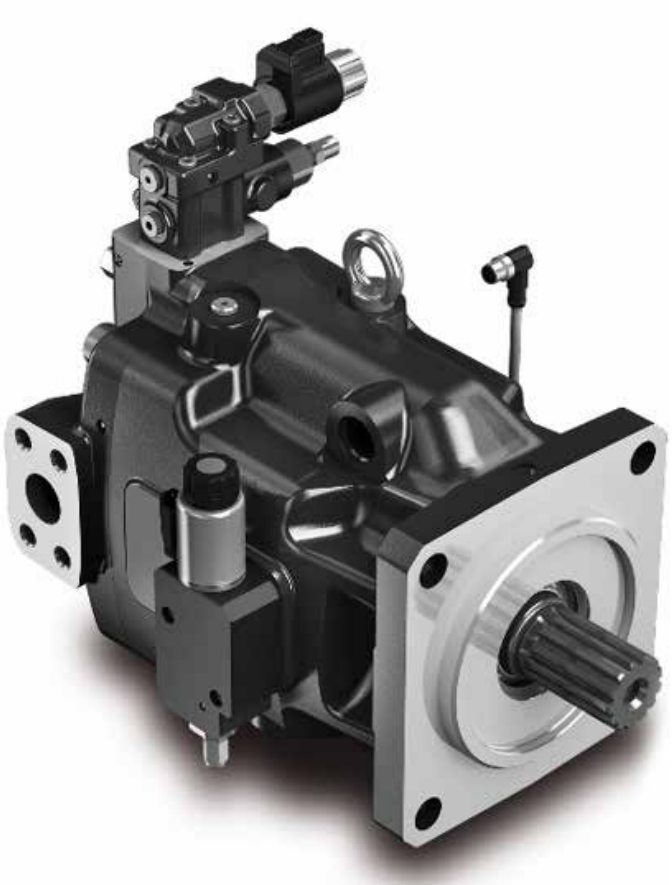

Fig. 1 - Casappa LVP140 axial piston pump

Case study: the Casappa LVP140 piston pump

The case study was Casappa's new LVP140 piston pump, a swashplate piston pump with a maximum displacement of 140 cc/rev (see Fig. 1), capable of working in mobile and stationary applications, with an open circuit and a hydraulic pressure of up to 420 bar.

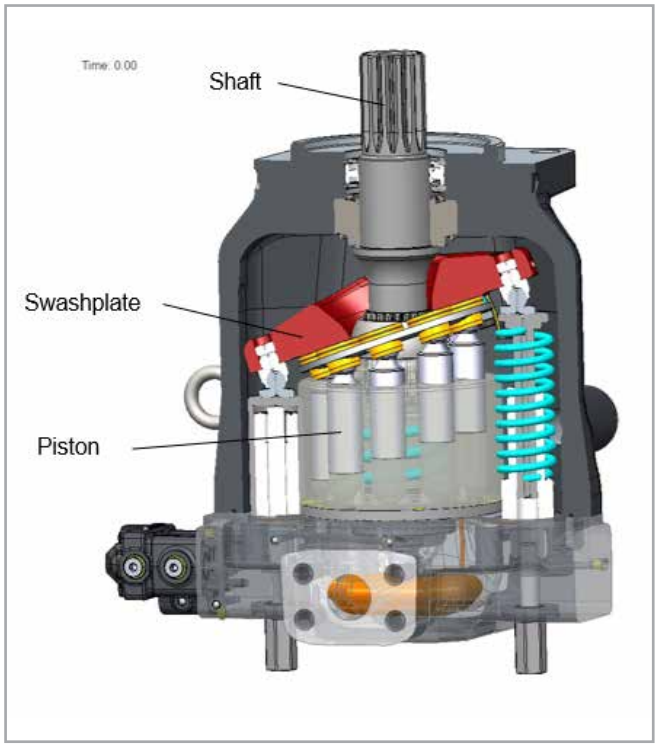

Fig. 2 - Basic principle of an axial piston pump

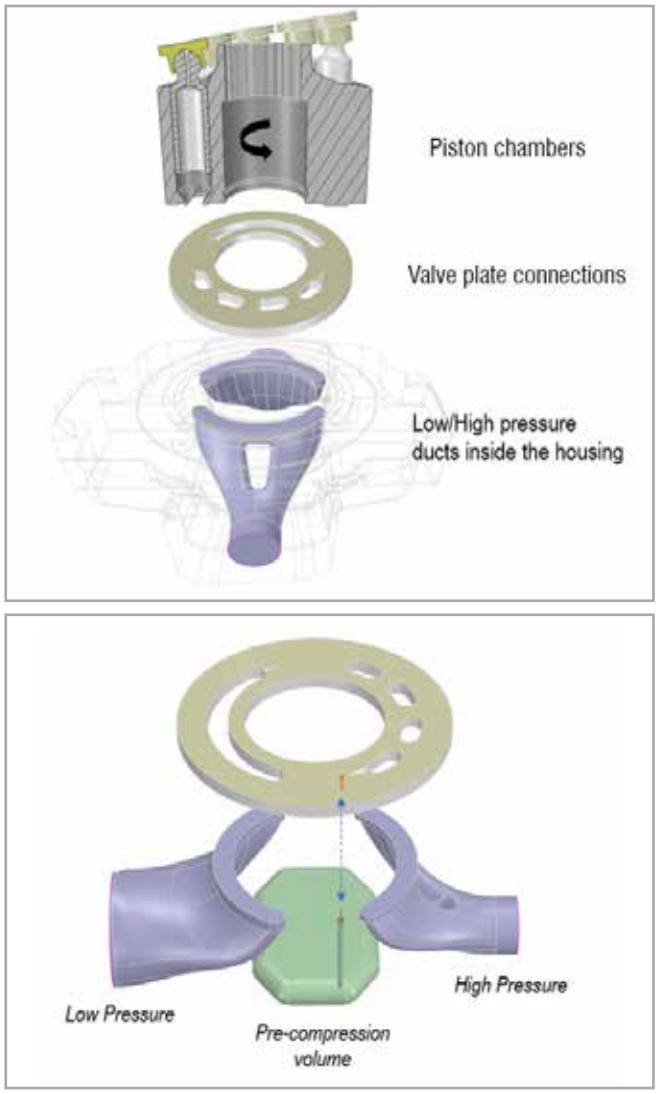

Fig. 3 - Main volumes inside the pump

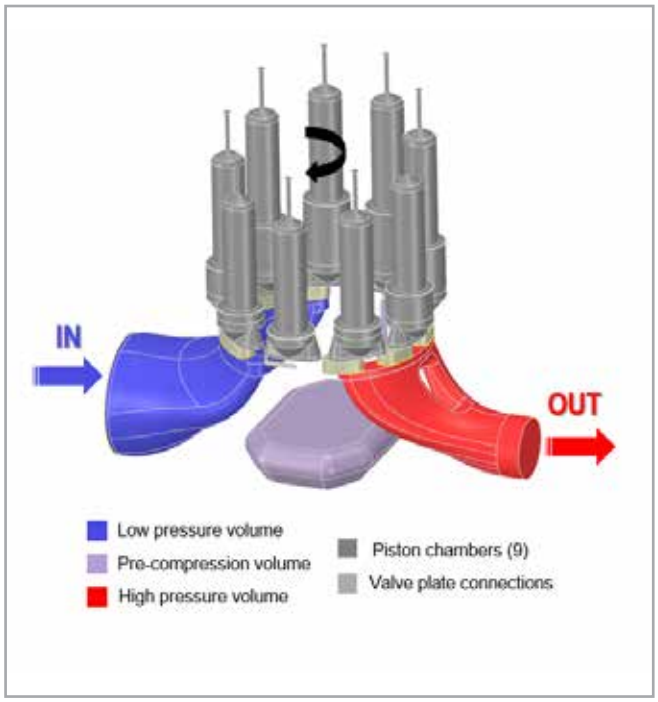

Reference pressure	1 bar
Inlet pressure	0 bar
Outlet pressure	180 bar
Rotating speed	1500 rpm
Fluid	ISO VG 46 mineral oil monophase
Heat transfer option	Isothermal (T = 50 C)
Turbolence model	SST
Number of elements	7'900'000
Simulation time	48 hours (Running on 32 cores Intel Xeon Gold 6240 CPU @ 2.60 GHz)

Fig. 4 - CFD model

In order to simulate the main fluid dynamic aspects that are involved in a working cycle, it is necessary to consider the main volumes inside the pump (Fig. 3), including:

- the variable volume inside each cylinder, called "piston chamber"
- high- and low-pressure ducts inside the pump housing
- valve plate connection: kidneys, grooves and orifices, whose shapes and positions define the pump's timing.

Special attention was paid to the valve plate design because the transition between the low-pressure and high-pressure connections and vice versa affects the pump's performance in terms of efficiency and noise generation.

In addition to the volumes described above, LVP140 is characterized by the presence of a noise-reduction feature, called "pre-compression volume". This feature makes this pump ideal for industrial applications where, due to the presence of electric motors, the pump becomes one of the first sources of noise.

The pre-compression volume is an isolated chamber realized in the rear cover of the pump: it is connected to the outside only through an orifice in the valve plate, located in the transition region from low pressure to high pressure.

Its function is to partially pressurize the fluid inside each piston before it is connected to the high-pressure line, in order to ensure a smoother pressure transition. In this way, flow ripple (the most important source of noise) can be minimized, by reducing backflows from the delivery to the suction line, and peak flow rates in the delivery.

The CFD model

The computational fluid dynamics (CFD) model of the pump was developed using the commercial software Ansys CFX (Fig. 4). The simulation was time dependent to account for the rotational and reciprocating movements of the pistons. Fig. 4 shows the simulated working condition.

Modeling the entire pump, in particular the pre-compression volume, was especially challenging because of the high pressure drops (in the order of hundreds of bar) and the small transition zones: special attention was paid to the meshing phase, using high mesh refinement in the transition zones in the valve plate,

such as the grooves and orifices, where the highest fluid velocities are reached.

The rotating and reciprocating motions of the pistons was managed using the domain motion and mesh deformation features within CFX. The rotary motion was obtained by setting each piston domain as rotating, while the reciprocating motion was achieved through mesh deformation, which involves a displacement diffusion model with constant mesh stiffness.

Results and validation

The model was validated by comparing the predicted pressures and flow rates with those obtained from a well-established 0D circuital model developed in the Simcenter Amesim environment (Fig. 5). The lumped parameter model, which has been developed

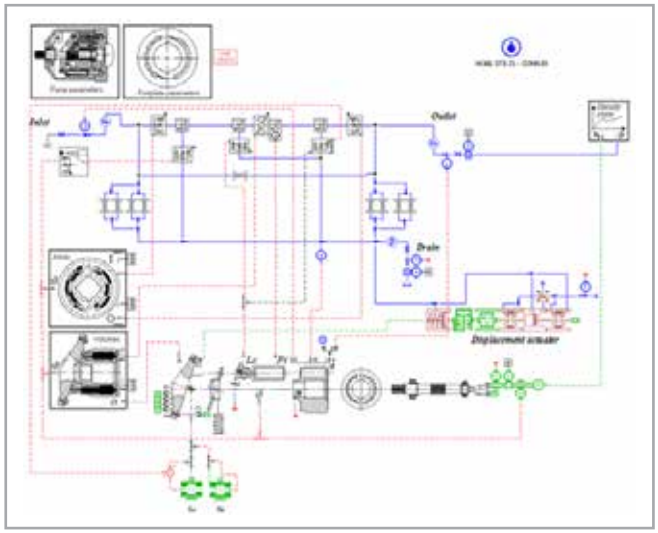

Fig. 5 - Amesim model of the LVP140 pump

over the years in collaboration with the Polytechnic of Turin and validated through experimental tests, is frequently used in the design phase of Casappa's components.

In just a few minutes of simulation, the 0D model estimates pump performance such as piston pressure peaks, internal backflows, flow ripples, and forces between internal components. In addition, it can predict cavitation conditions by simulating the dynamics of aeration (air release and dissolution in oil) and of vapor generation. However, since the fluid was considered as monophase in the 3D model, Amesim's full cavitation model was disabled in this study to obtain a consistent comparison between the two approaches.

Fig. 6 shows the comparison of the pressure inside a piston chamber and its corresponding flowrate. The results are perfectly comparable in all the phases. Owing to the absence of the gas phase, a non-physical negative pressure is achieved inside the pump chamber.

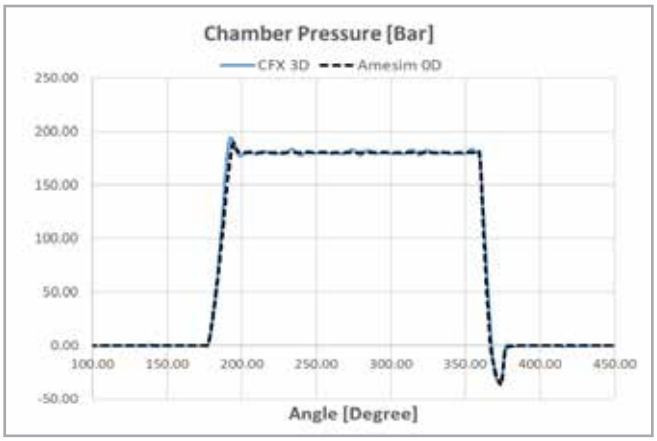

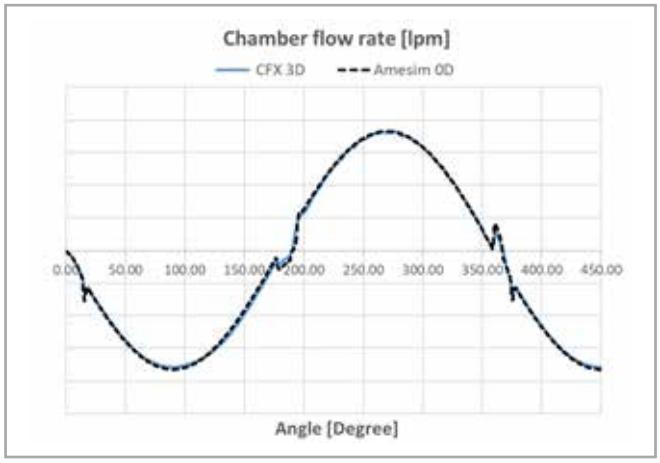

Fig. 6 - Comparisons of pressure and flow rate inside a piston chamber

Fig. 7 shows the flowrate exchanged between the pre-compression volume and one piston. As soon as the transition area is uncovered, oil flows from the pre-compression volume to the piston chamber, which is at lower pressure (1).

Due to the high pressure drop, the oil jet is particularly intense and, in a reduced angular phase, is able to pressurize the piston chamber (2). Therefore, when the piston is connected to the delivery line, a re-charge flow is established from the delivery to the pre-compression volume (3-4).

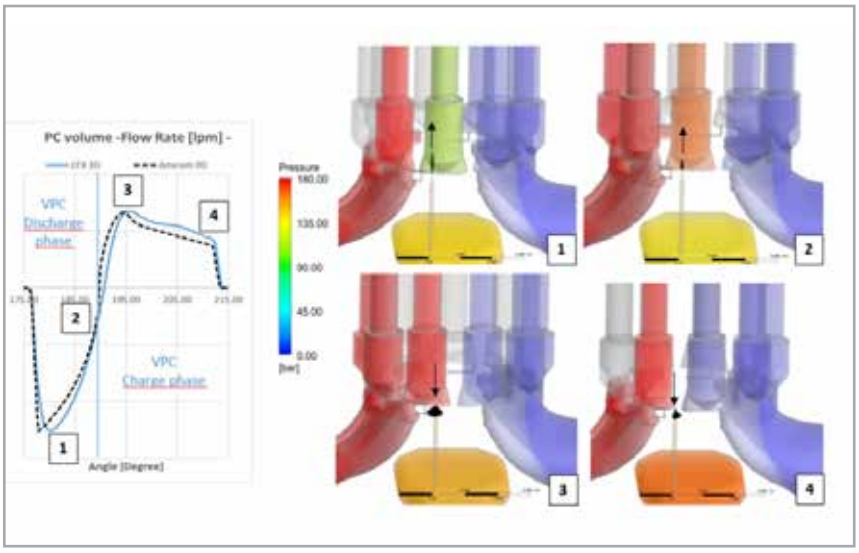

Fig. 7 - Flow field inside the pump

The comparisons reported show an excellent correspondence between the two models. Although the 0D model remains the best tool in terms of computation time and ease of reaching convergence, a three-dimensional approach is the most advanced and accurate method. A CFD model can predict the spatial distribution of pressure and velocity within the pump allowing the following to be explained: filling-emptyng dynamics, flow field distribution, identifying vorticity and stagnation areas (Fig. 8).

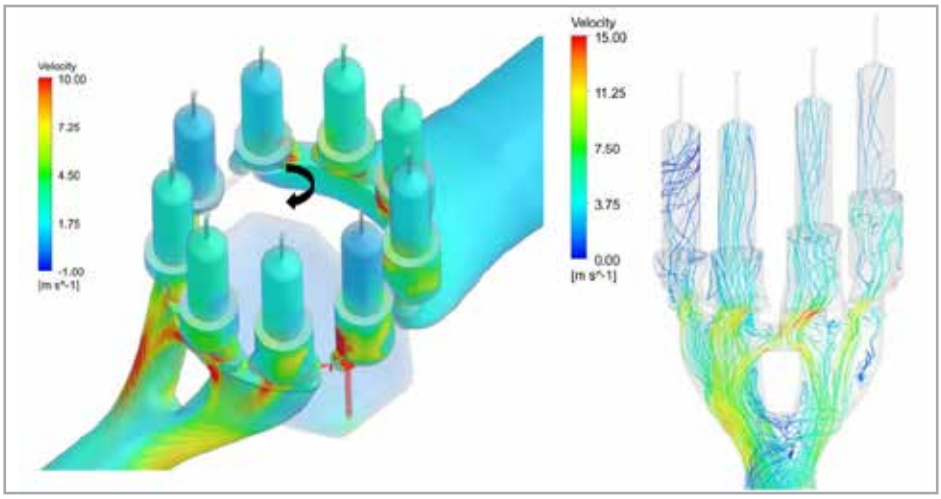

Fig. 8 - Flow field inside the pump

It was also useful in understanding the erosion phenomena that was observed on the test bench under extreme working conditions.

For example, Fig. 9 shows the velocity contour and its corresponding normalized vectors within the piston chambers while it begins opening the connection with the pre-compression volume as it moves from the suction region.

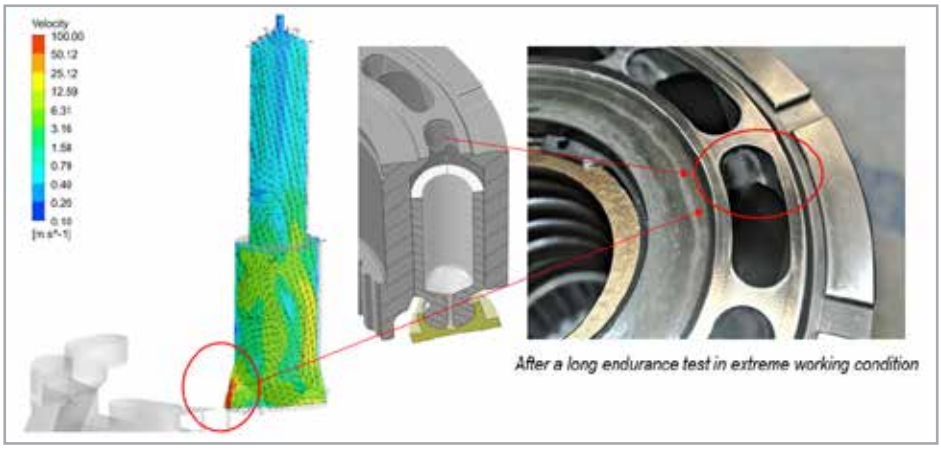

Fig. 9 - Example of detection of the erosion phenomena

Due to the high pressure drop, a high-speed oil jet with a component of near-axial velocity hits the surface of the cylindrical piston seat. Only later, when the piston intercepts the delivery groove, the flow is partially diverted.

The oil jet reaches high speeds, therefore the impact against the cylinder surface probably generates the erosion visible on the surface of the actual component subjected to the endurance test.

About CASAPPA

Casappa is an Italian company that has been working worldwide for more than sixty years in the field of fluid power.
We design and manufacture the main components of the hydraulic system for applications that range from construction to industrial vehicles, material handling, agriculture and industry. Our main products are aluminum and cast iron gear pumps and motors, variable displacement axial piston pumps, electronic controls and filters.

We strongly believe in product customization, to target the specific needs of each customer, creating long term collaborations with them; we achieve this flexibility thanks to the use of the most modern design engineering, innovative simulations and lab testing technologies.

Conclusions

In this work, a CFD model of an axial piston pump, operating at high pressure, was created to investigate the fluid dynamic aspects involving the main volumes inside the pump.
The model was validated using a quantitative comparison of predicted pressure and flow rates with those obtained from a validated lumped parameter model; the comparison shows an excellent correspondence between the two models.

Although the 0D model remains the best tool in terms of computation time and ease of reaching convergence, the 3D model proved to be the most advanced and accurate method to investigate the fill-empty dynamics, flow field distribution, and the erosion phenomena observed on the test bench under extreme working conditions.

The activity does not end here; the next steps will include the simulation of the most critical working conditions, i.e. the highest speed and pressure, and the introduction of a full cavitation model that will consider the release of air and steam, in order to investigate the spatial distribution of gas inside the pump.

For more information:
Giorgio Ceresa - EnginSoft
g.ceresa@enginsoft.com

Balancing multiple disciplines to design adaptable and sustainable buildings

ESTECO Technology helped Bouygues Construction automate the simulation process to identify appropriate designs more quickly

by ESTECO

Bouygues Construction develops innovations to support companies with new construction methods and materials, while considering future uses. The main requirements for any new construction include objective measurements, flexibility, industrialization, collaboration, and sustainability. Furthermore, clients are requesting innovative and evolving buildings. Bouygues manages to keep developing innovative processes by using a collaborative multidisciplinary design optimization (MDO) platform, which enables the various project stakeholders to make faster decisions and have a clear overview of possible solutions.

Challenge

A building is a prototype that is produced once. It is not a functional project like a car or an airplane, where the use of a design process can be profitable due to the sales volumes involved. Moreover, a building is created at the site with local resources and labor, and local environmental challenges that must be considered. Engineers must combine multiple engineering disciplines such as costing, methods, structures (reinforced concrete, steel, timber etc.), and the life cycle of the building.

Bouygues Construction had to blend a variety of disciplines and consider multiple variables to optimize the building and propose the most suitable design for its client.

Solution

Using modeFRONTIER, Bouygues automated a process to design a single floor of a building considering 26 input parameters such as geometry, solutions, use specifications, structural dimensions, unit prices, and unit rates of construction.

The outputs were the costs, rate of construction, and carbon footprint. VOLTA's collaborative platform allowed the company

"Thanks to MDO, we were able to objectively quantify the advantages of the various types of construction."

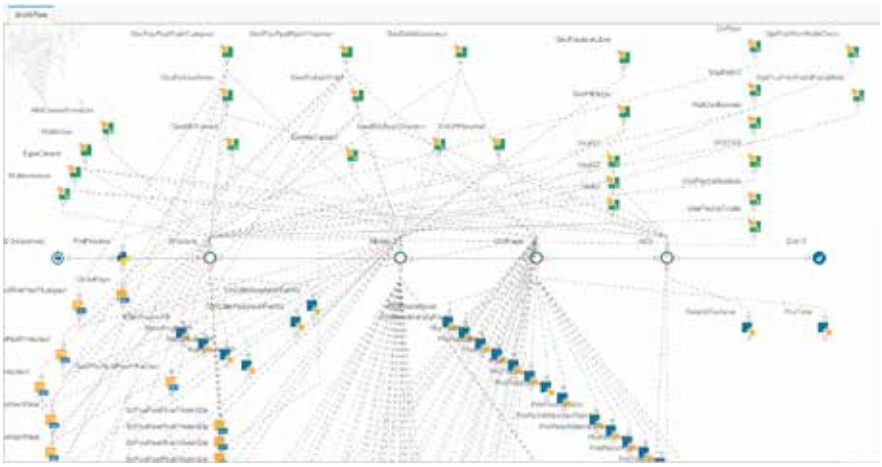

VOLTA workflow including multiple disciplines

to evaluate multiple construction designs and provide the most profitable and sustainable solutions to the construction team. This was possible because of the seamless integration between the simulation tools currently used at Bouygues.

The process was executed in just two days by a single engineer. *"A designer will learn and master a good software program,"* explained Sylvain Géry, Senior Structural Engineer at Bouygues Construction, *"ESTECO Technology seamlessly integrates with any simulation solver. This is particularly useful when a project spans different countries and involves companies who are used to working with different tools."*

Benefits

With ESTECO Technologies for process automation, design optimization and simulation data management, Bouygues expedited the simulation process and reduced the overall project design time.

The company's engineers created multidisciplinary processes and effectively coordinated all the steps involved. They were also able to evaluate the final outcome of the design by considering the costs and the carbon footprint.

Furthermore, the management of the project was simplified due to the ability for experts from different areas to collaborate, and as a result of the traceability of the evolution of the simulation model. There are many digital solutions available in the construction industry. *"Thanks to MDO,"* Géry said, *"We were able to objectively quantify the benefits of the various types of construction and identify the most appropriate combination of material usage, material technology and labor costs."*

For more information:
info@esteco.com

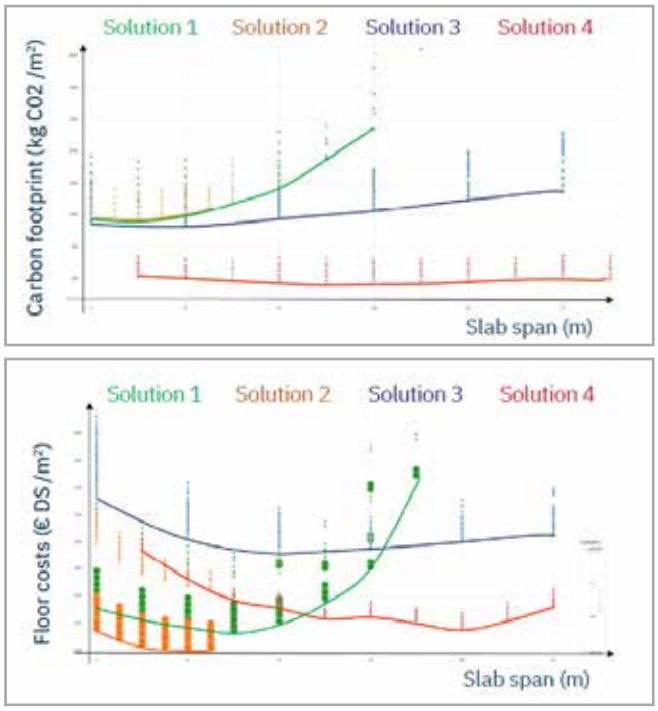

Results of the study, focusing on the carbon footprint and costs.

About Bouygues Construction

With 58,000 responsible and committed employees in more than 60 countries, Bouygues Construction designs, builds and operates projects in the sectors of building, civil works and energies and services. A leader in sustainable construction, the Group sees shared innovation as its primary added value and ensures that Health and safety are its top priorities. It has pledged to cut its greenhouse gas emissions by 30% by 2030 and offers its customers a wide range of low-carbon solutions. In 2020, Bouygues Construction generated sales of €12 billion.

by Dmitry Stepanov
CADFEM CIS

Using a combination of ParticleWorks and Ansys Fluent to simulate snow drift volume and deposition

In civilian residential area, the formation and distribution of snow cover has a significant impact on people's lives, affecting the movement of vehicles, safety and the maintenance costs of facilities. Two of the most important factors in this regard are heavy snowfalls and the high wind speeds during blizzards. Snow fences are often used to protect larger areas, but the selection of their shape and position are critical for their effectiveness. This study evaluates the combined use of ParticleWorks and Ansys Fluent to simulate the volume and deposition of snow transported around such snow fences and compares the simulation results with experimental results, showing a strong correspondence.

The formation and distribution of snow cover in places where people live affect their livelihoods: snow drifts negatively affect the movement of vehicles, and the accumulation of drifts determines the safety and maintenance costs of facilities. Heavy snowfall and high wind speed (blizzards) in particular become significant factors for people living in areas with harsh climatic conditions. Residential areas in such regions need to be protected in some way. Snow fences of various configurations are often installed to protect large areas. But in order to choose the right shape of and position for the fence, it is necessary to know the volume of snow that is transported.

At present, there are a number of Russian and foreign methods that allow the volumes of snow to be calculated [1-5]. These methods can be used for the initial estimation of this parameter. However, when solving practical problems, for example, the formation of snow drifts behind a snow-retaining fence, the data obtained using these methods is insufficient. Furthermore, the snow drifts formed also affect the parameters of the atmospheric boundary layer. This suggests that choosing the correct type of fence and its location is a critical task.

The numerical simulation of these complex processes makes it possible to obtain sufficiently complete information about the nature of the snow drift, taking into account the influence of various factors. To determine the correct placement and the required number of rows of snow fences, it is necessary to create a model that couples the continuous flow and the particle flow, so that the direction, wind speed, and snow properties (particle size, density), as well as the values of the coefficients responsible for interaction with the fence (such as the friction coefficient) become the input variables. This paper illustrates the combined use of ParticleWorks and Ansys Fluent to simulate the process of snow drift, while considering the effect of snow fences.

Description of the mathematical model

With respect to the simulated process, the motion of snow in an air flow can be considered as a primary flow of inert particles, where the particle size has no inverse effect on the primary phase.

This problem can be easily solved using a combination of two solvers: Ansys Fluent and ParticleWorks. Ansys Fluent performs the aerodynamics calculation and the output data should be a csv-file containing the values of the velocity components at each node of the mesh. Then, based on the resulting aerodynamic flow field obtained, ParticleWorks calculates the motion of the discrete particles and simulates their interaction with the downstream objects using the discrete element method. Each calculation is performed independently of the other. It should be noted, however, that the two modules can currently be coupled through the Ansys Workbench platform.

The geometry of simulation domain is a parallelepiped with sides of $1.5 \times 7.1 \times 117.5$ m. The mesh size in Ansys Fluent was approximately 4.3 million elements with 28.1 million nodes. ParticleWorks reads csv-files with up to 40 million lines fairly easily. The velocity profile was set in Ansys Fluent as the boundary condition, and the symmetry at the lateral boundaries was taken into account. In ParticleWorks, the properties of the snow were specified, and its polydispersity was taken into account: the particle diameter was set to a range of d=10...20 mm. The initial

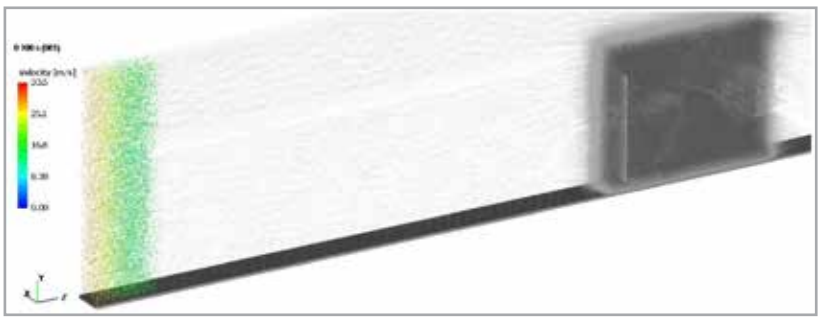

Fig. 1 - Vector field of air and snow particle velocity at time t=0.1 sec

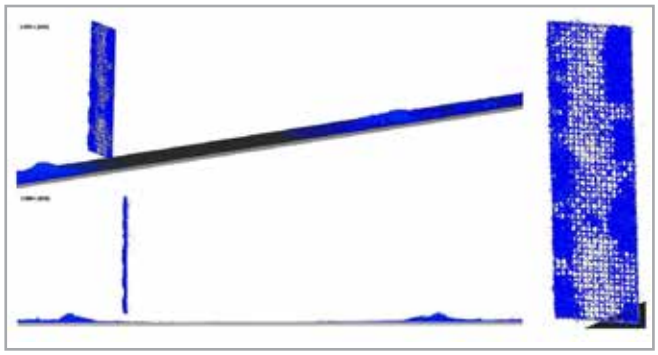

Fig. 2 – Distribution of particles deposited on the wall of the fence and on the surface of the ground at the time t=5 sec

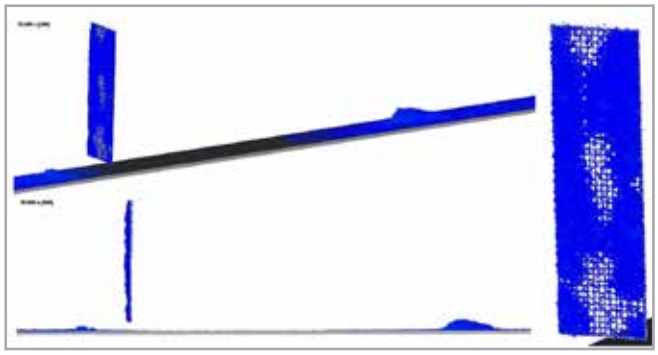

Fig. 3 – Distribution of the particles deposited on the wall of the fence and on the surface of the ground at the time t=30 sec

moment of time was taken as the distribution of air in the simulated area (see Fig. 1). The results presented below in Figs. 2-3 characterize the distribution of the snow cover at different points in time.

Concluding observations

The simulation results were compared with the experimental data presented in the reference [3] (see Fig. 4). It can be noted that there is a qualitative agreement between the results of numerical simulation and the results of the experiments: two snow drifts are formed in front of the first fence and behind it. The position of the snow cover did not change during the 30 seconds simulated. In addition, one can note that the snow cover between the first and the second fences, which were spaced 40 m apart, had the appearance of small drifts with a regular structure (see Fig. 5). It was observed that snow particles between the drifts moved due to the effect of saltation: in the air flow, moving particles collide with static ones thereby dislodging them and engaging them in further movement. This type of inert particle motion is only inherent to the discrete phase where the particles have a diameter of d=10...40 mm. This thesis is confirmed in the references [3,4].

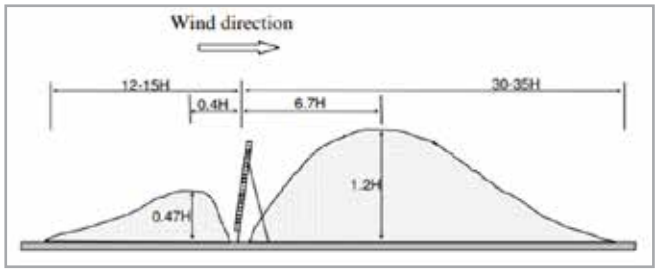

Fig. 4 – Dependence of snow drift size on the effective height (H) of the wall [3]

About CADFEM CIS

CADFEM CIS is the largest CAE systems distributor and Ansys, Inc. certified elite channel partner in Russia. CADFEM CIS provides delivery, implementation and technical support for Ansys multidisciplinary solutions and related software products. The company also offers engineering consulting services, including customized calculations, development of methods to resolve specific issues, and software adjustment. CADFEM CIS helps solve all issues, offering an effective computing IT infrastructure for resource-intensive simulation. In the transition to Industry 4.0, the company helps its customers to reduce time and costs and shorten the production cycle.
For further information, visit: ***www.cadfem-cis.ru***

Conclusion

The results of this study showed that the ParticleWorks solver is an effective tool for modeling dispersed flow. The validity of the simulation results was confirmed by comparing them with the results of an experimental study. Therefore, the combined use of ParticleWorks and Ansys Fluent may be considered as a promising method for solving various types of problems in civilian environments.

For more information:
Dmitry Stepanov and Denis Khitrykh - CADFEM CIS
dmitry.stepanov@cadfem-cis.ru
denis.khitrykh@cadfem-cis.ru

References

[1] Lobkina V., Kazakova E., Gensiorovsky Y., "The calculation technique for transport of snow in poorly-studied areas (Sakhalin Island)", Ice and Snow Journal 52 (3):58, 2015;

[2] Soloviev A., Lebedev O., Kalach A., "Mathematical Modelling of Behavior of Snow Weight on the Hillside" Journal of Voronezh State Technical University, P 116-117, 2011;

[3] Tabler R., "Snow fence guide", Strategic Highway Research Program, National Research Council, Washington DC, report number, SHRP-W/FR-91-106, pp. 1-61, 1991b;

[4] Giangreco S., "Validation of Lattice Boltzmann model for snow transport and deposition by wind": Doctoral dissertation. 2010;

[5] Matsuzawa M., Ito Y., Ueda M., "Method of Calculating the Amount of Accumulated Snow Transported during a Single Blizzard", Sirwee 2010. Conference Papers, Presentations and Workshops, abstract n°25. 2010 P.1-7.

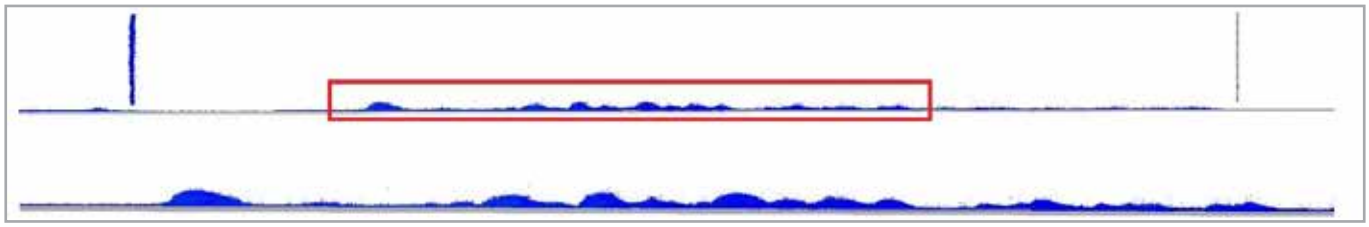

Fig. 5 – Distribution of snow between the two fences

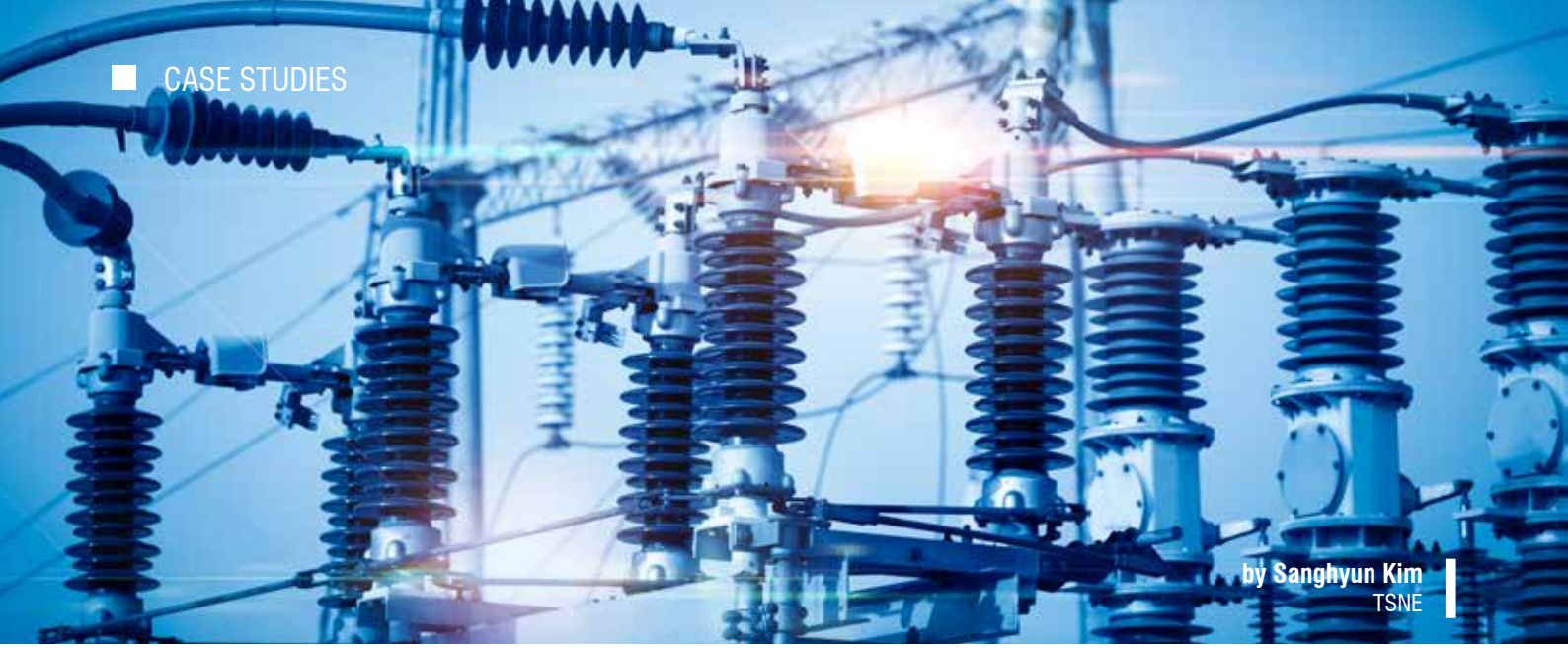

by Sanghyun Kim
TSNE

An analysis of stray load loss reduction of a distribution transformer using STS for the bushing flange plate

Many new products are being actively developed in the field of transformers including high-efficiency, low noise, and lightweight models. To develop high-efficiency power distribution transformers, it is important to minimize copper and iron losses, but studies on stray load losses are relatively scarce. This article addresses how to reduce the stray load losses in low-voltage side bushings for highly efficient distribution transformers.

Industrialized countries around the world are working to reduce greenhouse gas emissions through international agreements to combat the environmental impacts of climate change. According to a press release from its Ministry of Environment, Korea aims to reduce greenhouse gas emissions by 37% by 2030 in a pre-emptive response to international agreements. Transformers do not directly emit CO_2, but losses can lead to indirect CO_2 emissions. The reason for this is that fewer transformer losses mean fewer raw materials are needed by power plants. Moreover, an analysis by EPRI (Electric Power Research Institute) shows that a 0.1% increase in transformer efficiency could yield $300-million in annual economic benefits. New transformer products are actively being developed, including high efficiency, low noise, and lightweight models. To ensure a high-efficiency power distribution transformer, it is important to minimize copper and iron losses, but research and development on these losses has reached saturation level, and studies on stray load losses are relatively inadequate.

This article discusses how to reduce stray load losses in low-voltage side bushings for highly efficient distribution transformers. The basic transformer model is designed using steel (SS400) for the housing material. The second transformer model's design has a slit in the area where the magnetic flux of the plate is concentrated and attaches to the STS (Stainless steel). In the third model, the flange plate around the bushing terminal is cut into a large square and then the STS is attached. We verified the effects of the three models presented in this paper by conducting finite element method (FEM) analysis using Ansys Maxwell, and then we manufactured a customized transformer and tested it.

Modeling the transformer housing and bushing for a 100kVA single-phase transformer

In this article, the basic model used for the analysis is a 100kVA single-phase transformer, with the following specifications:

- Rated capacity = 100 kVA
- Primary rated voltage = 13,200V
- Secondary rated voltage = 230V
- Primary rated current = 7.58A
- Secondary rated current = 434.8A
- Frequency = 60Hz

Fig. 1 shows the transformer model, its housing and bushing terminal. The housing is 2.5mm thick. The transformer model includes the housing and a low-voltage side bushing. All insulated structures that did not affect the results of the electromagnetic field analysis

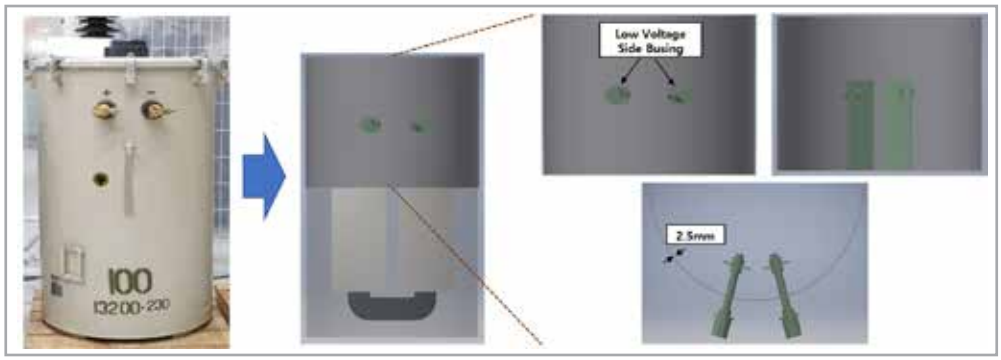

Fig. 1 – Transformer model including the housing and the bushing terminal

were omitted from the model. Ansys Maxwell was used for the FEM calculations, and a 3D electromagnetic field analysis was performed.

The magnetic field generated by the two bushing terminals with different current directions can be expected to affect the transformer case, and this magnetic flux would concentrate at the center of the flange plate. Firstly, a basic transformer model (Model#1) is

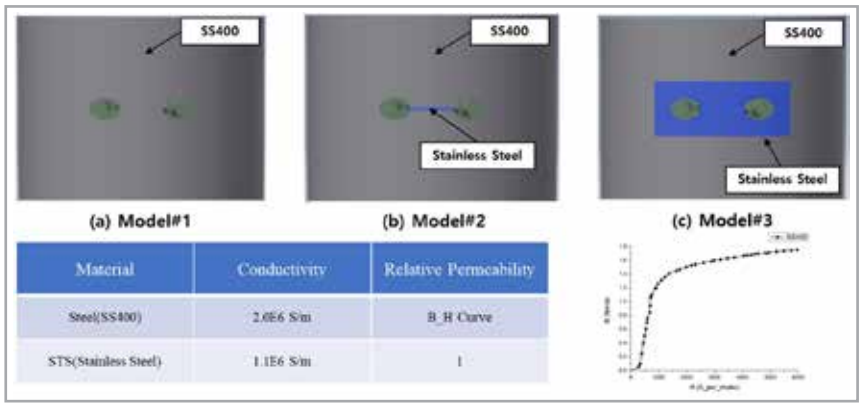

Material	Conductivity	Relative Permeability
Steel(SS400)	2.0E6 S/m	B_H Curve
STS(Stainless Steel)	1.1E6 S/m	1

Fig. 2 – Analysis model and material properties

designed using steel for the housing. Model#2 is designed with a slit at the area of the plate where the magnetic flux is concentrated. The slit on the plate is shown in Fig. 2 (b). In the third model, the flange plate around the bushing terminals is cut into a large square and an STS plate is attached. The STS plate is shown in Fig. 2 (c). The calculations for each model were performed with FEM and the physical properties of each model are shown in the table in Fig. 2.

Stray load loss analysis after using STS for the bushing flange plate

Fig. 3 (a) shows the results of magnetic flux density analysis and the eddy current analysis for the first model. The analysis confirmed that the leakage flux is concentrated between the two terminals of the bushings, and the loss was also concentrated as a result of the induced current generated in the magnetic flux.

To reduce the stray load loss on the bushing flange plate, various STS shapes were attached to the flange plate at the position where the leakage is concentrated. Fig. 3 (b) shows the results of the magnetic flux density analysis and the eddy current analysis for Model#2 with the slit in the STS, and Fig. 3 (c) shows the results for Model#3 with the STS plate.

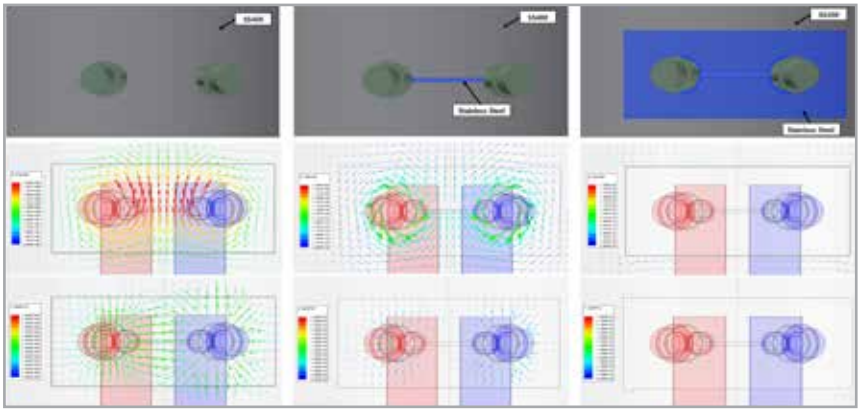

Fig. 3 – Results of magnetic flux and eddy current analyses

Fig. 4 shows the distribution of stray load loss for each model, and it is clear that using STS at the position where the leakage is concentrated greatly reduces the stray load loss. The stray load loss in Model#1 is 21.4W, while in Model#2, the loss is 2.7W, and in model#3 it is 0.2W. The difference in loss for each model is shown relative to Model#1, as can be seen in the table in Fig. 4. Compared with Model#1, the stray load loss reduction rates are 74.4% and 98.1%, respectively. Model#3's stray load loss at the bushing flange plate is remarkably reduced.

The verification tests on the proposed stray load loss reduction methods

In this article, a 100kVA single-phase transformer was specially manufactured to verify the results of the calculations. This 100kVA single-phase transformer used for the experiments was manufactured specifically to be the same as the models used for the FEM calculations. The transformer produced to verify the stray load loss reduction methods proposed in this article is shown in Fig. 5. The test method used was to measure the total loss using a power analyzer on the low-voltage side bushing terminal after applying a rated current to the high-voltage side bushing terminal. The copper loss was quantified by measuring the load current and the resistance. Moreover, the experiment was performed using the same winding and iron core; only the transformer housing was changed.

The load experiment provides data about the total copper loss and the DC loss. The stray load losses can be acquired by calculating the difference between the total copper losses and the DC losses, but

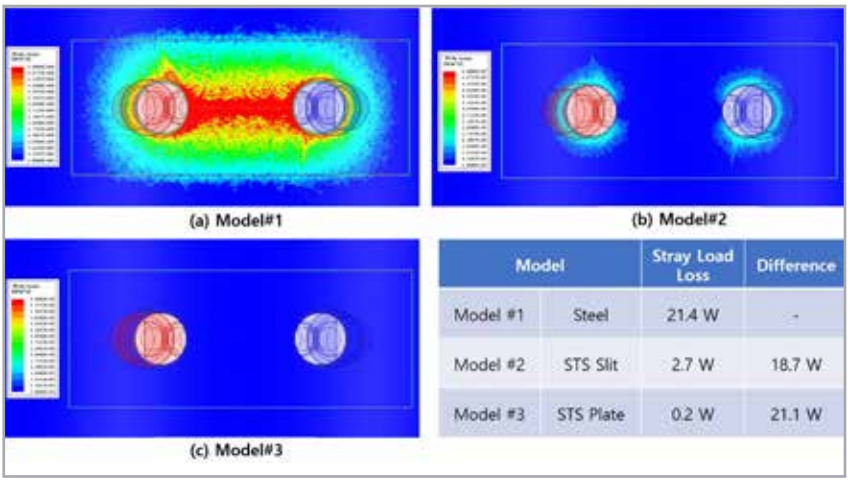

Model		Stray Load Loss	Difference
Model #1	Steel	21.4 W	-
Model #2	STS Slit	2.7 W	18.7 W
Model #3	STS Plate	0.2 W	21.1 W

Fig. 4 – Result of stray load loss analysis

Conclusion

In this article, FEM calculations and verification experiments were performed to reduce the stray load loss at the low-voltage side bushing of a power distribution transformer. The FEM calculations confirmed that the loss mainly occurs between the two bushing terminals, and that the partial use of STS on the bushing flange plate can reduce these losses.

Transformer Model#2 with an STS slit and Model#3 with an STS square plate are proposed in this article. The experiment confirmed that the use of the STS plate reduced the loss by 22.6W.

this figure also includes the eddy current losses from the windings and other structures. These eddy current losses are indistinguishable experimentally from the stray load losses. All loss measurements were performed at an ambient temperature of 25°C, but the measured values were calculated after first converting them to the transformer's operating reference temperature of 75°C.

In the experimental load test, each model used the same winding and iron core. Therefore, it can be assumed that the eddy current loss occurring in the winding (except for the bushing flange plate) and the eddy current loss occurring in the other structures are the same. As a result, as shown in Fig. 5, the difference in total stray load loss found in the experiments can be proven to be the loss reduction effect of using STS. The experiments verified that the partial use of STS on the bushing flange plate reduced the total stray load loss by 29.7% compared to the basic model.

The transformer used to verify the results of the FEM calculations was specially customized. A load test was performed during the experiment which verified the effectiveness of the proposed methods. It should be noted, however, that if the transformer body is added to the analysis, the stray load loss should be expected to further increase as a result of the leakage magnetic flux generated by the transformer winding. This aspect of the problem will form the subject of further studies.

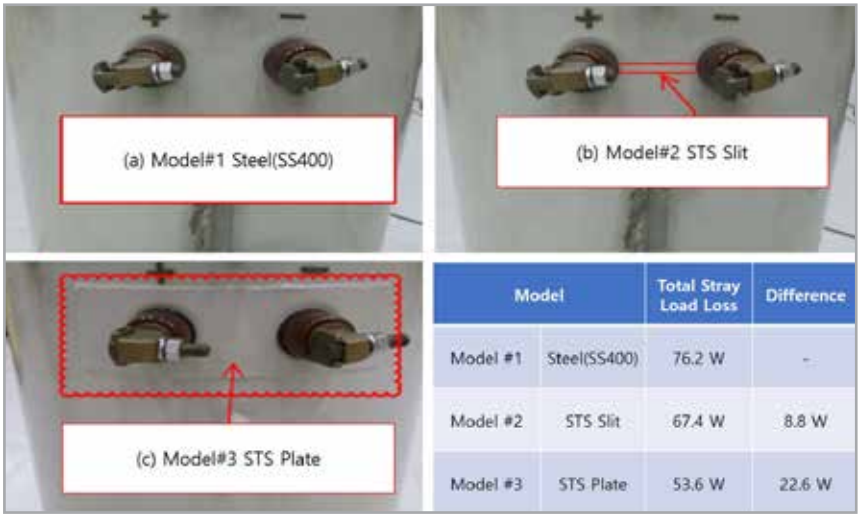

Model		Total Stray Load Loss	Difference
Model #1	Steel(SS400)	76.2 W	-
Model #2	STS Slit	67.4 W	8.8 W
Model #3	STS Plate	53.6 W	22.6 W

Fig. 5 – Verification test models and the results of the total stray load loss

About TSNE

Since its establishment in 1988, TSNE has specialized in CAE, providing engineering programs and services to Korean customers. Tae Sung S&E (TSNE) aims to be the "One Stop Total CAE Solution Provider" (OSTS) both in domestic and global markets.
TSNE leverages its large base of business capabilities and its team of CAE experts to provide services to customers in various industries (aerospace, automotive, civil engineering, biomedical, shipbuilding, electrical and electronics, energy, defense, chemical industries, etc.) and is expanding its business scope to research innovative technologies and apply them in the field.

The company is striving to become a global engineering company and increase its potential to become a sustainable engineering company. Tae Sung S&E is partner to all engineers who strive to solve challenges. Tae Sung S&E will work with you to achieve "NO PROBLEM, BE HAPPY".

This article is based on a paper written by the same author entitled: *Sang-Hyun Kim, Jung-Kyu Jin, Young-Joo Kim, Bum-In Shin, Hyang-Beom Lee, "The Reduction Method of a Stray Load Loss of Distribution Transformer on the Bushing Flange Plate with STS", Journal of Electrical Engineering & Technology, Vol. 14, pp. 1607-1613, 2019.*

For more information:
Sanghyun Kim - TSNE
shkim20@tsne.co.kr

by Fidesys

A stress-strain model of a soil massif

An extract from the 2017 Ufa Tunnel Survey Report

The following article is an extract from the 2017 Ufa Tunnel Survey report and presents the analysis of the seismic and geological characteristics of the natural technical system known as a "tunnel-rock massif" in order to design the tunnel for greater stability and security during operations.

In order to develop a model of the natural-technical system known as a "tunnel - rock massif" using the Micromine mining-geological system, a database was created with frame models of the actual surface and of the tunnel's underground structure (see Fig. 1). The raster models of the seismic parameters for all linear directions of the seismic studies (see Fig. 2), and frame models of the seismic engineering elements were loaded into the database.

The strategy of modeling the stress-strain state in the conditions under consideration should take into account the following factors:

- long-term construction of the tunnel structure will guarantee the recovery of deformations in the rock massif and the stabilization of the natural technical system (NTS) "tunnel - rock massif";
- significant differences in the elastic moduli of the rocks in the soil of the future tunnel will determine the different response of the NTS to dynamic (quasi-seismic) effects during use of the tunnel;
- formation of the elastic moduli model is based on the seismic properties of the rock mass, which allows an objective assessment of the level of additional stresses and strains in case of dynamic effects on the NTS under consideration.

Based on this strategy, the first version of the elastic model is formed, a fragment of which is shown in Fig. 3. In addition to the geometry and properties of the seismic engineering elements, the model takes into account disjunctive elements f3-f5 with reduced

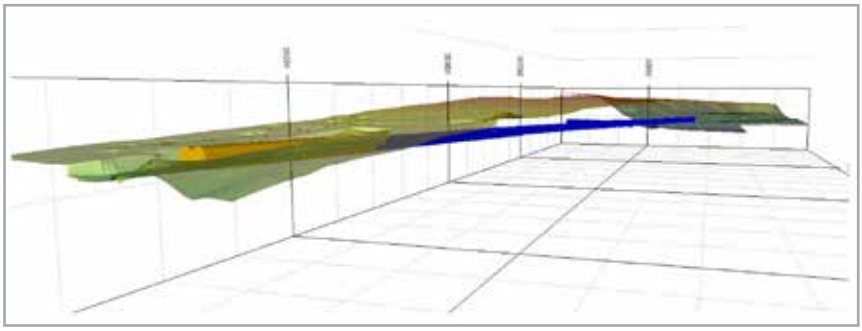

Fig. 1 – Frame model of the actual surface and of the tunnel's underground structure.

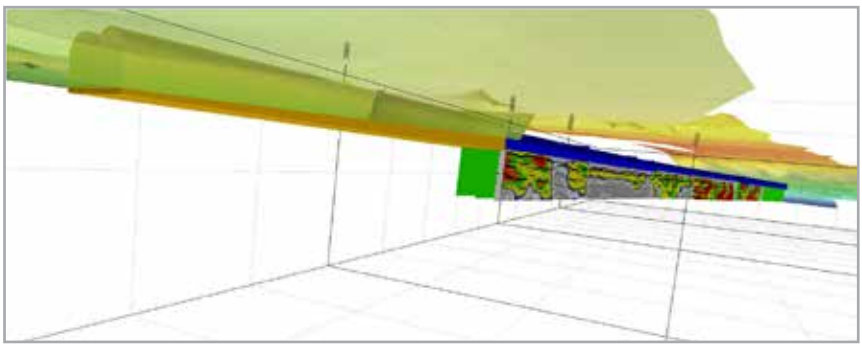

Fig. 2 – Frame models of the structure and parts of the engineering and seismic models in raster sections

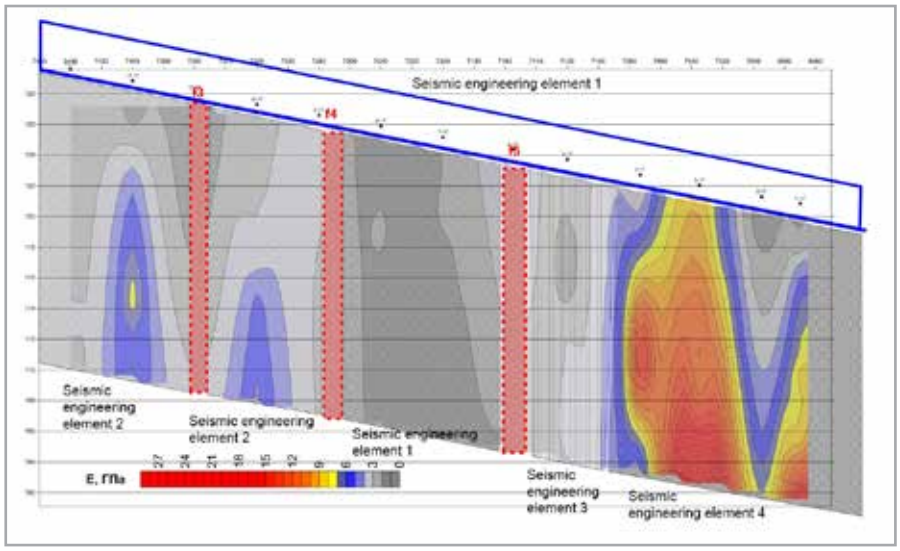

Fig. 3 - Part of 3D frame model of the geometry and properties of the seismic engineering elements in the tunnel soil

dynamic elastic moduli (E = 500MPa, Poisson's ratio = 0.4, density = 1.8kg/cm^3).

Taking into account the frame and raster models of the mining and geological database, block models of the elastic moduli are generated, which are then exported into the database of the Fidesys 3D strength analysis package and further algorithms for calculating the components of the stress-strain state in the "tunnel - rock massif" natural-technical system are implemented.

The initial version of the simulation provided a block-based 3D model with the seismic engineering properties and the position of disjunctive elements as shown in Fig. 3. Fig. 4. shows a general view of the geometry of the 3D block model upon which the stress-strain state modeling process is performed. As a result of modeling the components of the stress-strain state, a database of 3D massifs was created using the components of stresses, strains, and displacements that can be analyzed in detail in different sections using a specialized viewer.

Figs. 5-9 show several parts of the 3D views of the components of the stress-strain state of the massif.

In general, the initial options for modeling the stress-strain state in the seismic engineering (dynamic) model of the NTS "tunnel - rock massif" indicate a possible continuous strain disturbance in the following tunnel intervals:

- at the intersections of the tunnel axis with disjunctive elements f1 - f6, the instantaneous type variable strains (relative values) reach 35mm, and the displacements

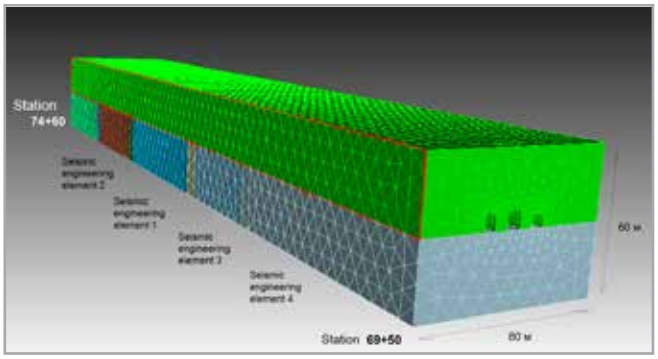

Fig. 4 - General view of the block model of the NTS "tunnel - rock massif" in seismic engineering

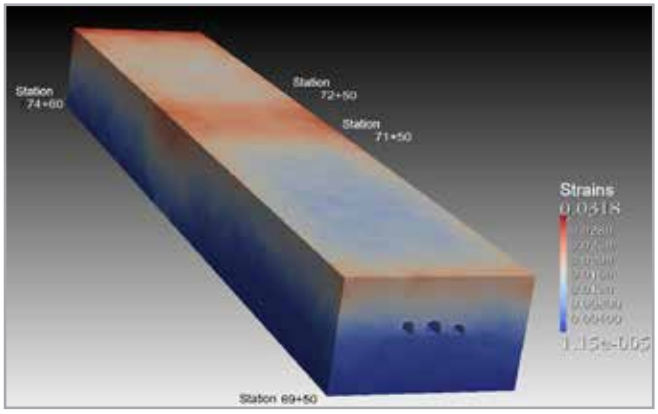

Fig. 5 - Array of displacement values in general (scale in meters)

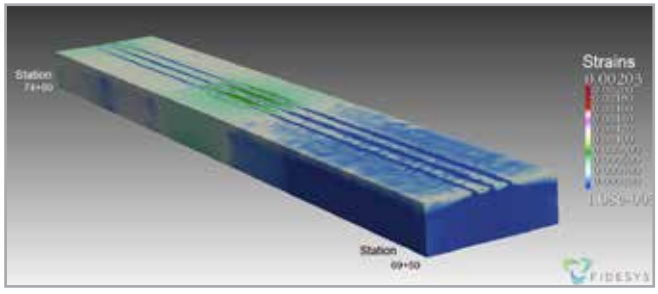

Fig. 6 - Horizontal section of the array of total strain values (scale in meters)

About Fidesys

The Fidesys CAE software package for high-precision strength calculations is the flagship product of the Russian company FIDESYS. The software package is available in both traditional desktop and cloud versions. The project began in 2009 at the Moscow State Lomonosov University under the guidance of Professor Vladimir Levin [8-12]. The company then became part of the Russian Skolkovo Foundation, which was the impetus for the creation of the first commercial version of the product, and subsequently the cloud version of CAE. Today the company employs 25 mathematicians, graduates of leading specialized universities and PhDs. In addition, the organization employs 11 consulting professors from Moscow State University (MEPhI), Moscow Institute of Physics and Technology (MIPT), scientific institutions of the Russian Academy of Sciences, the University of New Hampshire, and Columbia University. FIDESYS provides engineering consulting and custom software development services to solve highly specialized tasks for its customers. The company is involved in: complex problems of mechanical resistance and the stability of structures; geophysics and geomechanics; strength of composites; intelligent materials; solid phase transitions.

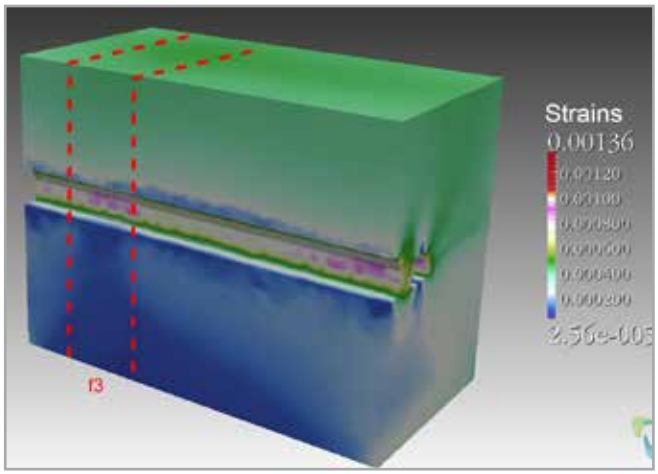

Fig. 7 – Part of the vertical section of the total strain values

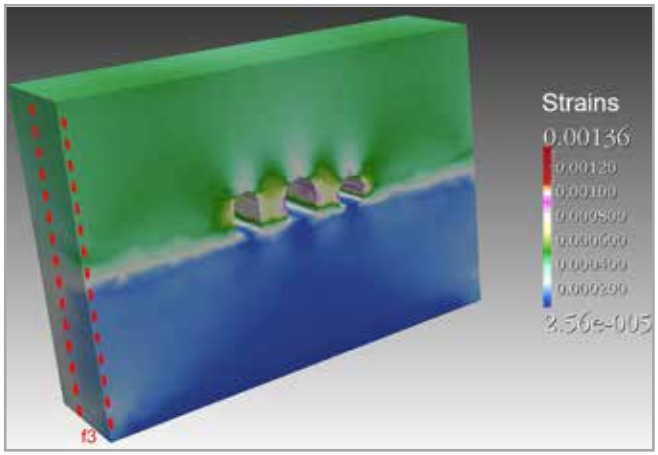

Fig. 8 - Part of the vertical section of the array of total strain values in the area of disjunctive element f-3

(absolute values) reach up to 10-15 mm;at the station interval 71+50 - 72+50 (the weakest rocks) alternating deformations can be 2-4mm, and displacements can be up to 15 mm.

After analysing the whole complex of survey materials and considering the options for the structural design elements of the tunnel, the designers made further detailed calculations in the specified intervals, based on the electronic model. This

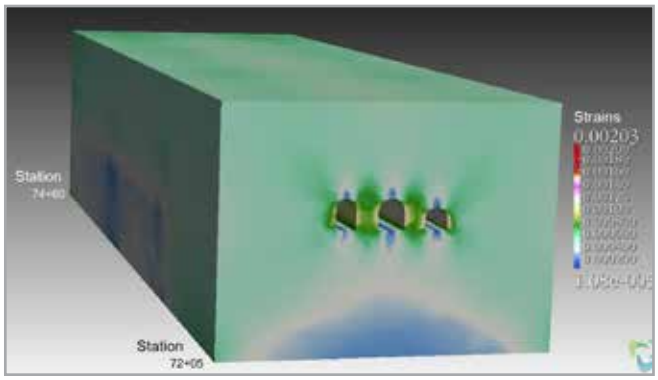

Fig. 9 – Part of the general view of the array of total strain values in the station interval 72+5 - 34+60

will significantly reduce the initial values of the components of the stress-strain state established for adverse scenarios in the development of geological-engineering processes.

Table 1 below shows the physical and mechanical properties of the soil mass according to complex analytical and seismic studies of the area surrounding the tunnel impact zone, and recommendations for additional measures to improve the stability of the "soil massif – tunnel" system so that optimal design solutions can be developed.

Conclusions

It should be specially emphasized that in order to correctly solve geomechanical problems concerning the assessment of the stability of underground structures, it is necessary to use a seismic method of determining the elastic moduli (deformation modulus and Poisson's ratio) on the existing tunnel's zones of influence on the rock mass for at least 50m in all directions from the sides and the face of the main and auxiliary excavations.

For more information:
Vladimir B. Pisetsky*
pisetski@yandex.ru

Vladimir B.Pisetsky is Doctor of Geological and Mineralogical Sciences, Professor, Head of the Department of Geoinformatics of the Ural State Mining University

Intervals of dangerous strain processes development		Stress-strain modulus, MPa	co Specific Pa hesion, M	Internal friction angle, degree	Poisson's ratio	Density, g/cm³	EGE	Predictive maximum value full strain, mm	Recommendations and notes
Initial station	End station								
73+20	73+70	20	0.05	20	0.4	1.9	6-1	10	Disjunctive element zone with possible development of deformation processes under dynamic loads and evolution of filtration flows. It is recommended that the massif be secured with cement solutions.
71+00	71+50	600	0.1	23	0.35	2.1	6-1, 6-2, 6-3, 7-1	10	Disjunctive element zone in contact with dispersed and rocky soils. Development of additional bending strains. Anchoring is recommended.
The entire tunnel route		2000	0.2	25	0.3	2.2	6-2, 6-3	5	Predominance of semi-rocky soil with low water saturation.

Table 1 - Recommended values of the physical and mechanical properties of soil for calculating the main structural elements of the tunnel

by Francesca Lago
EnginSoft

Virtual fluid dynamic and thermal optimization study of the die and production process for a high-end gearmotor housing component

One of the central themes in Industry 4.0 and smart manufacturing is the development of highly efficient production systems that minimize production costs and improve productivity and product quality. Highly efficient production enables companies to become more competitive in the market by improving their performance, thus enabling them to differentiate themselves from low-cost nations. Hence, it is essential to produce high quality products while at the same time reducing waste, which is also important in terms of environmental sustainability and energy efficiency.

The diecasting production process with its high production rates is certainly one of those sectors in which high efficiency plays a strategic role. The implementation of intelligent monitoring platforms is fundamental to the creation of efficient production processes. These platforms identify any anomalies in the process parameters by means of signals from sensors positioned in the die and correlate them with the defect levels identified for the specific process being analyzed.

Product part acceptability thresholds will guide the user in determining the optimal working ranges for the process parameters and any significant deviation from these will trigger an alert.

This article will illustrate how numerical simulation, in addition to playing a key role in the optimization of the die design and the production process, is also a valuable support in defining the position of the sensors in the die and in identifying the most significant process variables, which are fundamental aspects for the development of intelligent monitoring platforms.

Fig. 1 – Die-casting product: housing for a gearmotor

This study is part of the research project PREMANI (MANIFATTURA PREDITTIVA): design, development, and implementation of Digital Manufacturing solutions for Quality Prediction and Intelligent Maintenance, funded as part of the POR FESR VENETO 2014-2020 Action 1.1.4 "Call for the support of Research and Development projects developed by Industrial Districts and Regional Innovative Networks".

The project aims to develop techniques for predicting the operating characteristics of machines and plants by combining product quality analysis with plant efficiency analysis in a context described as Predictive Manufacturing.

The case study

The component being studied is the housing for a gearmotor used in various applications such as escalators (Fig. 1). The part is produced by RDS Moulding Technology with a die-casting process using a single impression die in EN AB 44100 alloy (AlSi12).

From the very first stages of production, non-conformities were detected in the component that resulted in part of the production being discarded. These defects were:

- cold joints in the upper part of the casting,
- air pockets in the central hub and in the upper part of the component,
- shrinkage porosity in the central hub and in the upper part of the body,
- erosion of the die in the frontal area of the ingate, and
- cracks in the die after only a few cycles of production which resulted in a short die lifetime.

A preliminary analysis of the production process, conducted with MAGMASOFT, allowed the causes to be identified and the corrective actions to be evaluated (Fig. 2)

Die redesign

The redesign phase was divided into two steps: a fluid dynamics optimization and a thermal optimization. The fluid dynamics optimization concerns the redesign of the casting and venting system to improve the quality of the component in terms of incorporated air, subcooling and the maximum speed of the alloy inside the die.

The preparation phase consists of defining the parametric geometries for the casting and venting system, and assigning specific variables used by the system (MAGMA Optimizator) to autonomously identify the optimal configuration to meet the quality improvement objectives listed above.

After the optimization, the optimal geometry can be graphically identified. In this specific case, Design 18 represents an excellent compromise between avoiding the risks of incorporating air in the

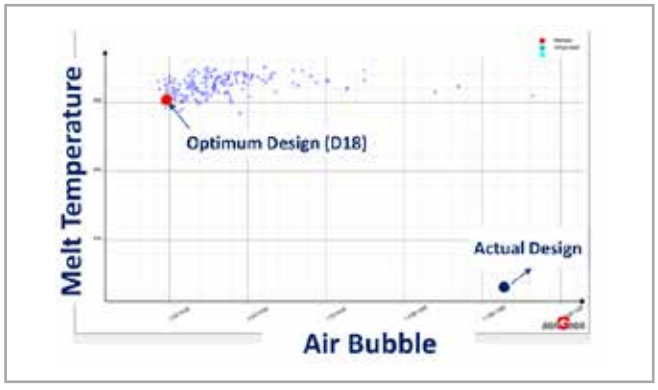

Fig. 3 – Filling dynamics check: ratio between air pockets in the part and alloy temperature

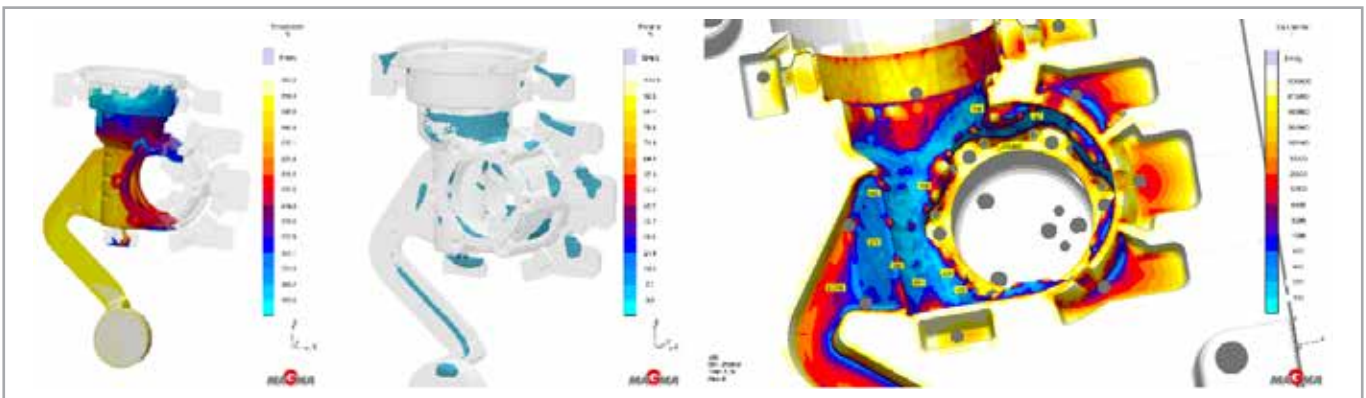

Temperature distribution during filling to assess the risk of cold joints

Porosity criterion to evaluate shrinkage porosity

Die life criterion to evaluate the risk of cracks in the die.

Fig. 2 – Examples of defects found in the first phase of production

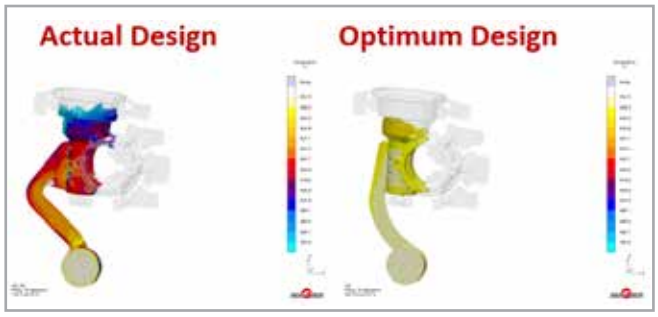

Fig. 4 – Temperature curve at 42% of filling

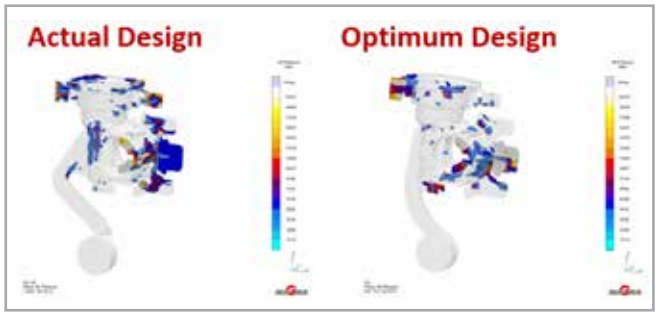

Fig. 5 – Distribution of air pockets after filling

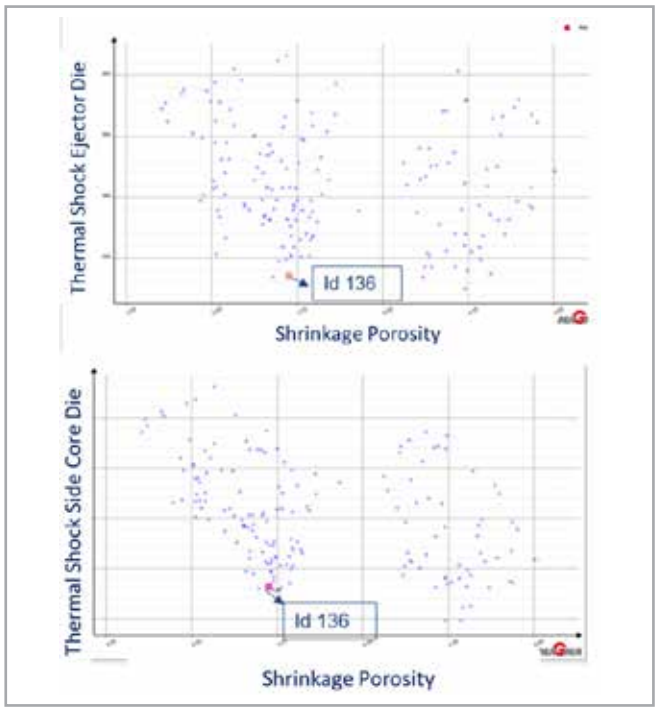

Fig. 6 – Scatter chart: ratio between shrinkage porosity and thermal shock

casting and drops in temperature during filling (Fig. 3), significantly improving the quality of the component (Figs. 4 - 5).

The thermal optimization aims to find the optimal configuration of the thermoregulation circuits and their governing parameters (type, temperature, and flow rate of the thermoregulating medium). In this case the two objectives are conflicting: on the one hand, the aim is to minimize the areas in the casting at risk of shrinkage porosity and, on the other hand, to reduce the thermal shock on the die surface to reduce the occurrence of thermal fatigue cracks.

Similarly to the fluid dynamics optimization, the variables governing the circuit geometries and temperature control parameters were introduced, allowing MAGMA Optimizator to independently identify the optimal design that met the above-mentioned objectives.

Analysis of the results reveals the optimal design to be Design 136, which improves the fatigue life of the molding parts at significantly reduced shrinkage porosity (Figs. 6 - 7).

Virtual DOE to study casting and die defects

After the redesign of the die, a virtual design of experiment (DOE) of 300 designs was calculated to evaluate the correlation between the process parameters and the casting defects. This study showed the

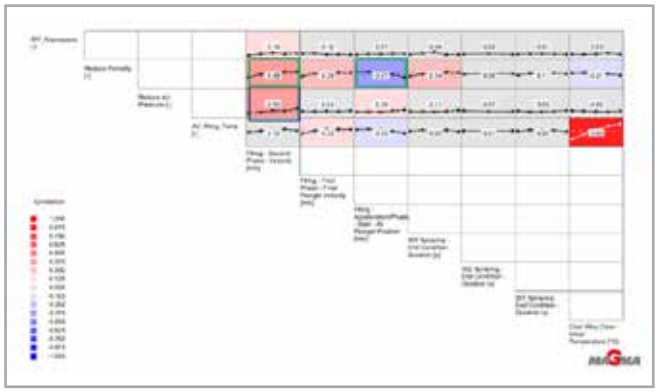

Fig. 8 – Correlation matrix of input-output variables

sensitive variables to be: the second phase speed of the piston, the switching point between the first and second phase speed, and the casting temperature (Fig. 8).

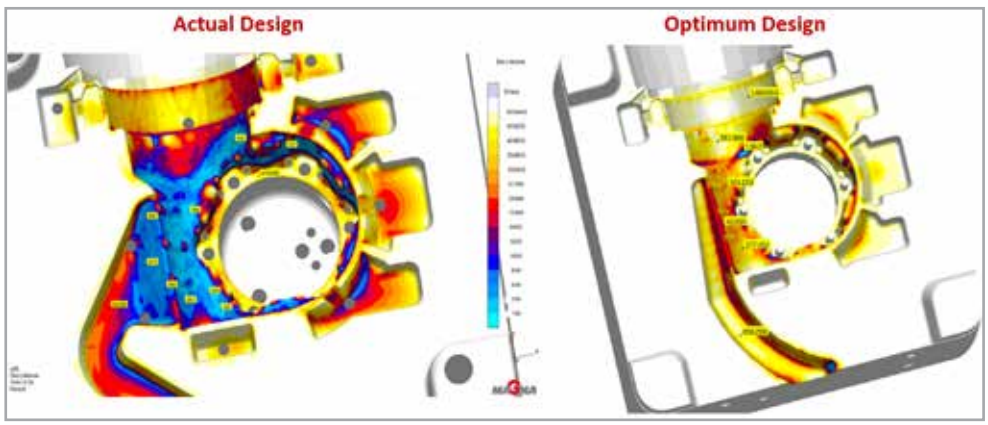

Fig. 7 – Die life: current design vs optimal design (D136)

In addition to the analysis of the component, we also investigated the impact of the process parameters on the thermal fatigue life of the dies. It was found that, even in the worst case, the number of cycles at which the die should begin to deteriorate is about 17 times higher than in the initial configuration in which the first cracks began to develop after 10,000 cycles.

Production with the redesigned die was undertaken (Fig. 9) by controlling

Fig. 9 – Produced die; Coordinate Measuring Machine (CMM) and optical dimensional control

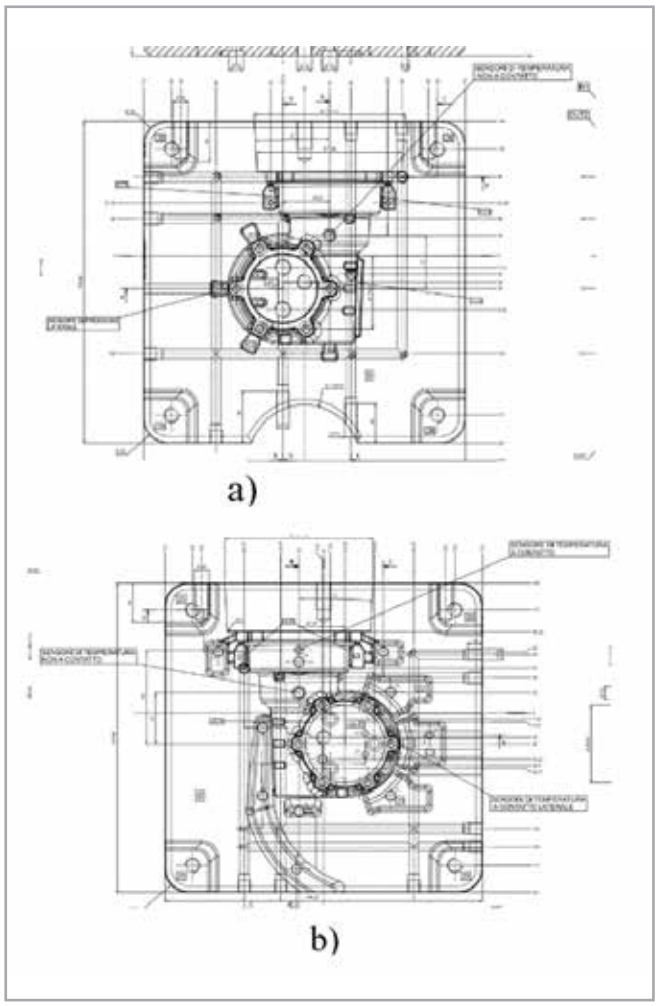

Fig. 10 – Sensor diagram of (a) fixed array and (b) movable array

the process parameters using the Smart ProdACTIVE monitoring system. This system is used to monitor the stability of the process while guaranteeing the quality of the component and the life of the molding parts.

The installation of special sensors on the dies and on the machine (Fig. 10) makes it possible to monitor the production process and instantly identify any deviation in the parameters susceptible to the generation of defects.

This system monitors the stability of the process (Fig. 11) guaranteeing the quality of the component and the lifetime of the molding parts.

Conclusions

Once again, the virtual optimization of the die by means of numerical simulation proves to be fundamental in producing products of increasingly high quality. However, the need to combine product quality with a highly efficient production process to improve competitiveness against low-cost nations makes it necessary to develop intelligent monitoring platforms to identify any anomalies in the process parameters in real time, detecting potential waste castings without performing any quality control and allowing the machine operator to intervene promptly.

Research projects make an increasingly important contribution to supporting innovation in new areas as in the project described.

Acknowledgements

We would like to thank the SPRING Consortium, leader of the PREMANI project, and all the project partners with particular reference to the Department of Management and Engineering (Dipartimento di Tecnica e Gestione dei Sistemi Industriali, DTG) of the University of Padua, and the companies RDS Moulding Technology and Unilab.

References

[1] N. Gramegna, M. Bucci, S. Poles, "Optimization of casting parameters for aluminum alloy suspension arm using new MAGMAfrontier module", 10th Int. MAGMASOFT Users' Meeting, 2002

[2] "Alluminio e sue leghe: Classificazioni e trattamenti termici." Elio Gianotti. Trattamenti Termici Ferioli & Gianotti (Torino)

[3] F. Bonollo, N. Gramegna, S. Odorizzi: "La pressocolata delle leghe di alluminio: simulazione numerica del processo", Edimet (1999)

[4] F. Bonollo, S. Odorizzi: "Numerical simulation of Foundry Processes", SGEditoriali 2001

[5] E. Gariboldi, F. Bonollo, P. Parona: "Manuale della difettologia nei getti pressocolati – Handbook of defects in high pressure diecasting", Associazione Italiana di Metallurgia, 2010

For more information:
Francesca Lago - EnginSoft
f.lago@enginsoft.com

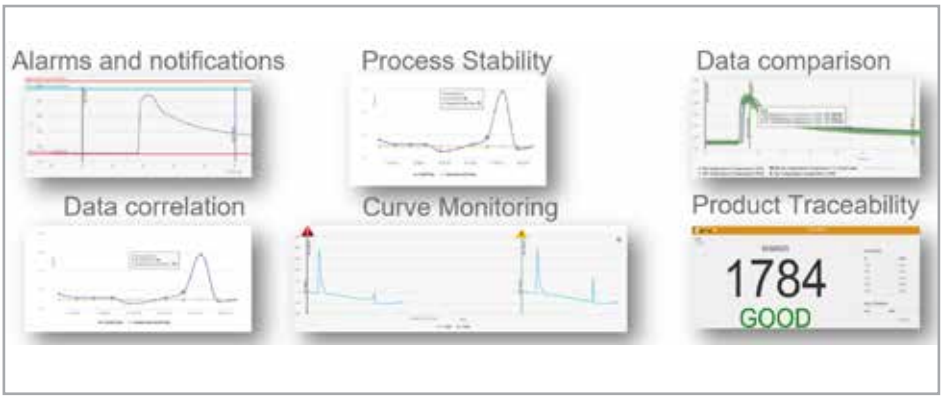

Fig. 11 – Smart ProdACTIVE monitoring system

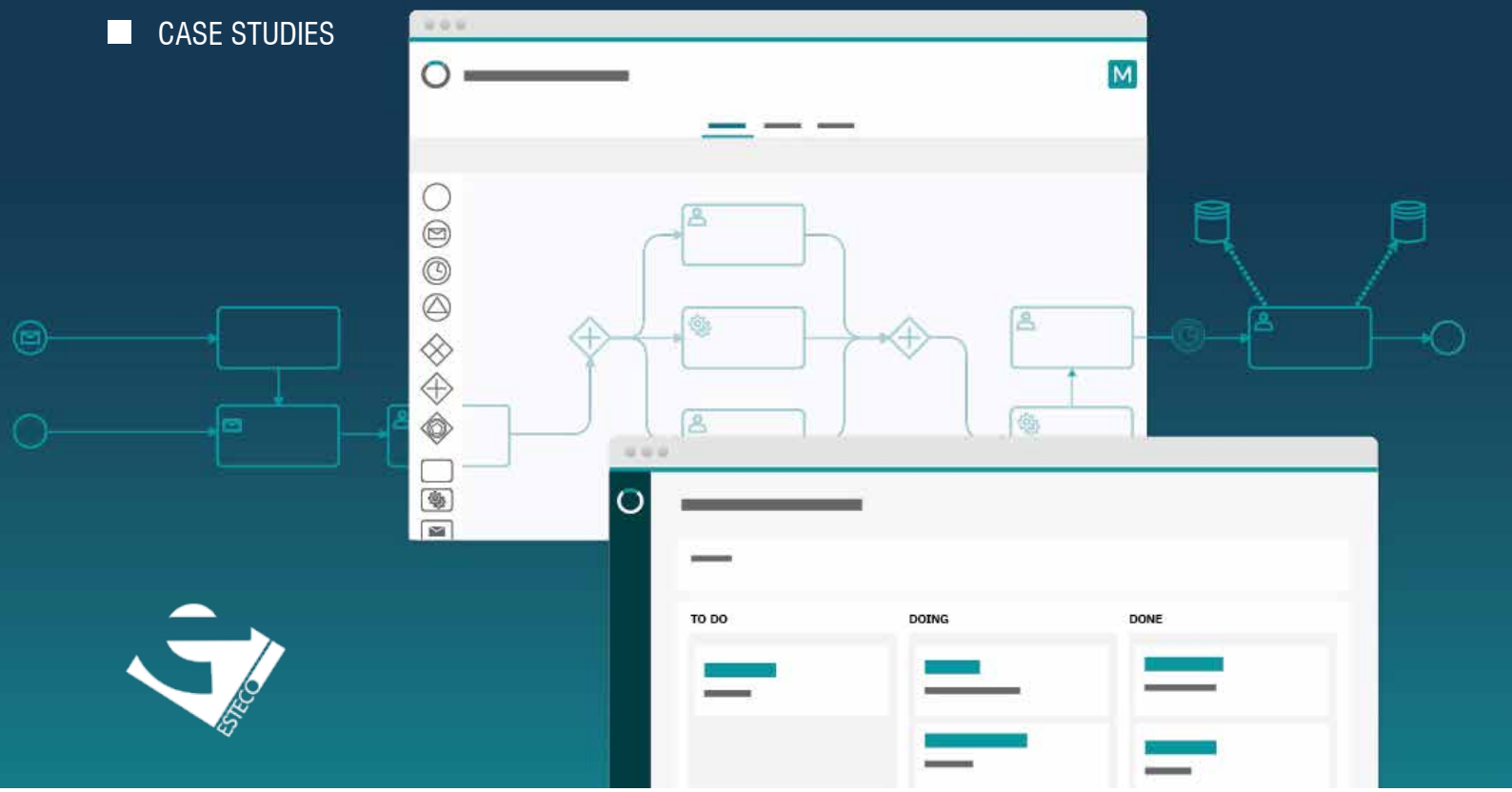

Introducing Business Process Management in VOLTA: a brand-new environment to map and execute engineering design processes

Interview with Marco Turchetto, VOLTA product manager

ESTECO has added business process management (BPM) capabilities to the VOLTA enterprise platform for simulation process and data management (SPDM) and design optimization. Could you explain how BPM affects engineering simulation?

First, allow me to explain what BPM actually is. Gartner defines BPM as a discipline that uses various methods to discover, model, analyze, measure, improve and optimize business processes. A business process coordinates the behavior of people, systems, information, and things to produce business results that support a business strategy. At ESTECO, we believe that BPM can help organizations to map, standardize and execute engineering design processes that are sometimes not formally documented. The danger is that engineering disciplines may work in a siloed manner, especially in simulation. Therefore, researchers at our R&D department studied and examined business process modeling techniques. In particular, they chose the business process model and notation (BPMN) standard to create a business process mapping tool with a view to introducing it into the VOLTA enterprise platform. In so doing, we aim to enhance VOLTA's existing simulation data management capabilities, maximizing the enterprise-wide flow of engineering data. Companies can expect to increase process visibility, improve interaction between management, the engineering, and simulation departments and accelerate product development. This approach was validated in the COMPOSELECTOR

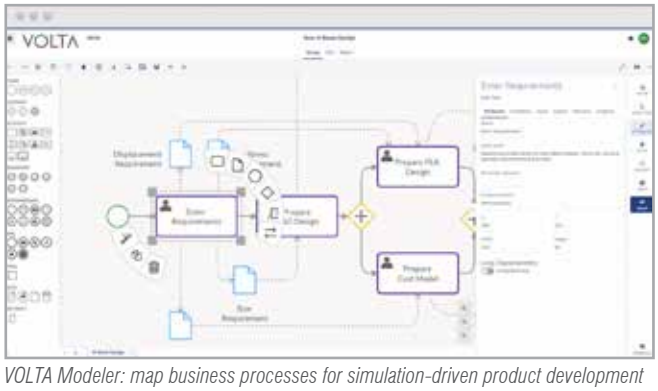

VOLTA Modeler: map business processes for simulation-driven product development

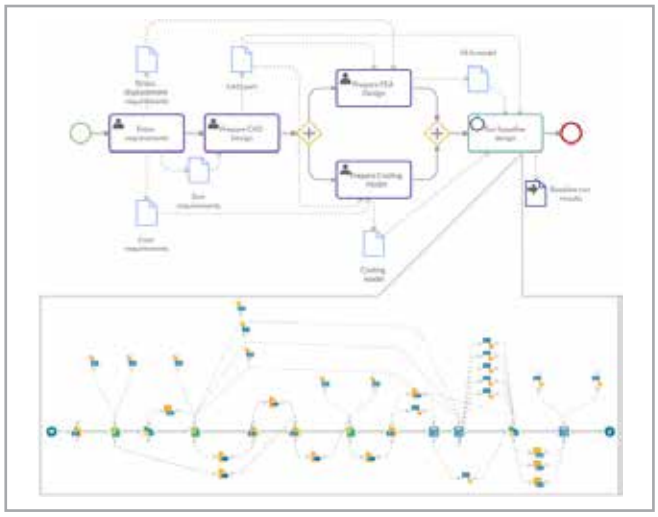

VOLTA Service Task: automatically invokes the execution of a simulation workflow

research project, funded by the European Union's Horizon 2020 Research and Innovation Programme. The scope of that project was to develop a decision support system integrating materials modeling, business process management tools, and multidisciplinary design optimization into a single workflow to support the complex decision-making process involved in selecting and designing composite components.

You mentioned that companies still rely on undefined processes to manage simulation. How does BPM help address organizational issues and break down technical silos between departments?

Paperwork, emails, phone calls, simulation models without versioning, and the use of shared drives are still common practices in simulation-based product development. This may involve numerous manual tasks often performed by single-domain experts who are sometimes disconnected from the rest of the organization. The risk of working with a siloed approach is that it exponentially increases the time spent searching for the right data. Senior management needs to initiate organizational change to slowly embrace and promote the acceptance of routines, thereby enabling better real-time collaboration on simulation data and results. Most SPDM software solutions promise to overcome these challenges by incorporating traditional project management tools such as Gantt charts and PERTs. However, while it is possible to illustrate project schedules and visualize project tasks, the visibility is restricted to single tasks and their proximities. For example, an assignee may not know where a simulation request originated, who is responsible for preparing a CAD or performing a CAE analysis, or where the data is stored. This is where our BPM-enabled VOLTA SPDM platform comes in. Organizations can now map a range of activities and convert them into a standardized business process, allowing them to coordinate repeatable user tasks, automatically execute simulation analyses, and track the activity of each individual engineering analyst. As a result, teams will be able to reuse existing analyses or established best practices to accelerate product development and meet customer requirements more quickly.

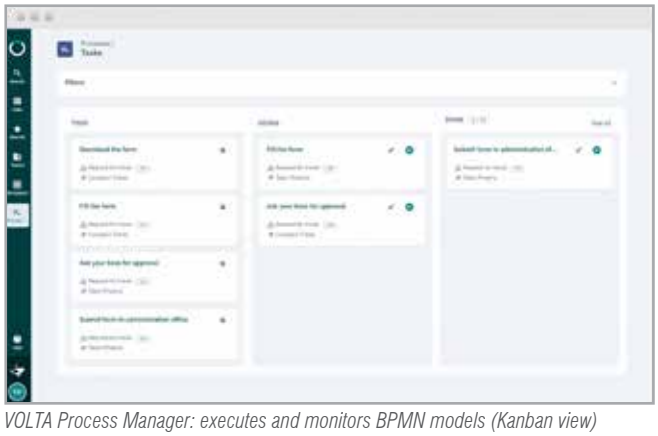

VOLTA Process Manager: executes and monitors BPMN models (Kanban view)

How do you map and execute business processes in VOLTA enterprise software? What are the VOLTA Modeler and the VOLTA Process Manager?

VOLTA Modeler is a workflow editor based on the business process model and notation (BPMN) 2.0 standard that uses graphical notations to map the flow of activities in a business process. Tasks represent these activities in the process. They can be user tasks (human activities), script tasks, or service tasks to invoke the execution of simulation workflows to predict design behavior. The "VOLTA Service Task" is the link between the business process and the simulation workflow for modeling and for executing complex simulations. When the process reaches the simulation service task, a simulation workflow is automatically called to be executed. By connecting engineering solvers into the automated workflow, it seamlessly executes simulation analysis chains and performs design space exploration studies. BPMN graphical representation clarifies the dependencies among tasks. The sequence of execution is made explicit by highlighting the relationship among the different tasks, whether in sequence or in parallel, enabling the company to understand how the process flows.

Once the business process has been designed with VOLTA Modeler, the next step is to execute it. VOLTA Process Manager reads the XML codification of a BPMN process and executes its elements by delivering the tasks to the right assignees, whether they are people or machines, invoking the simulation workflows to perform the design exploration studies. As a result, the right people get the right task at the right time and the automated tasks are triggered precisely when needed. The software also automates the flow of data, manages the input resources and task outputs, and maintains full traceability of every action performed during the execution of the process.

What's in the roadmap for BPM?

In release 2021R3, we have given our customers early access to BPM tools in the VOLTA SPDM platform. We plan to support an increasing number of use cases to achieve full interaction between the simulation workflow and business process. In future releases, we will also improve the VOLTA Service Task by making it possible to request simulations for input data as defined in the business process layer and have the results available for use later in the business process.

Ansys CFD-Pro: a new entry-level license for fluid dynamic simulations

In 2021, the Ansys computational fluid dynamics (CFD) tools took a large step forward in terms of model depth and workflow capabilities. In addition to the many other features of the flagship product, a new license called Ansys CFD-Pro is also available. The Ansys CFD-Pro package is based on the Fluent Solver and provides tools to tackle a range of common entry-level CFD applications using a high-fidelity approach.

This new license can be used in two different ways: linked to a Discovery license or stand alone.

A combined Discovery + CFD-Pro license gives users Discovery's real-time geometry and physics capabilities, as well as highly accurate fluid solutions using the Fluent solver behind the scenes, all in the Discovery interface. With this option, the user can: manipulate geometries and prepare computer-aided design (CAD) models for simulation (Model mode); study designs in few seconds using graphics processing unit (GPU) solvers (Explore mode); and refine analyses using high-fidelity CFD physics without leaving the Discovery interface (Refine mode).

A stand-alone CFD-Pro license allows users to use a "Pro" version of Fluent. This has the same Fluent interface and solver, but with a limited set of physics capabilities for less complex CFD simulations.

Users can therefore control the accuracy of simulations by accessing the industry leading meshing capabilities of Fluent Meshing technology. They can analyze products in the well-known CFD interface, while hiding capabilities unnecessary for entry-level applications for a simplified and easy process. Finally, results can be enhanced with additional Ansys Fluent solver controls, capabilities, and accuracy.

A more detailed list of capabilities is explained in Fig. 1. With the CFD-Pro license in the Discovery interface, it is possible to simulate incompressible steady state flows and conduct conjugate heat transfer analysis; porous media and several basic turbulence models are available; and the effect of gravity can be included through the Boussinesq approximation.

In addition to the previous ones, more models are available in the Fluent interface: compressible (ideal-gas) model and non-Newtonian fluids, 2D fan model, multiple reference frames, and multi-species flows. This allows simulation of fans, pumps, and basic turbomachinery in general, as well as species mixing problems.

The pre- and post-processing operations are also enhanced. Fluent Meshing is available with the Watertight Geometry workflow for complex geometries and meshing needs, which enables the generation of high-quality tetra/poly/mosaic grids. Parameters and expressions can be created to explore different configurations and to simplify the setup procedure. Reports can be generated to summarize the setup and results in one document, which can be shared to communicate the simulation results. Finally, Polyflow features such as extrusion, co-extrusion, fiber spinning, blow molding and thermoforming are also available.

CFD Capabilities Chart	Pro
CAD Import	✓ ✓
Steady-state flow and heat transfer (excluding radiation)	✓ ✓
Basic turbulence models – inviscid, laminar, k-epsilon, k-omega (standard and SST) and Spalart-Allmaras	✓ ✓
HPC: 4 HPC cores included, additional core accessed via ANSYS HPC licensing	✓ ✓
Conjugate Heat Transfer (CHT) in solids; Porous media (isotropic, orthotropic and conical)	✓ ✓
Fluid state models: Incompressible, Bousinesq approximation	✓ ✓
Fluid state models: Compressible (ideal gas), non-Newtonian fluids	✓
Rotating reference frames, multiple reference frames, 2D fan model, multi-stream mixing (multiple non-reacting species)	✓
Fluent Meshing: Watertight Meshing workflow including Polyhedral, Poly-Hexcore with Mosaic technology, Tetrahedral and Prism meshing	✓
Fluent Setup and Post Processing, including Reports	✓
Parameters and expressions	✓
Ansys Polyflow: extrusion, co-extrusion, fiber spinning, blow molding and thermoforming (no viscoelasticity or yield stress models)	✓

✓ Fluent Interface
✓ Discovery Interface

Fig. 1 - List of capabilities

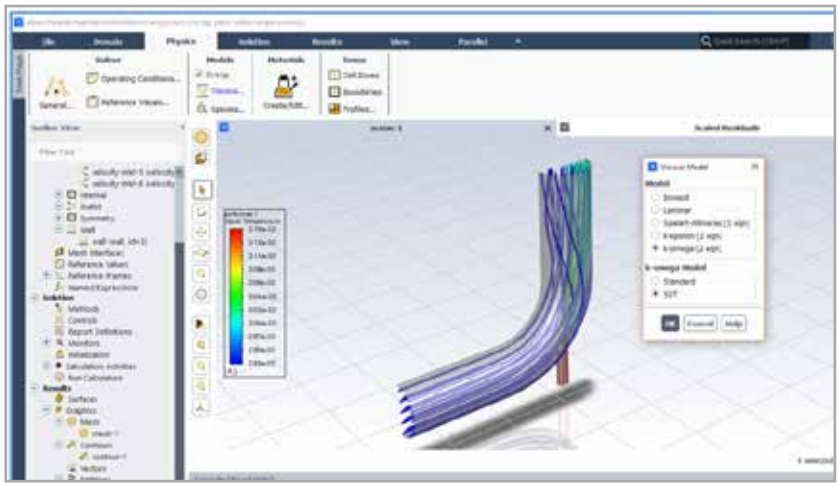

Fig. 2 CFD-Pro with Fluent interface

The entire package is consistent with the Premium and Enterprise versions of Fluent used by experienced analysts, but adapted to entry-level needs. Based on the Single-Windows Workflow concept, it allows users to execute the entire process in a single interface: from the mesh in Fluent Meshing, they can switch to the Fluent Solver mode for setup and execution, and then conclude in Fluent Post, maintaining the same consistent user experience.

CFD-Pro is also compatible with parallel computing as it includes four high-performance computing (HPC) cores. If required, additional cores can be accessed through the Ansys HPC license to accelerate complex simulations.

In conclusion, the CFD-Pro license offers advanced technologies and Fluent accuracy with a reduced set of physical and modeling capabilities for high-fidelity entry-level CFD applications.

For more information:
Diana Magnabosco - EnginSoft
d.magnabosco@enginsoft.com

EnginSoft attains ISO 9001:2015 certification for training

EnginSoft is proud to announce that it has obtained ISO 9001:2015 certification as a training provider (EA37). *"This is a further demonstration of our commitment to technology and knowledge transfer and the high quality of our training courses,"* states Angelo Messina, Education and Training Manager at EnginSoft.

He continues, *"Training is a strategic imperative for companies to remain competitive and keep pace with the rapid changes in technology. Upgrading and developing their staff's digital skills, particularly in more technical areas is fundamental to product evolution and manufacturing excellence."*

He adds that the Italian government's tax credit incentive related to industry 4.0 training expenses has been extended for the two-year 2021-2022 period to support companies in their up-skilling and re-skilling efforts. *"This incentive offers tax credits of up to 50% not only on training costs, but also on the costs of the trained personnel,"* Messina explains. *"With this ISO 9001:2015 certification EnginSoft is in an even stronger position to assure its clients of the eligibility of the training courses it provides."*

Since the tax credits can also be claimed on the so-called "Corporate Academy" courses, which EnginSoft builds with its clients according to their specific requirements, this recognition represents a new opportunity not to be missed. The incentive scheme is applicable not only to traditional training but also to technology transfer training projects.

For further information, contact the EnginSoft Training Secretariat Tel: +39 035 368 711 or visit www.enginsoft.com/training

EnginSoft ha ottenuto la certificazione ISO 9001:2015 per la formazione

EnginSoft è orgogliosa di annunciare di aver ottenuto la certificazione ISO 9001:2015 per il settore EA37 della formazione. *"Questa è un'ulteriore dimostrazione del nostro costante impegno nella diffusione della cultura tecnologica e dell'elevata qualità dei nostri corsi di formazione"*, afferma Angelo Messina, Education and Training Manager di EnginSoft.
E prosegue: *"La formazione è un imperativo strategico per le imprese che puntano a rimanere competitive e a stare al passo con i rapidi cambiamenti tecnologici. L'aggiornamento e lo sviluppo delle competenze digitali del proprio personale, ed in particolare in alcune aree ad alto contenuto innovativo, è fondamentale per l'evoluzione dei prodotti e per l'eccellenza produttiva".*
Angelo Messina ricorda che il governo italiano ha prorogato per il biennio 2021-2022 l'incentivo relativo alle spese di formazione Industry 4.0 per facilitare le imprese nei percorsi di riqualificazione e sviluppo delle competenze delle proprie risorse. *"Questo incentivo offre crediti d'imposta fino al 50% non solo dei costi della formazione, ma anche del costo del personale formato"*, spiega Messina. *"Con questa certificazione ISO 9001:2015 EnginSoft è in grado di garantire ai propri clienti l'erogazione di percorsi formativi agevolabili."*
Poiché i crediti d'imposta possono essere applicati anche ai corsi cosiddetti "Corporate Academy", che EnginSoft costruisce con i propri clienti sulla base delle loro specifiche esigenze, questo riconoscimento rappresenta una nuova opportunità da non perdere. Il regime di incentivazione è applicabile non solo alla formazione tradizionale ma anche ai progetti di formazione al trasferimento tecnologico.

Per ulteriori informazioni contattare la Segreteria Corsi EnginSoft Tel: +39 035 368 711 o consulta www.enginsoft.com/training

INTERNATIONAL CAE CONFERENCE

HYBRID EVENT

2021

37th INTERNATIONAL CAE CONFERENCE AND EXHIBITION

ORCHESTRATING DIGITAL TRANSFORMATION THROUGH SIMULATION

All video recordings and conference papers are now freely available

PROCEEDINGS, PROTAGONISTS AND SALIENT MOMENTS

proceedings2021.caeconference.com
www.caeconference.com